Investigation of Planar Channeling Radiation on Diamond and Quartz Crystals at Electron Energies between 14 and 34 MeV and Probing the Influence of Ultrasonic Waves on Channeling Radiation

D I S S E R T A T I O N

zur Erlangung des akademischen Grades

Doctor rerum naturalium
(Dr. rer. nat.)

vorgelegt

der Fakultät für Mathematik und Naturwissenschaften
der Technischen Universität Dresden

von

M. Sc. Phys. Behnam Azadegan

Gutachter: **Prof. E. Grosse**

Prof. H. Backe

Prof. L. Grigoryan

Tag der Einreichung: 02.07.2007

Tag der Verteidigung: 15.11.2007

Contents

Introduction

After the theoretical prediction of channeling radiation (CR) and the first exact description of the main features expected for this new type of electromagnetic radiation by M.A Kumakhov in 1976, an intense experimental investigation of CR has been started in many research centers of the world. This effort aimed at the verification of the effect and the validation of the properties of CR as well. While CR has been proclaimed as a unique source of quasi-monochromatic X-rays already in the first works published, suggestions for some practical realization of such a nonconventional X-ray source appeared in the 1990ies, not least stimulated also by the development of brilliant superconducting linear electron accelerators of relatively moderate energy, i.e., several tens of MeV.

The first measurements of CR at the Radiation source ELBE of the Forschungszentrum Dresden-Rossendorf have been performed in the fall of 2003, where the most important attempt for an application of CR in radiobiological research was the optimization of its yield and spectral line width as well. Since diamond single crystals have been found to probably be the most suitable ones for an intense CR production because of their outstanding properties to withstand rather high average electron currents, a first measurement series was directed to the studying of the dependence of the yield of planar CR on the thickness of the diamond crystal.

The processing of the experimental data obtained and their physical interpretation needed an effective interactive computer code for theoretical calculations and simulation of CR. The well-known many-beam formalism had to be applied for this purpose on the base of the commercial software package Mathematica. Instead of phenomenological potentials with best-fit parameters, real thermally averaged continuum potentials of the crystal planes considered had to be implemented. The method of the complex optical potential should be applied for the estimation of the intrinsic CR line widths, but a variety of other line-broadening mechanisms had to be taken into account for a realistic simulation of the principally asymmetric and energy-shifted CR lines as registered in CR measurements. Furthermore, concerning the formation of the CR line shape, different approaches could be found in the literature, where the influence of electron multiple scattering during channeling, which plays an increasing role with increasing crystal thickness, was rather poorly known. Finally, the calculation of the CR intensities had to be performed by numerical integration of the population of the channeling states over the crystal thickness and combined with the transition probabilities between transversely bound states.

Motivated by the challenge to install the first tunable quasi-monochromatic CR X-ray source for practical application at the ELBE facility, the results of the forthcoming theoretical as well as experimental investigations of planar electron CR produced on diamond crystals should provide the

necessary data for its design and construction. This X-ray source came into operation at the end of 2006.

Since recent activities in CR research are even directed to probing an active stimulation of CR emission by means of ultrasonic vibrations excited in the crystal, the measurement of the up to now unknown undisturbed CR spectra, generated on piezoelectric crystals such as, e.g., quartz at low electron energy, became a highly actual topic. The developed theoretical instrument checked in the more simple measurements of CR on diamond crystals should be applied for disentangling the expectedly more complicate CR spectra to be obtained from channeling of electrons in polyatomic crystals. To start with the investigation of CR on quartz crystals was reasonable because the combination of a pillbox resonator with easily available piezoelectric quartz crystals should provide a suitable method for the excitation of GHz-frequent ultrasonic waves in the source crystal used for CR production. Although quantum calculations of the influence of ultrasound on CR emission predict intensity amplification effects only near to a rather narrow resonance region, a systematic investigation of CR stimulation by ultrasound seemed to be unpreventable for the deeper understanding of the acting mechanism, and this the more, because relevant theories available to date proclaim slightly different results.

After a brief historical outline on the discovery of CR, comprising the above described topics, the present work deals in chapter 1 with a comprehensive demonstration of the theory of CR and its application and implementation into the current research carried out by the Department of Radiation Physics of the Institute of Radiation Physics of the Forschungszentrum Dresden-Rossendorf. The measurements of CR on diamond crystals, performed at the electron beam of ELBE, are described and compared with theoretical calculations in chapter 2. The application of the developed experimental and theoretical methods for the spectrometric investigation of CR on quartz, which has for the first time been realized in the frame of this work, is explained in chapter 3. The principle used for the excitation of ultrasonic waves in a piezoelectric quartz crystal is described in chapter 4. Finally, chapter 5 of the present work deals with the theoretical description of the influence of ultrasound on CR emission and expected effects as well as with the first experiments of CR stimulation performed at ELBE in 2007. Important conclusions could be drawn for the refined investigation of CR stimulation by ultrasound, where, at present, the possible practical output of the research in this field cannot be overseen yet.

Chapter 1

Theory of channeling radiation

1.1 Essential historical moments

The channeling effect of charged particles, i.e. the steering of their motion through single crystals along crystallographic strings or planes, has astonishingly been discovered by computer simulations of the motion of ions in crystals in the early 1960ies [Rob62, 63]. The principal description of channeling succeeded with the introduction of the continuum approximation for the interaction potential by Lindhard [Lin65]. Channeling of both low-energy electrons as well as positrons was first observed experimentally by Uggerhøj who used the β^+/β^--decay of radioactive ^{64}Cu ions which were implanted into a copper single crystal [Ugg66].

In 1976 Kumakhov published a work where the emission of intense electromagnetic radiation by channeled relativistic electrons or positrons was theoretically predicted [Kum76]. The exact treatment of relativistic effects led him conclude that the "channeled particle radiation" is more "powerful" than bremsstrahlung, more "monochromatic" than synchrotron radiation, directed into a narrow forward cone and energetically shifted into the domain of X- or γ-rays. The idea of a new (nonconventional) radiation source was born.

This prediction stimulated a sedulous search for the channeling radiation (CR) in many accelerator laboratories of the world and a large interest in the further investigation of this type of radiation. In 1977 Andersen et al. presented a classical and also quantum mechanical description of the effect [And77], and only little later CR has been observed from channeled 56 MeV positrons [Alg79] as well as from ultra-relativistic positrons [Mir79]. Measurements of CR using positron and/or electron beams of low (several MeV), medium (tens of MeV) and high energy (from about 100 MeV to several GeV) and single crystals such as Ni, Si, diamond, Ge, LiF, LiH, SiO_2, Au, W etc. followed at research centers such as Århus, CERN, TU Darmstadt, Kharkov, Lawrence-Livermore, Mainz, Saclay, Sepukhov, Stanford, Tokyo, Tomsk and Yerevan, aimed at the investigation of the fundamental

characteristics of CR. At present, most of the results of those pioneering works are reviewed in monographs (see, e.g., Sae85, Kum89, Kum91) containing numerous references to original works, and CR (as well as other phenomena of radiation physics) is included into textbooks.

It is necessary to mention that an increased interest in CR appeared again during the 1990ies, when dedicated suggestions have been made to eventually apply CR as an easily tunable, rather intense quasi-monochromatic source of X-rays at medium electron energies [Gen90, Gary91]. The newly-developed superconducting linear electron accelerators (e.g. S-DALINAC Darmstadt) provide beams of low transverse emittance advantageous for effective CR generation. For the purpose of application, the optimization of the yield and the spectral line width of CR became an issue of intensive investigation [cf. Gou82, Bur84].

Diamond crystals have been discovered to be probably the most suitable ones for the production of intense CR because of their outstanding parameters such as low atomic number, nearly perfect structure, high Debye temperature, large thermal conductivity, etc. Unfortunately, most of the experimental investigations, which have been performed on diamond up to now, were restricted to either relatively high [Gou82, Kep91] or low electron energies [Gen90, Net94, Rei99]. Furthermore, in these works, only relatively thin crystals (from several μm up to about 50 μm) were considered.

The influence of the thickness of diamond crystals on the yield as well as on the line width of CR still needed a systematic quantitative investigation for proving of different hypotheses (cf. Net94, Rei99), where the available range of electron energy at ELBE (10 ÷ 35 MeV) provided ideal preconditions to perform such measurements in the frame of the present work.

The theoretical concept of CR at electron energies less then 100 MeV will be discussed in detail in the following paragraphs. The computer codes developed in this work were applied for the numerical calculation of the expected CR photon energies, line widths and photon yields and enabled the direct comparison with the measured data.

1.2 Theoretical description of channeling radiation at medium electron energies

When a beam of relativistic electrons passes through a randomly oriented single crystal, it will be incoherently scattered (like in an amorphous material) due to interactions of the particles with the individual crystal atoms. The continuous transfer of transverse momentum to the charged particles results in the emission of the ordinary polychromatic spectrum of bremsstrahlung.

Channeling occurs when the beam enters into the single crystal in direction near to a crystallographic axis or plane, being elements of high symmetry in the crystal lattice. In the frame of the classical model, the scattering at the ordered crystal atoms becomes coherent now, causing an oscillatory motion of the electrons along the corresponding string or plane of atoms. Considering this oscillatory motion as an accelerated one in the rest frame of the electron, it emits electromagnetic radiation called

channeling radiation (CR). Although the oscillation frequency ω_0 is rather low and correspond to a radiation energy $\hbar\omega_0$ in the optical region, relativistic effects such as the Lorentz contraction of the longitudinal coordinate and the Doppler effect transform the energy of emitted CR photons observed in beam direction into the domain of X-rays.

At the electron energies considered, the phenomenon of CR emission has to be described by a quantum mechanical formalism. The steering of the electrons to crystal axes or planes is modeled by the interaction of the particles with a continuous axial or planar potential formed by the spatially and thermally averaged action of the individual electrostatic potentials of the crystal atoms positioned in the corresponding axis or plane [Lin65]. Despite their relativistic energy, the transverse motion of the channeled electrons of mass $m\gamma$, where γ denotes the Lorentz factor, stays being nonrelativistic and can be described by a one (planar) or two dimensional (axial) Schrödinger equation which contains the averaged potential of the crystal plan or axis. The transverse motion of the channeled electrons is, therefore, restricted to discrete (bound) channeling states of the so called continuum potential. Spontaneous transitions between these eigenstates lead to the emission of CR, the energy spectrum of which is, consequently, characterized by a line structure of possible photon energies. Since usually the number of bound states is relatively small at electron energies less than 100 MeV, the quantum mechanical approach for the description of CR proves to be necessary.

1.3 Continuum potential

Let us exemplarily consider planar electron channeling. Since the longitudinal component of the velocity of the relativistic particle is assumed to be $v \approx c$, where c denotes the velocity of light (i.e. $\beta \approx 1$ or $\gamma \gg 1$), according to [Lin65] the electron perceives the common action of the individual atomic potentials of the plane as such of a continuous one. This means that the crystal plane is assumed to be charged continuously, forming an average one dimensional transverse continuum potential. Supposed the electron moves along the plane in direction z, this potential is given for a single plane by

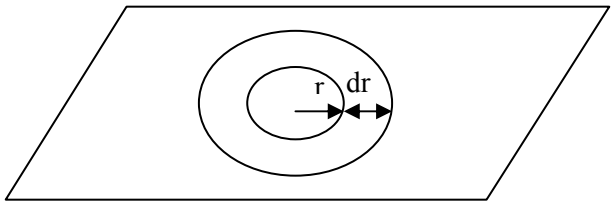

Fig.1.1 Geometry for the derivation of the continuum potential for planar channeling.

$$V(x) = 2\pi N d_p \int_0^\infty V_{atom}(\sqrt{x^2 + r^2}) r dr \tag{1.1}$$

where x is the vertical distance from the plane, N is the atomic density in the plane, and d_p is the interplanar distance [Kum89]. The atomic interaction potential V_{atom} introduced in Eq. (1.1) may be taken in different form or approximation, respectively. The Moliere potential (cf. [Atk82]) is one of the most commonly used potentials, which predicts the channeling states as well as CR energies rather well. The Moliere approximation to the Thomas-Fermi potential is a screened Coulomb potential with the screening function given by

$$V_{atom}(r) = \frac{z_1 z_2 e^2}{4\pi\varepsilon_0 r} \sum_{i=1}^{3} \alpha_i \exp\left(-\beta_i r / a_T\right) \tag{1.2}$$

where $\alpha_i = \{0.1, 0.55, 0.35\}$, $\beta_i = \{6.0, 1.2, 0.3\}$, z_1 and z_2 are the atomic numbers of projectile and target, respectively, r is the distance between the particle and the crystal atom, $e^2 = 14.4$ eV Å, and a_T is the Thomas-Fermi screening length given by

$$a_T = 0.8853 a_0 (z_1^{1/2} + z_2^{1/2})^{-2/3} \tag{1.3}$$

with a_0 being the Bohr radius (0.529 Å).

A more accurate approach is that of Doyle-Turner [Doy68]. Here the interatomic potential is obtained by fitting the electron scattering factor determined by a Hartree-Fock calculation to experimental results

$$V_{atom}(r) = 16\pi z_1 a_0 e^2 \sum_{i=1}^{4} \frac{a_i}{(b_i/\pi)^{3/2}} \exp\left[\frac{r^2}{(b_i/4\pi)^2}\right] \tag{1.4}$$

where a_i and b_i are tabulated coefficients [Doy68].

Substitution of expression (1.2) into (1.1) leads to the planar-averaged static Moliere potential for a single crystallographic plane

$$V(x) = 2\pi z_1 z_2 (N d_p) a_T \sum_{i=1}^{3} (\alpha_i / \beta_i) \exp\left(-\beta_i x / a_T\right). \tag{1.5}$$

Similarly, the planar static continuum potential according to Doyle-Turner reads

$$V(x) = 2\sqrt{\pi} z_1 a_0 e^2 (N d_p) \sum_{i=1}^{4} \frac{a_i}{\sqrt{\beta_i}} \exp\left(-x^2 / \beta_i\right) \tag{1.6}$$

with $\beta_i = b_i / 4\pi^2$.

The obtained static continuum potential must be corrected yet for thermal vibrations of the lattice atoms. This can be performed by convolving the expressions given by Eqs. (1.5) and (1.6) with a Gaussian distribution which describes the thermal displacements of the atoms from the plane. Since each individual atom vibrates independently, the one-dimensional thermal vibration amplitude is characterized by a root-mean-squared (rms) displacement u_1. With this assumption, the operation of thermal averaging is given by

$$V(x, u_1) = \int_{-\infty}^{\infty} V(x - x') P(x') dx' \tag{1.7}$$

with

$$P(x') = (2\pi u_1^2)^{-1/2} \exp\left(-x'^2 / 2u_1^2\right). \tag{1.8}$$

This transformation converts the static Doyle-Turner potential into a thermally averaged form which reads

$$V(x, u_1) = 2\sqrt{\pi} z_1 a_0 e^2 (N d_p) \sum_{i=1}^{4} \frac{a_i}{(\beta_i + 2u_1^2)^{1/2}} \exp\left(-x^2 / (\beta_i + 2u_1^2)\right) \tag{1.9}$$

and will be applied in the following paragraphs for the calculation of the planar CR photon energies and yields.

1.4 Transverse wave equation of channeled electrons

At planar channeling the relativistic particle enters the crystal under a small incidence angle relative to the crystal plane considered. The description of planar CR bases on the division of the particle motion into a longitudinal and a transverse component. Since the longitudinal motion along the plane is not affected by the above given continuum potential, the velocity in z direction is actually nearly constant and amounts to $v_z \approx c$. However, under channeling condition, the transverse momentum p_x of the channeled particle is small compared with the longitudinal one p_z and, therefore, its transverse energy

can be defined by the nonrelativistic expression

$$E_x = \frac{p_x^2}{2m\gamma} + V(x) \,, \tag{1.10}$$

but taking into account the relativistic particle mass $m\gamma$ [Kum91].

In order to describe the radiation emitted by the charged particle during channeling, the applicability of both the classical and quantum theory has to be considered. At medium particle energy (≤ 100 MeV), the motion of the particle has quantum characteristics, i.e., it is bound to discrete transverse channeling states, and the number of bound states is small. So CR is emitted in result of a transition of the channeled particle between to energy levels. With increasing particle energy, the density of bound states increases leading to an overlap of states. This situation can be handled by a classical calculation. In the present work, the energy of the electrons was limited between 10 and 40 MeV. Therefore, the quantum mechanical solution of Eq. (1.10) will be discussed in detail in the next paragraph.

1.5 Quantum mechanical description of planar channeling

As mentioned above, the planar interaction potential is one-dimensional, and the transverse motion of the electron along the coordinate *x* can be described by a Schrödinger equation (rather than by a Dirac equation) which reads

$$\left[\frac{p_x^2}{2m\gamma} + V(x)\right] u(x) = E_x u(x) \tag{1.11}$$

where E_x and $u(x)$ are the transverse energy and wave function of the electron, respectively, and $V(x)$ is the transverse planar continuum potential in the laboratory frame.

Since the planar potential is periodic, it can be expanded to a Fourier series

$$V(x) = \sum_n v_n e^{ingx} \, (n = ...,-1,0,1,2,...) \tag{1.12}$$

where v_n are the Fourier coefficients of the potential (which will be explained in section 1.6.), and ng are the reciprocal lattice vectors normal to the planes as shown in Fig. 1.2.

The eigenfunctions of Eq. (1.11) are one dimensional Bloch waves of the form

$$u(x) = e^{ikx} \sum_n c_n e^{ingx} \, (n = ...,-1,0,1,2,...) \tag{1.13}$$

where k is the transverse crystal momentum lying in the first Brillouin zone, i. e., $0 \le k \le g/2$. Since the potential as well as the eigenvalues converge very fast, the sum over n can be truncated after a finite number of terms. By substituting the expressions (1.12) and (1.13) into Eq. (1.11) the problem reduces to the finding of the eigenvalues and eigenfunctions of a matrix A which in the planar case consists of the components

$$A_{nm} = v_{n-m} \qquad (m \neq n)$$

$$A_{nn} = \frac{\hbar^2}{2m\gamma}(k + ng)^2 + v_0 \,. \tag{1.14}$$

If the origin of coordinates in the crystal is chosen such that the transverse potential is symmetric, i.e., $V(x) = V(-x)$, then the matrix A is Hermitian, i. e., $A^*_{nm} = A_{mn}$, the eigenvalues are real, and for $k = 0$ the eigenfunctions have a definite parity and alternates from even to odd, where the ground state has even parity.

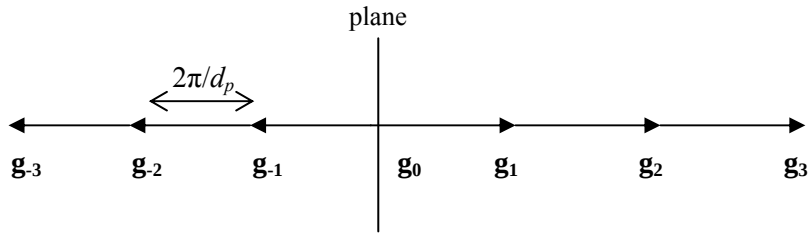

Fig.1.2 Illustration of the reciprocal lattice vectors normal to the crystal plane

1.6 Fourier coefficients of the continuum potential

Since the transverse potential has the periodicity of the lattice, its expansion to a Fourier series represents the most general form of the continuum potential. In order to define the Fourier coefficients, one has to consider some properties of the structure of the crystal lattice.

1.6.1 Reciprocal lattice vectors

The position of an atom in the crystal lattice can be defined by a vector $\vec{R}$

$$\vec{R} = u_1\vec{a}_1 + u_2\vec{a}_2 + u_3\vec{a}_3 \tag{1.15}$$

where $\{\vec{a}_1, \vec{a}_2, \vec{a}_3\}$ are primitive vectors and (u_1, u_2, u_3) are integers. For every crystal lattice there exists an equivalent reciprocal lattice which is important for the description of the scattering of particles in the crystal. Every reciprocal lattice vector $\vec{g}$ represents a set of parallel crystal planes perpendicular to $\vec{g}$. The distance between these adjacent planes is $d_p = 2\pi/g$, and equivalent planes are usually denoted by the Miller indices (*hkl*). The reciprocal lattice vector associated with these Miller indices is given by

$$\vec{g} = h\vec{b}_1 + k\vec{b}_2 + l\vec{b}_3 \tag{1.16}$$

where $\{\vec{b}_1, \vec{b}_2, \vec{b}_3\}$ are primitive vectors of the reciprocal lattice. The primitive vectors of the reciprocal lattice are related to those of the real lattice by the expressions

$$\vec{b}_1 = 2\pi\frac{\vec{a}_2 \times \vec{a}_3}{\vec{a}_1 \cdot (\vec{a}_2 \times \vec{a}_3)}, \vec{b}_2 = 2\pi\frac{\vec{a}_3 \times \vec{a}_1}{\vec{a}_1 \cdot (\vec{a}_2 \times \vec{a}_3)}, \vec{b}_3 = 2\pi\frac{\vec{a}_1 \times \vec{a}_2}{\vec{a}_1 \cdot (\vec{a}_2 \times \vec{a}_3)}. \tag{1.17}$$

For a cubic crystal structure such as that of diamond (see Fig. 1.3), the set of primitive vectors is given by the expressions

$$\vec{a}_1 = a\hat{x}, \vec{a}_2 = a\hat{y}, \vec{a}_3 = a\hat{z} \tag{1.18}$$

$$\vec{b}_1 = \frac{2\pi}{a}\hat{x}, \vec{b}_2 = \frac{2\pi}{a}\hat{y}, \vec{b}_3 = \frac{2\pi}{a}\hat{z}\ , \tag{1.19}$$

and the interplanar distance is defined by

$$d_p = \frac{a}{\sqrt{h^2 + k^2 + l^2}}\ . \tag{1.20}$$

In the simplest crystal structure, there is only one atom at each lattice site. More complicate crystal structures may be described by more than one atom at each lattice site.

For example, the crystal structure of diamond may be represented by an fcc lattice with a 2-atom basis {(0,0,0),(1/4,1/4,1/4)} or, equivalently, by a cubic lattice with an 8-atom basis {(0,0,0), (1/4,1/4,1/4), (0,1/2,1/2), (1/4,3/4,3/4), (1/2,0,1/2), (3/4,1/4,3/4), (1/2,1/2,0), {3/4,3/4,1/4)}. For this structure given

in the 8-atom basis, the primitive vectors are those of Eqs. (1.18) and (1.19), but in the 2-atom basis they are given by the relations

$$\vec{a}_1 = \frac{a}{2}(\hat{x}+\hat{y}), \vec{a}_2 = \frac{a}{2}(\hat{y}+\hat{z}), \vec{a}_3 = \frac{a}{2}(\hat{x}+\hat{z}) \tag{1.21}$$

$$\vec{b}_1 = \frac{2\pi}{a}(\hat{x}+\hat{y}-\hat{z}), \vec{b}_2 = \frac{2\pi}{a}(-\hat{x}+\hat{y}+\hat{z}), \vec{b}_3 = \frac{2\pi}{a}(\hat{x}-\hat{y}+\hat{z}). \tag{1.22}$$

One can notice that the Miller indices for the (111) plane of diamond are indeed (*111*), when this basis is used. For the (110) plane, however, the Miller indices then are (*211*), and for the (100) plane they are (*101*).

The unit cell of the cubic diamond structure contains 8-atoms as shown in Fig. 1.3.

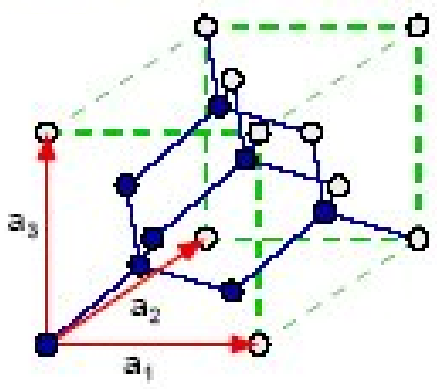

Fig.1.3 Unit cell of the diamond structure with 8-atoms

1.6.2 Structure factor of the crystal

When a charged particle (electron) enters a crystal, it will be scattered on the individual crystal atoms. Depending on the direction of the incident electron beam as well as on the spatial spacing of the atoms in a crystal plane, there will be different planar interaction potentials. In order to describe these potentials, one can split the problem in two parts. First one considers scattering on a single atom, and secondly one describes scattering on the crystal lattice.

The scattering on a single atom leads to a scattering form factor, and if the atomic potential $V_{atom}(r)$ is spherically symmetric with respect to the nucleus, it is defined by [Doy68]

$$f_{el}(s) = \frac{2m}{\hbar^2}\int_0^\infty r^2 V_{atom}(r)\frac{\sin(4\pi sr)}{4\pi sr}dr \tag{1.23}$$

where $4\pi s$ denotes the change of the magnitude of the electron wave vector in a scattering event, and s = sin(θ)/λ (Å^{-1}) where θ means the angle between the incident and the reflected electron wave vector. An analytical approximation of $f_{el}(s)$ is

$$f_{el}(s) = \sum_{i=1}^{4} a_i e^{-b_i s^2} \tag{1.24}$$

where a_i and b_i are parameters determined by the curve fitting procedure performed by Doyle and Turner [Doy68]. However, this approximation is valid only for s ≤ 2Å^{-1}, and calculations must fail at increasing number of Bloch waves. Therefore, a non-linear least-squares-fit of $f_{el}(s)$ to six Gaussians [Cho99a] has been applied in this work (see Table 1.1). If the potential for planar channeling converges fast, the application of different sets for the coefficients a_i and b_i leads to the same result.
In order to describe scattering at the lattice, a structure factor S is involved

$$S = \frac{1}{V_c} \sum_j e^{i\vec{g}\cdot\vec{r}_j} \tag{1.25}$$

where the sum extends over all atoms in the unit cell. The structure factor determines those sets of Miller indices, the reflections from the corresponding planes are strong. It can be shown that S vanishes for every value s different to $s = ng/4\pi$. Therefore, the atomic scattering form factor can be written in the following form

$$f_{el}(\frac{ng}{4\pi}) = \frac{2m}{V_c \hbar^2} \sum_j e^{i\vec{g}\cdot\vec{r}_j} \int_0^\infty r^2 V_{atom}(r) \frac{\sin(gr)}{gr} dr \,. \tag{1.26}$$

The Fourier components of the planar continuum potential can be computed using tabulated electron-scattering form factors $f_{el}(s)$ which are proportional to the Fourier transforms of the atomic potential. As an analysis shows, the Fourier components of the planar continuum potential can be written

$$v_n = \frac{h^2}{2\pi m} f_{el}(\frac{ng}{4\pi}) \,. \tag{1.27}$$

If the thermal vibrations of the lattice atoms are taken into account, then the Fourier coefficients read

$$v_n = \frac{4\pi}{V_c}\sum_j e^{-M_j(\vec{g})} e^{(-i\vec{g}.\vec{r_j})} \int_0^\infty r^2 V_{atom}(r)\frac{\sin(gr)}{gr}dr \qquad (1.28)$$

where V_c denotes the volume of the unit cell, $\vec{r_j}$ is the lattice site of atom j in the unit cell, $M_j(\vec{g}) = \frac{1}{2}g^2\langle u_j^2\rangle$ is the Debye-Waller factor for atom j taking into account its thermal motion, and u_j is the one-dimensional vibration amplitude.

The potential $V_{atom}(r)$ used for the electron-atom interaction may be the screened Coulomb potential given by Eq. (1.2) or the more accurate Doyle-Turner potential given by Eq. (1.4). For the screened Coulomb potential, the Fourier coefficients defined by Eq. (1.28) read

$$v_n = \frac{4\pi\hbar^2 z_1 z_2}{m a_0 V_c} a_0^2.(e^2/a_0)\sum_j e^{-M_j(\vec{g})}\cdot e^{(-i\vec{g}.\vec{r_j})}\sum_{i=1}^{4}\frac{\alpha_i}{(\beta_i/a_n)^2+(ng)^2}, \qquad (1.29)$$

and for the Doyle-Turner potential they are given by the expression

$$v_n = \frac{2\pi z_1}{V_c} a_0^2.(e^2/a_0)\sum_j e^{-M_j(\vec{g})}\cdot e^{(-i\vec{g}.\vec{r_j})}\sum_{i=1}^{4} a_i e^{\left(-\frac{1}{4}(\frac{b_i}{4\pi^2})(ng)^2\right)}. \qquad (1.30)$$

Table 1.1 Values of the parameters a_i and b_i as determined for diamond by different authors.

Reference	a_1(Å)	a_2(Å)	a_3(Å)	a_4(Å)	a_5(Å)	a_6(Å)
[Doy68]	0.7307	1.1951	0.4563	0.1247		
[Cho99a]	0.4370215	1.085384	0.68448047	0.0716327	0.0166049	0.213033
	b_1(Å^2)	b_2(Å^2)	b_3(Å^2)	b_4(Å^2)	b_5(Å^2)	b_6(Å^2)
[Doy68]	36.9951	11.2966	2.8139	0.3456		
[Cho99a]	46.353418	16.726551	5.6137232	0.3270024	0.0406705	1.508868

1.7 Numerical calculation of CR photon energies for different crystal planes of diamond

The theoretical approach to planar electron channeling explained in the previous paragraphs has been applied in this work for the establishment of an interactive computer code based on the software package Mathematica 4.1. In the frame of the many-beam formalism, the program calculates planar continuum potentials as well as wave functions and eigenvalues of channeled electrons. From these data, transition energies between transversely bound states and, hence, CR photon energies are deduced. The calculations have been performed for such electron energies as well as crystal planes in diamond which had been chosen for experimental investigation of CR at ELBE. The results of the calculations and a comparison with measured CR data are presented in the following paragraphs, even if the CR measurements will be described in detail in chapter 2.

1.7.1 Continuum potential

The convergence of the continuum potential and, consequently, of the corresponding eigenvalues depends on the number of reciprocal lattice vectors (i.e. the number of planes) which contributes to the numerical value of this potential. The number of the planes is always odd because positive and negative reciprocal lattice vectors have to be included.

The Fourier coefficients of the continuum potential were calculated using Eq. (1.30). A value of 0.042 Å was assumed for the one-dimensional (rms) vibration amplitude of diamond at room temperature. The structure factors of diamond were calculated for both the 2-atom and the 8-atom basis (cf. 1.6.1). Since in the case of diamond the potential and the eigenvalues converge very fast, the continuum potential was calculated for 21 Bloch waves.

For illustration, the continuum potentials of the (100), (110) and (111) planes of diamond are shown in Fig. 1.4. From these figures one can realize that the interplanar spacing between (110) planes is a factor of $\sqrt{2}$ larger than that for (100) planes. Therefore, the potential of the (110) plane is twice as deep as that of the (100) plane and, at fixed electron energy, the number of bound states for the (110) plane is larger than that for the (100) plane. Furthermore, the potential of the (111) plane shows two minima which correspond to the unequally spaced crystal planes. The spacing of the (111) planes by turns amounts to $\frac{a}{4\sqrt{3}}$ and $\frac{3a}{4\sqrt{3}}$. Therefore, the interplanar distance within the same family of planes is $\frac{a}{\sqrt{3}}$.

1.7.2 Eigenvalues

The energy levels of the channeled electrons have been calculated for the electron energies of 14.6, 17, 25, 30 and 34 MeV as chosen in the measurements. The truncation to 21 Bloch waves defines the

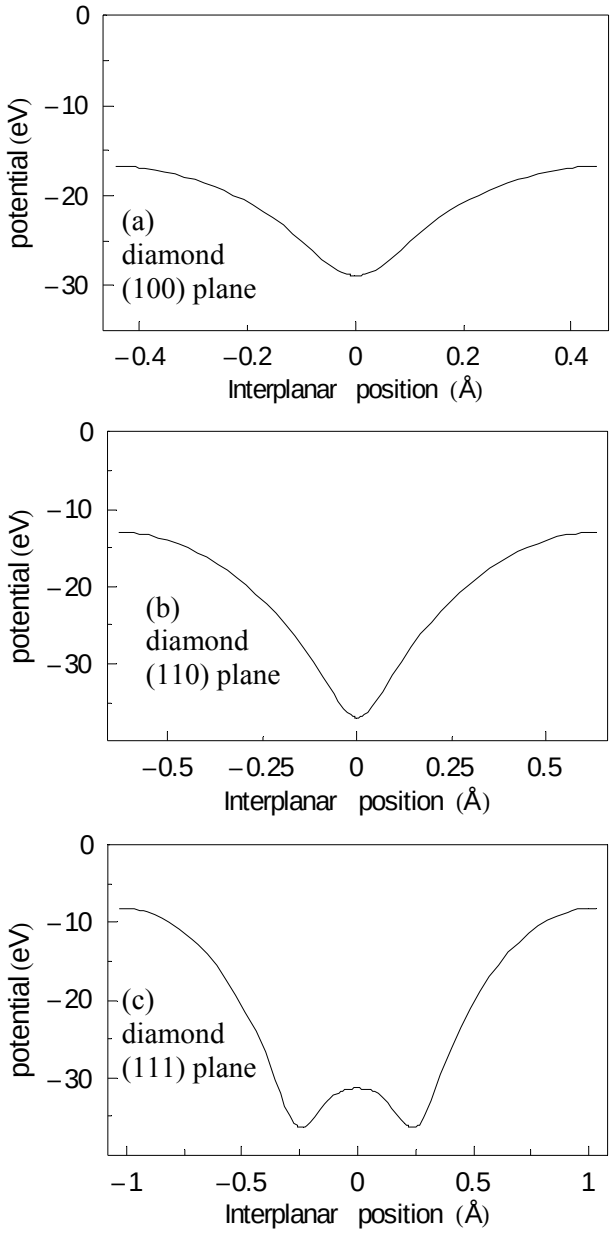

Fig.1.4 Potentials of crystal planes in diamond calculated for 21 beams. (a) (100), (b) (110), (c) (111). The potentials are plotted for one period of planes.

Table 1.2 Lowest eigenvalues for 14.6 MeV electrons planar channeled in diamond at a transverse crystal momentum k=0. The energies are given in unit of eV.

Plane	E_0	E_1	E_2	E_3	E_4	E_5
(111)	-32.09	-29.07	-21.91	-16.24	-12.06	-7.95
(110)	-29.27	-18.95	-14.41	-12.89	-11.40	-6.98
(100)	-23.30	-17.25	-16.34	-14.25	-13.67	-10.46

dimension of the matrix A to 21×21. Further input data of the computer code are the electron energy and the Miller indices (*hkl*) of the plane considered. Output data are the eigenvalues and eigenfunctions of the electrons channeled in the corresponding planar continuum potential. The eigenvalues for 14.6 MeV electrons channeled in different planes of diamond are listed in Table 1.2. The energy of the emitted CR photons in the laboratory frame is given by

$$E_{if} = \frac{\hbar\omega_{if}}{(1-\beta\cos\theta)} \tag{1.31}$$

where ω_{if} is the frequency of CR in the electron rest system, θ denotes the angle of observation with respect to the direction of the electron beam and $\beta = v/c = \sqrt{1-1/\gamma^2}$. For $\theta = 0$ Eq. (1.31) can be approximated by

$$E_{if} = 2\gamma^2\hbar\omega_{if} = 2\gamma^2(E_i - E_f) \tag{1.32}$$

with E_i and E_f being the eigenvalues of the initial and final state, respectively. Since the planar continuum potential is one-dimensional, the eigenvalues and eigenfunctions are characterized by a single quantum number n. As shown in Fig. 1.4, the continuum potentials are symmetric. Therefore, the eigenfunctions for the transverse crystal momentum $k = 0$ have a definite parity, starting from $n = 0$ with even parity and alternating between even and odd.

Table 1.3 CR photon energies for the lowest transitions of 14.6 MeV electrons planar channeled in diamond.

Plane	Transition	CR photon energy measured (keV)	CR photon energy calculated Continuum model (keV)	CR photon Energy calculated Single potential (keV)
(100)	1→0	9.38±0.04	9.56	10.73
(110)	1→0	16.54±0.05	17.06	17.48
	2→1	7.89±0.04	7.13	8.06
(111)	2→1	11.07±0.04	11.69	–
	3→2	8.14±0.03	9.26	–
	4→3, 5→4	6.05±0.05	6.83, 6.71	–

The CR photon energies calculated for the lowest transitions of 14.6 MeV electrons channeled in the (100), (110) and (111) planes of diamond are compared with measured data in Tab. 1.3. The errors of the measured values given in Tab. 1.3 result from the fitting procedure only (see chapter 2). The uncertainty of the electron beam energy (assumed to be ≈ 200 keV) governs the maximum error of the measured CR photon energies which amounts to about 0.4 keV. Therefore, the calculated CR photon energies are in good agreement with the measured ones.

1.7.3 Single potential approximation

For electron energies E > 10 MeV, the potentials of simple planes can be approximated by an analytical expression of the form

$$V(x) = -\frac{u_0}{\cosh^2 x/b} \tag{1.33}$$

where u_0 and b are parameters. They amount to u_0 = 22.8 eV, b = 0.215Å for the (110) plane and to u_0 = 12.4 eV, b = 0.168Å for the (100) plane of diamond [Kum89].

The transverse energies of planar channeled electrons can be calculated by

$$E_{xn} = -\frac{\hbar^2}{2m\gamma b^2}\left(-\frac{1}{2}+\sqrt{\frac{1}{4}+\frac{2m\gamma u_0 b^2}{\hbar^2}}-n\right)^2 \tag{1.34}$$

with $n \le -\frac{1}{2}+\sqrt{\frac{1}{4}+\frac{2m\gamma u_0 b^2}{\hbar^2}}$.

The transition energies calculated in the single potential approximation for 14.6 MeV electrons channeled along the (110) and (100) planes of diamond are included in Table 1.3 for comparison with the results obtained by means of the continuum model. Note that this method is not applicable for the (111) plane because of the more complicate shape of its planar potential (see Fig. 1.4c).

1.8 Line width of quasi-monochromatic channeling radiation

Several mechanisms contribute to the residual width and the line shape of CR as registered by means of an X-ray spectrometer. They will briefly be considered in the following.

1.8.1 Coherence length

The intrinsic line width of CR is connected with the finite lifetime of the channeling states. In the case of diamond, it is mainly determined by incoherent scattering of the channeled electrons on phonons

(thermal scattering) [Rad70, Whe65], but also by scattering on the crystal atoms [Cho99, Bur84, And83, Bir82, Web95]. The resulting CR line shape is a Lorentzian with a width given by

$$\Gamma_{coh} = \frac{2\gamma^2 \hbar c}{l}. \tag{1.35}$$

The total coherence length l is defined by

$$\frac{1}{l} = \frac{1}{l_1} + \frac{1}{l_2} \tag{1.36}$$

where l_1 and l_2 are the coherence lengths of the initial and final states of some transition considered. In the framework of the theory of the complex potential, $U(X) = V(x) + iW(x)$, the coherence length reads

$$l_j = -\frac{\hbar \beta c}{2\langle W \rangle_j} \tag{1.37}$$

where $\langle W \rangle_j = \langle \psi_j | W | \psi_j \rangle$ is the expectation value of the imaginary part of the complex potential for the state j.

Such as the real part V(x) [cf. Eq. (1.12)], the imaginary part W(x) can be expanded into a Fourier series

$$W(x) = \sum_n v_n^i e^{ingx} \quad \text{(n=…,-1,0,1,2,..)} \tag{1.38}$$

where the Fourier coefficients are given by [Cho99a, Rad70]

$$v_{\vec{g}}^i = \frac{\hbar^3 \beta N_V}{2m_0^2 c V_c} \int f_{el}(|\vec{q}|) f_{el}(|\vec{q} - \vec{g}|)[e^{-M_j(\vec{g})} - e^{-M_j(\vec{g}) - M_j(\vec{q} - \vec{g})}] q dq d\varphi, \tag{1.39}$$

$\vec{q} = \vec{k} - \vec{k}_0$ is the change of the electron wave vector, and $f_{el}(|\vec{q}|)$ is the scattering amplitude. Equation (1.39) can be reduced to the form [Cho99a]

$$v_n^i = -\frac{\hbar^3 \pi N_v}{2m_0{}^2 c V_c} \sum_i \sum_j a_i a_j \left[\frac{e^{-M_j(\vec{g}) - B_i B_j n^2 g^2/(B_i + B_j)}}{B_i + B_j} - \frac{e^{-C_i C_j n^2 g^2/(C_i + C_j)}}{C_i + C_j} \right] \tag{1.40}$$

with $B_i = b_i/(16\pi^2)$ and $C_i = B_i + 0.5\langle u_i^2\rangle$ using the Gaussian approximation of the electron-scattering form factor $f_{el}(s)$ [Doy68]. N_v denotes the atomic density, and V_c is the volume of the unit cell. The expectation value $\langle W \rangle_j$, therefore, describes the decay of a particular eigenstate due to incoherent scattering, where l_j gives the characteristic length for attenuation of the initial electron wave function. The lifetime of that channeling state is then $\tau = l_j/c$.

As already discussed in § 1.6.2, the approximation of the electron-scattering form factor $f_{el}(s)$ given by Doyle and Turner is valid for values of $s < 2$ Å^{-1}. When this may be acceptable yet for the calculation of the eigenvalues, it, however, will lead to inaccurate coherence lengths because incoherent scattering is effective at short distances from the channeling plane. Consequently, the Fourier components of *W(x)* have to be evaluated for sufficiently large values of *s*. With reference to the results of Ref. [Cho99], which apply for values of $s \leq 6$ Å^{-1}, calculated coherence lengths for the 1→0 and 2→1 transitions of electrons channeled in the (110) plane of diamond are listed in Table 1.4. With these values one obtains intrinsic line widths increased by about 15 ÷ 20 %.

Table 1.4 Coherence lengths (μm) calculated for the two lowest transitions of electrons of energy E_e channeled in the (110) plane of diamond.

E_e (MeV)	1→0	2→1
14.6	1.11	3.21
17	1.06	2.91
30	0.90	1.99
34	0.87	1.86

The complex potential and the probability density distributions calculated for channeling of 17 MeV electrons in the (110) plane of diamond (Figs. 1.5 − 1.7) demonstrate important features:

(i) The imaginary part of the complex potential is weaker than the real continuum potential and more strongly located at the channeling plane.

(ii) Scattering acts differently on different channeling states described by the corresponding probability densities (or wave functions).

(iii) The coherence length (or lifetime) of a more tightly bound channeling state is shorter than that of a weaker bound one.

(iv) The coherence lengths become shorter with increasing electron energy, because the wave functions of channeled electrons become more constrained to the plane.

(v) The intrinsic CR line widths for transitions between low lying channeling states are larger than those for higher transitions.

(vi) The intrinsic CR line width increases with increasing electron energy.

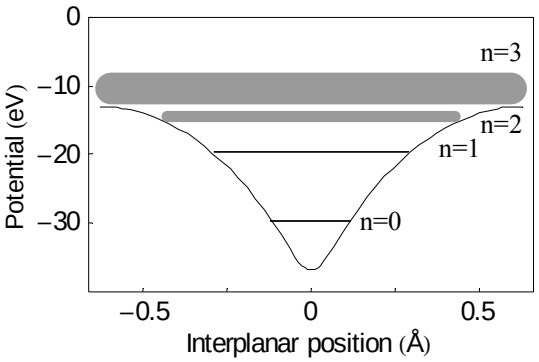

Fig. 1.5 Real part of the continuum potential of the (110) plane of diamond and eigenvalues (bands) calculated for channeled electrons of energy17 MeV.

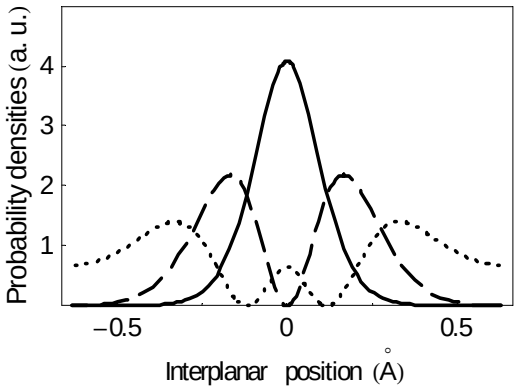

Fig. 1.6 Probability density distributions calculated for electrons of energy 17 MeV channeled in the (110) plane of diamond. Ground state with n = 0 (full line) , channeling states with n = 1 (dashed line) and n = 2 (dotted line).

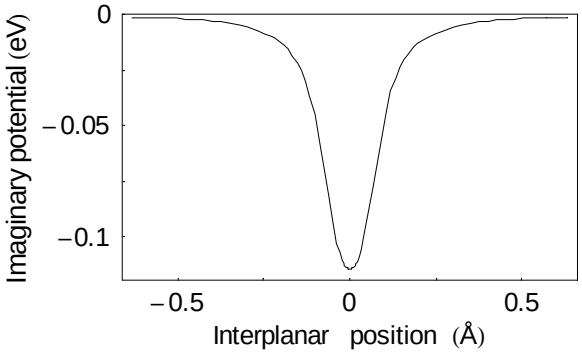

Fig.1.7 Imaginary part of the potential of the (110) plane of diamond calculated for 17 MeV electrons.

1.8.2 Finite crystal thickness

The contribution to line broadening due to the finite thickness L of the crystal [Bur84, Cho99] reads

$$\Gamma_L = \frac{4\pi\gamma^2\hbar c}{L}. \tag{1.41}$$

It also relates to the life time of the channeling states but can be neglected at larger L.

1.8.3 Bloch-wave broadening

It is inherent to the many-beam approach of channeling that the eigenvalues depend upon the electron wave vector k which can vary such as $-g/2 \le k \le g/2$. This effect causes a band structure of the channeling states (see Fig. 1.5). The variation of the transverse energy with the electron wave vector is small for tightly bound states. For states near the top of the potential and within the continuum, however, this effect becomes the dominating line-broadening mechanism.

At small observation angles, Bloch-wave line broadening is given by the sum of the band widths of the initial and the final states

$$\Gamma_{Bloch} = 2\gamma^2 \left(\left| \varepsilon_i^{k=0} - \varepsilon_i^{k=\frac{g}{2}} \right| + \left| \varepsilon_f^{k=0} - \varepsilon_f^{k=\frac{g}{2}} \right| \right) \tag{1.42}$$

or, accurately speaking, by the band dispersions [Cho99].

Apart from line broadening inherent to channeling, the experimental conditions of production as well as registration of CR involve further components affecting the observed CR line shape.

1.8.4 Energy spread of the electron beam

The energy E_x of a CR line scales with the electron energy E_e such as

$$E_x \propto \gamma^a \tag{1.43}$$

where a is a constant ranging from 1.5 to 2 in dependence on the transition considered [Kle85]. Therefore, an initial beam-energy spread ΔE_e causes the energy spread of the observed CR photons

$$\Delta E_x = a \frac{\Delta E_e}{E_e} . \tag{1.44}$$

While ΔE_e of the ELBE beam is small and can be neglected, an exact tuning of the beam energy is, however, an important requirement [cf. Eq. (1.43)].

1.8.5 Detector resolution

If the response function of the X-ray detector applied for CR spectrometry is a Gaussian, its width contributes to the CR line width observed, and the CR line shape now represents a convolution of the (intrinsic) Lorentzian with this Gaussian, a so called Voigt profile.

1.8.6 Doppler broadening

Since the channeled electron is relativistic, the Lorentz transformation deepens the crystal potential by a factor γ. The dipole emission pattern of CR in the electron rest system transforms into an extremely forward directed cone. Due to the Doppler shift, the CR photon energy E_x observed at an angle θ with respect to the axis of the electron beam becomes

$$E_x = \frac{\hbar\omega_{if}}{(1-\beta\cos\theta)} \approx \frac{2\gamma^2\hbar\omega_{if}}{1+\gamma^2\theta^2} \tag{1.45}$$

where the transition energy $\hbar\omega_{if}$ relates to the transverse energy difference of the channeling states involved (cf. Fig. 1.5). Consequently, the CR photons with maximum energy are emitted into the direction $\theta = 0$, and E_x decreases with increasing observation angle. For the electron energies available at ELBE, the residual CR photon energies reach values between about 10 and 100 keV.

Concerning the measurement of the CR photon energy, it directly follows from Eq. (1.45) that an accurate adjustment of the detector position is very important. The finite solid angle of the X-ray detector principally also influences the observed CR line shape. However, this effect is mostly negligible at typical measurement conditions. Otherwise, a large beam divergence may cause CR line broadening because the average observation angle then becomes different from zero. In accordance with Eq. (1.45), line broadening due to $\theta \neq 0$ is always directed towards smaller photon energy. Therefore, the registered CR line shape becomes asymmetric.

1.8.7 Multiple scattering

Multiple scattering of the electrons in the crystal effectively affects the beam divergence at a depth z and, consequently, contributes to CR line broadening and asymmetry. For diamond crystals this line-broadening mechanism becomes relevant at a thickness of several tens of μm.

Multiple scattering of electrons in amorphous materials (or randomly oriented crystals) is well understood. Its effect on the line shape of planar CR, i. e., when the channeled electron moves parallel to a crystal plane, is less investigated. The asymmetry of the line shape of planar CR from diamond at electron energies of 54.2 and 80 MeV was first studied in Ref. [Gou88]. Measured CR spectra on Si crystals could be interpreted by introducing some mean multiple-scattering angle in Ref. [Kep91]. The asymptotic behavior of CR spectra at large crystal thicknesses has been considered in Ref. [Ogn94].

The angular distribution of multiple scattering can be described by a Gaussian

$$f(\theta, z) = \frac{1}{\sqrt{2\pi}\theta_{ms}(z)} e^{-\theta^2/2\theta^2_{ms}(z)}. \tag{1.46}$$

The (rms) multiple-scattering angle of electrons in amorphous media is given by [Hig79]

$$\Theta_{ms} = (\frac{14MeV}{E_e})\sqrt{\frac{z}{L_0}}\left(1 + 0.038\ln(\frac{z}{L_0})\right) \tag{1.47}$$

where L_0 denotes the radiation length, and z is the thickness of the layer. For a randomly oriented diamond crystal, the radiation length amounts to 12.23 cm [Tsa74, Eid04]. Note that L_0 means the path length in matter after which the electron energy was diminished by a factor of 1/e due to radiation losses. The Doppler broadening of planar CR due to multiple scattering can be evaluated by [Cho99a]

$$\Gamma_{Dopp} = \gamma^2\Theta_{ms,ch}^2 E_{CR} \tag{1.48}$$

Here $\Theta_{ms,ch}^2$ is an effective mean-squared multiple-scattering angle relevant for the conditions of CR production and measurement. The mean-squared multiple-scattering angle during planar channeling is expected to be less than that determined by Eq. (1.47) because the channeled particle is transversely bound in discrete states.

To clarify the matter of investigation, let us depict the effect of multiple scattering classically. When scattering in the crystal spreads the incoming electron beam of low emittance over a solid angle $\Delta\Omega_e(z;\phi,\theta)$, where ϕ denotes the azimuth with respect to the normal of the plane and θ means the scattering angle of the electron, planar channeling proceeds in the plane $(z;\phi = \frac{\pi}{2},\theta)$. Formally, there is no limit for θ, but the CR observation angle ϑ changes with θ. In accordance with Eq. (1.45), this causes a CR energy spread $-\gamma^2\vartheta^2$. With Eq. (1.47) one can find that Θ_{ms} for thick crystals may become even larger than $1/\gamma$. On the other hand, dechanneling is connected with scattering components directed perpendicular to the channeling plane. Such components may also lead to intra-band or inter-band scattering which governs the occupation dynamics due to migration of the channeled electrons to other states. Independent on the initial population, equilibrium occupation of bound states is assumed to be reached already after several μm of traveling of the electrons through the crystal.

Avoiding any assumptions about the scattering angle θ, in the present work the effect of multiple scattering on the line shape of planar CR has for the first time been investigated consistently, i.e., only relating to experimental data measured at ELBE. The method consists in the following. If some CR

line in a measured CR spectrum is sufficiently well separated from CR lines resulting from other transitions, it is possible to determine the effective (rms) multiple-scattering angle $\Theta_{ms,ch}(z)$ by fitting an appropriate asymmetric spectral distribution function to the observed line shape.

It must be mentioned that such an ansatz has already been drawn up in Refs. [Gou88, Kep91]. Furthermore, an analytical expression was suggested in Ref. [Cho99a] but it is erroneous, and a corresponding fit procedure does not converge. In the frame of this work, the correct analytical expression for the CR line shape has been deduced [Aza06], and an interactive computer code has been established and applied for the processing of the measured CR data. The dependence of the ratio $\Theta_{ms,ch} / \Theta_{ms}$ on the crystal thickness will be investigated in the following paragraphs.

1.8.8 Line shape of CR lines

All the line-broadening mechanisms discussed above contribute simultaneously to the residual shape of a measured CR line. The δ-function characterizing the differential transition rate between channeling states [Kep91, Gen96, And83, Web95] converts to a Lorentzian representing the intrinsic CR line shape. This Lorentzian is convolved by a Gaussian-like distribution which accounts for the detector resolution, the Bloch-wave broadening and the effect of multiple scattering. Therefore, as mentioned in Ref. [Gen96], the total CR line width cannot be simply determined neither by a linear nor by a quadratic summation of the partial widths. Indeed, the widths of two convolved Lorentzians add linearly, those of two Gaussians add quadratic. The width of a Voigt profile, however, has no adequate analytical expression and can be given only.

The often used estimation of the total width Γ of a registered CR line [Cho99, Net94]

$$\Gamma^2 = \Gamma_{coh}^2 + \Gamma_L^2 + \Gamma_{Bloch}^2 + \Gamma_{\mathrm{det}}^2 + \Gamma_{beam}^2 + \Gamma_{Dopp}^2 \tag{1.49}$$

ignores these circumstances and, hence, is not accurate but only an approximation.

In the present analysis, diamond crystals of rather large thickness (42,5 ÷ 500 μm) are considered where effects due to multiple scattering are expected to considerably influence the CR line shapes and photon energies. Therefore, the registered spectral lines of (110) planar CR have been approximated by a convolution of a Lorentzian of bandwidth Γ_T with a Gaussian-like distribution with the standard deviation $\theta_{ms,ch}$ accounting for multiple scattering during channeling [cf. Gou88, Cho99a]

$$P(E_x)dE_x = \pi^{-3/2} dE_x \times \int_0^\infty \frac{t^{-1/2}(\Gamma_T / 2)(1+2\alpha^2 t)e^{-t}}{(E_x(1+2\alpha^2 t) - E_0)^2 + 0.25(1+2\alpha^2 t)^2 \Gamma_T^2} dt \tag{1.50}$$

$$\alpha^2 = \gamma^2 \theta^2_{ms,ch},$$

where E_x denotes the registered CR peak energy, and E_0 is the maximum CR photon energy obtained

at $\theta = 0$. In such a representation of the CR line shape, the involved asymmetry parameter α relates to the energy spread due to multiple scattering, which causes a peak-energy shift and an asymmetric CR line shape as well. Note that the width Γ_T in Eq. (1.50) is a fit parameter incorporating all contributions to line broadening except Doppler broadening.

1.9 Intensity of channeling radiation

1.9.1 Selection rules and matrix elements

The electric field of the atomic planes of the crystal forces dipole oscillations of the charged particles during channeling. In a quantum mechanical approach, the transition strength between the channeling states depends on the magnitude of the dipole matrix element defined by $< u_f | p_x | u_i >$. In the considered case, p_x is the transverse momentum of the electron.

As discussed above, the eigenfunctions have definite parities for $k = 0$. The symmetry of the eigenfunctions leads to the selection rules for the transition matrix element. Dipole transitions of channeled electrons are allowed between such initial and final eigenstates, the eigenfunctions of which have opposite parities. Normally, the transitions with $\Delta n = 1$ are the strongest ones. Transitions with $\Delta n \geq 3$ are usually weak, but they may be observed in measured spectra.

The eigenfunctions normalized to one interval of planes read

$$u_i(x) = \frac{1}{\sqrt{d_p}} e^{ikx} \sum_{n=-m}^{m} c_n^i e^{ingx} \tag{1.51}$$

where c_n^i are components of column vectors in the matrix satisfying the condition

$$\sum_{n=-m}^{m} (c_n^i)^* c_n^i = 1 , \tag{1.52}$$

and $2m+1$ is the number of Bloch waves. In the framework of the many-beam formalism, the matrix elements read

$$\left\langle u_f | p_x | u_i \right\rangle = -i\hbar \int_{-d_p/2}^{d_p/2} u_f(x) \frac{d}{dx} u_i(x) dx = (2\pi\hbar / d_p) \sum_n (c_n^f)^* c_n^i (ng + k). \tag{1.53}$$

The eigenfunctions of low lying channeling states the (110) plane of diamond are shown in Fig. 1.8 for 14.6 MeV electrons. As can be seen, the ground state with $n = 0$ has even parity, the state with $n = 1$ has odd parity etc.

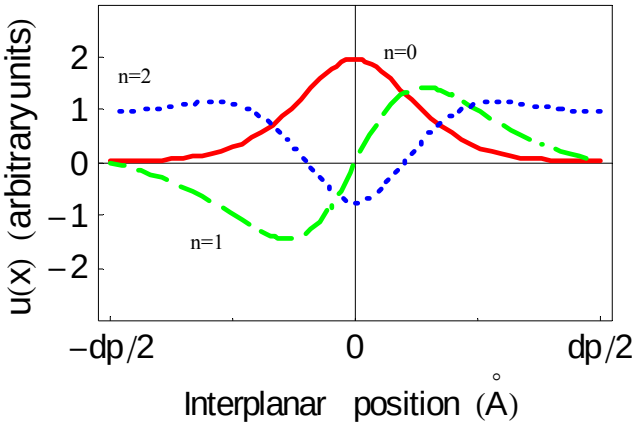

Fig. 1. 8 Eigenfunctions of low lying states in the potential of the (110) plane of diamond for 14.6 MeV electrons at k=0.

1.9.2 Population of channeling states

Channeling occurs if the electrons are incident to the crystal under a small angle θ_0 with respect to a crystal plane. The critical angle θ_c obtained from the equation $\frac{1}{2} pv\theta_c^2 = |V_{\max}(x)|$ reads

$$\theta_c = \sqrt{\frac{2\gamma |V_{\max}|}{mc^2(\gamma^2 - 1)}}. \tag{1.54}$$

For $\theta_0 > \theta_c$ the transverse energy of the electron is too large to be captured by the planar potential. Such particles cannot populate bound channeling states but are scattered into the continuum. It is convenient that states near the top of the potential are called quasi-free.

Obviously, CR can only occur if transverse eigenstates of the continuum potential were populated. This means that the incident plane wave (of the electron) must at the crystal surface match with eigenfunctions of the planar continuum potential. Hence, the initial population $P_j(\theta)$ of transverse

states j is determined by the overlap of these eigenfunctions with the incident plane wave [And83, Tul81]

$$P_j(\theta) = \left|\left\langle u_{j,k}(x)\middle|\exp(ik_x x)\right\rangle\right|^2 = \frac{1}{dp}\left|\int_{-d_p/2}^{d_p/2} dx u_i(x)\exp(ip\theta_0 x/\hbar)\right|^2 = \left|\frac{2\pi}{\sqrt{d_p}}\sum_n c_n^j(k)\delta_{k_x,k+ng}\right|^2, \quad (1.55)$$

where k is the crystal momentum, p is the momentum of the incident electron, $k_x = p\theta_0/\hbar$ is the transverse momentum of the incident electron, and θ_0 is the angle of incidence relative to the plane. As can be seen from Eq. (1.55), the matrix element differs from zero only if the condition $p\theta_0/\hbar = k + ng$ is fulfilled. Note that the integral of the initial population over θ is twice the Bragg angle $\theta_{brag} = \pi\hbar c/E_e d_p$.

The initial population of bound and quasi-free states drawn versus the angle of a 14.6 MeV electron incident to a diamond crystal nearly along the (110) plane is shown in Figs. 1.9a and 1.9b. The same is shown in Fig. 1.10 for 30 MeV electrons. It can be seen that electrons incident exactly at $\theta = 0$ may populate states with even quantum number n only. The population probability varies remarkably with θ. For incidence angles larger than the critical angle θ_c, the population of bound states is substantially reduced, and the population of quasi-free and free states increases. According to Eq. (1.54), the critical angles for channeling along the (110) plane of diamond and for the electron energies of 14.6 and 30 MeV amount to 2.25 and 1.57 mrad, respectively, and are indicated by arrows in Figs. 1.9a and 1.10.

In order to maximum populate the channeling state $n = 1$ in the (110) plane of diamond, which represents the initial state of the strongest transition 1→0 with CR emission, the electron beam must enter the crystal close to incidence angles of 0.7 mrad and 0.42 mrad at electron energies of 14.6 and 30 MeV, respectively.

Since a real electron beam has a nonzero beam divergence σ_θ, it must be taken into account in a many-beam calculation. Assuming a Gaussian distribution of the incidence angle centered at θ_0

$$f(\theta) = \frac{1}{\sqrt{2\pi}\sigma_\theta}\exp(-(\theta-\theta_0)^2/2\sigma_\theta^2) \quad (1.56)$$

the initial population $P_j(\theta)$ has to be average over $f(\theta)$.

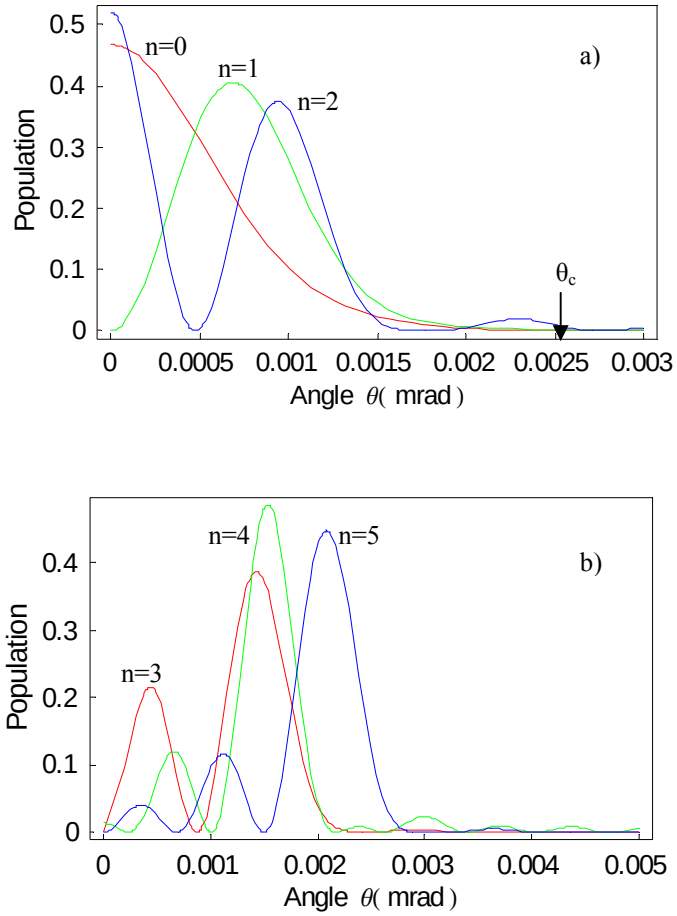

Fig. 1.9 Initial population of bound states (a) and quasi-free states (b) in the (110) plane of diamond drawn versus the incidence angle of 14.6 MeV electrons.

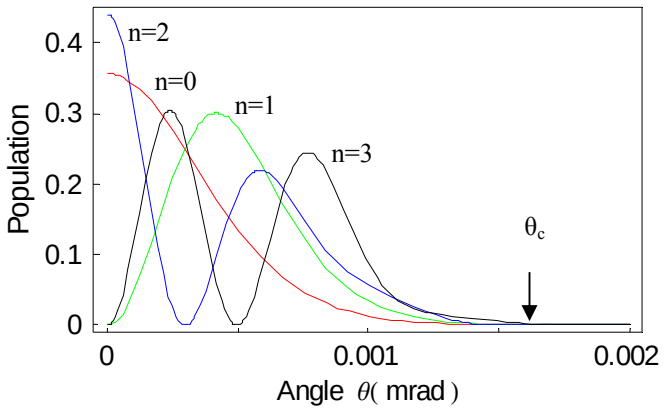

Fig. 1.10 The same as shown in Fig. 1.9a but for 30 MeV electrons.

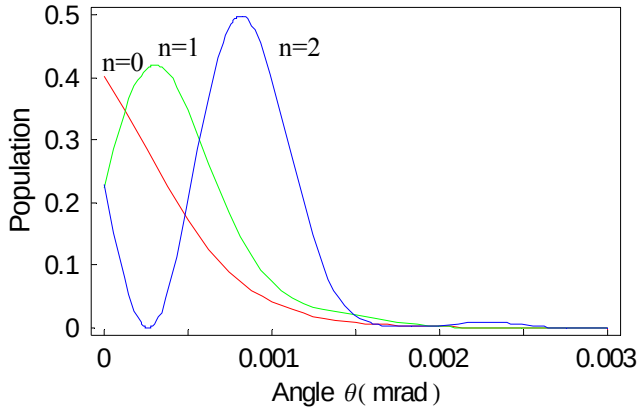

Fig. 1.11 Initial population of bound states in the (110) plane of diamond drawn versus the incidence angle θ of a 14.6 MeV electron beam at a beam divergence of 0.3 mrad.

The variation of the initial populations of bound states with the incidence angle for an electron beam of energy 14.6 MeV and with an angular divergence of 0.3 mrad is shown in Fig. 1.11. The comparison of Fig. 1.9a with Fig. 1.11 reveals that odd states are also populated at this given beam divergence just for $\theta_0 = 0$, and odd-even transitions with CR emission may occur.

The formula for the spectral density of CR has been derived from the dipole approximation to radiation emission. The spectral-angular density of planar CR per unit of crystal thickness dz, per unit of photon energy $dE\gamma$, per unit of solid angle $d\Omega$, and per electron [And81] reads

$$\frac{d^3 N_{CR}(i \to f)}{dz dE_\gamma d\Omega_\gamma} = \frac{\alpha \lambda_c^{\,2}}{\pi \hbar c} \frac{E_\gamma}{2\gamma^2 (1 - \beta \cos\theta)} \left| < u_f \left| p_x / \hbar \right| u_i > \right|^2 \times \delta\left(E_\gamma - \frac{E_i - E_f}{1 - \beta \cos\theta} \right) \times \left(\sin^2 \varphi + \cos^2 \varphi \frac{(\beta - \cos\theta)^2}{(1 - \beta \cos\theta)^2} \right) P_i(z) \tag{1.57}$$

where λ_c is the Compton wave length, and $P_i(z)$ is the occupation function of the state i at the crystal depth z. The angles θ and φ are the polar and azimuth angles of the emitted CR photons with respect to the direction of the incoming electron beam. It follows from Eq. (1.57) that the energy of the CR photons is given by the Doppler formula

$$E_{i \to f} = \frac{E_i - E_f}{1 - \beta \cos\theta} \tag{1.58}$$

By expanding β in terms of γ and $\cos\theta$ into a Taylor series one finds, that the maximum CR photon

energy observed in forward direction at $\theta = 0$ is approximately $2\gamma^2$ ($E_i - E_f$).

Taking the non-zero intrinsic CR line width (see § 1.8) into account, the δ-function in Eq. (1.57) has to be substituted by a Lorentzian. Multiple scattering has been involved by the convolution of this Lorentzian with a Gaussian given by Eq. (1.46). If CR is registered at zero degree within a narrow aperture $\Delta\vartheta \ll \gamma^{-1}$, one can set $\vartheta \cong \theta$, and with the commonly used approximation $\frac{1}{1-\beta\cos\theta} \cong \frac{2\gamma^2}{1+\gamma^2\theta^2}$ one finally obtains

$$\frac{d^2N_{CR}(i\to f)}{d\Omega_\gamma dE_\gamma} = \frac{\alpha\lambda_c^2}{\pi\hbar c} 2\gamma^2 (E_i - E_f) \left| \left\langle \psi_f \left| \frac{d}{dx} \right| \psi_i \right\rangle \right|^2 \int_0^L dz e^{-\mu_{(E_\gamma)}(L-z)} P_i(z) \times \pi^{-3/2} \int_0^\infty \frac{t^{-1/2}(\Gamma_T/2)(1+2\alpha^2 t)e^{-t}}{(E_\gamma(1+2\alpha^2 t) - E_0)^2 + 0.25(1+2\alpha^2 t)^2\Gamma_T^2} dt \quad . \tag{1.59}$$

Note that the first integral in Eq. (1.59) refers to the occupation of the state *i* over a chosen crystal thickness *L*, and the second one describes the shape of the registered CR line. The exponential factor in the first integral of Eq. (1.59) accounts for self absorption of CR photons in the crystal, and $\mu(E_\gamma)$ denotes the absorption coefficient of X-rays with energy E_γ.

The number of CR photons from the transition $i \to f$ is obtained by integration over the photon energy range related to the residual CR line shape

$$\frac{dN_{CR}(i\to f)}{d\Omega} = \int_{line} \frac{d^2N_{CR}(i\to f)}{d\Omega dE_\gamma} dE_\gamma \, . \tag{1.60}$$

This equation gives the CR photon yield per sr and per electron.

According to equation (1.59), the intensity of a CR line is proportional to the integral over $P_i(z)$. The occupation $P_i(z)$ of a channeling state *i* at the crystal depth *z* depends on the initial population, which is a function of the beam divergence and of the entrance angle of the beam into the crystal as well. Furthermore, $P_i(z)$ depends on various scattering processes during channeling, which may populate as well as depopulate the state under consideration. This population dynamics has been described by Anderson [And83] using a series of coupled differential equations

$$\frac{dP_n}{dz} = \sum_{n'} T_{n',n}(P_{n'} - P_n) \tag{1.61}$$

where $T_{n,n'}$ denotes the transition rate per unit length for a transition between states n and n', and the sum is taken over all bound, quasi-free and free states. Considering thermal scattering as the dominating process, the transition rate $T_{n,n'}$ reads

$$T_{n',n} = T_{n,n'} = \frac{2}{\hbar v}\left|\langle u_{n'}|W|u_n\rangle\right| \tag{1.62}$$

where v is the velocity of the electron, and W is the imaginary part of the complex potential given by Eq. (1.38) [And83, Cho99]. For a small interval of crystal depth δz, the occupation of the state n can be approximated by a Taylor series

$$P_n(z+\delta z) \cong P_n(z) + \delta z \frac{dP_n(z)}{dz} = P_n(z) + \delta z \times \sum_{n'} T_{n',n}(P_{n'}(z) - P_n(z)). \tag{1.63}$$

The term $T_{n,n'}P_{n'}(z)$ in Eq. (1.63) describes the feeding of state n, and the term $T_{n,n'}P_n(z)$ describes the depopulation of state n respective the feeding to other states.

The depth dependence of the occupation $P_n(z)$ of bound and quasi-free states determined for δz = 0.01 μm at an electron energy 14.6 MeV is shown in Figs. 1.12a and 1.12b, where an zero incidence angle of the electron beam has been assumed, and the beam divergence amounts to zero and σ_{beam} = 0.3 mrad, respectively. These figures demonstrate that

(i) at σ_{beam} = 0 only even states are populated at the crystal surface,

(ii) at σ_{beam} = 0.3 mrad several odd states are also populated although θ_0 = 0,

(iii) with increasing penetration depth of the electrons into the crystal, bound states are depopulated and quasi-free states are fed by interband scattering,

(iv) at a depth of about 8 μm, statistical equilibrium of occupation of states is reached,

(v) due to the selection rules for radiative transitions, no transition will be observed for σ_{beam} = 0 as well as for σ_{beam} = 0.3 mrad (i.e., the CR emission will be extremely weak).

The variation of the population of bound and quasi-free states for 14.6 MeV electrons incident at an angle of θ_{in} = 0.69 mrad (there the initial population of the state n = 1 reaches its maximum) is illustrated in Figs 1.13a and 1.13b for σ_{beam} = 0 and σ_{beam} = 0.3 mrad, respectively. As one can see, in these cases the odd states are also populated and, therefore, CR from the transitions 1→0 and 2→1 will be observed.

With an electron beam of small angular divergence, the variation of the population of different states with the incidence angle should be measurable by scanning θ_{in} with respect to the plane considered, but only if a sufficiently thin crystal is used. The latter condition is necessary because equilibrium occupation of states is reached within a relatively small penetration depth (as seen in Figs. 1.13a and 1.13a). Hence, measurements of CR on thicker crystals are insensitive to such variation. Otherwise, a

large beam divergence also leads to nearly equilibrium occupation of channeling states at the surface of the crystal. According to Eq. (1.61), this occupation is stable over the crystal depth.

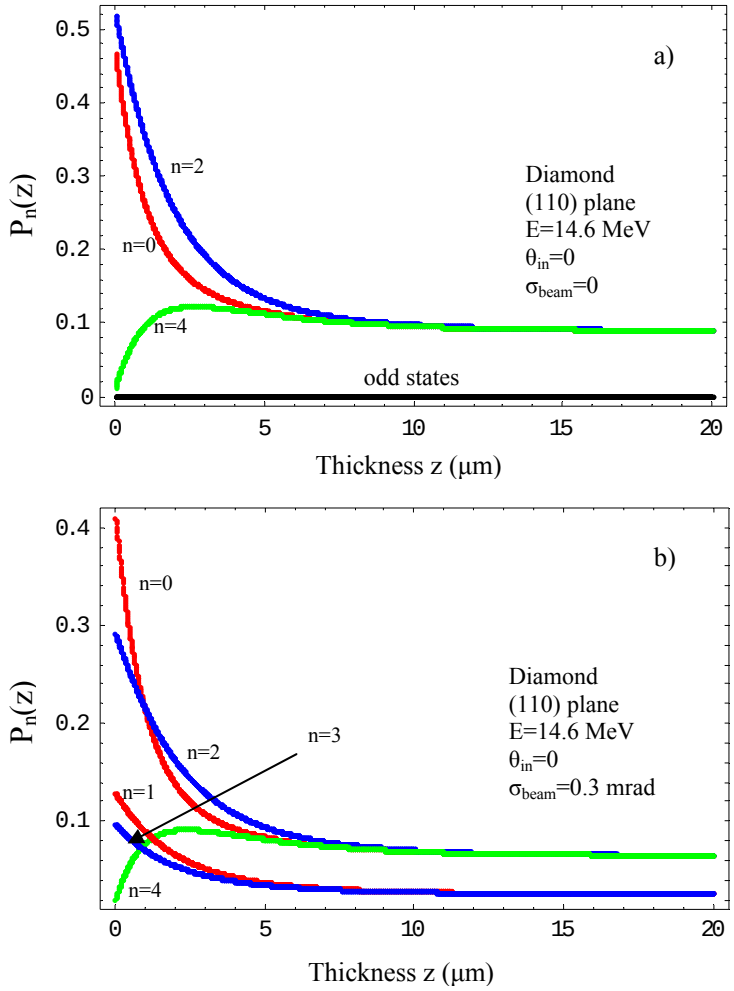

Fig. 1.12 Depth dependence of the occupation of states drawn versus the crystal thickness for 14.6 MeV electrons at zero incidence angle and zero beam divergence (a) and for a beam divergence of 0.3 mrad (b).

Finally, at fixed crystal thickness, the total CR photon yield can be obtained by integration of the occupation function over the entire crystal thickness. In order to illustrate the variation of the CR photon yield with the crystal thickness, a numerical integration has been performed for the 1→0 transition at the electron energy of 14.6 MeV. The result is shown in Fig. 1.14.

It is obvious that there are different dependences of the CR photon yield at small and large crystal thicknesses. It is hard to find an analytical function valid for a wide interval of crystal thickness, but for thin crystals both $p_n(z) = e^{-\lambda z}$ and $p_n(z) = z^{-1/2}$ can be considered as approximate solutions of Eq. (1.61) which allow reasonable fits to the experimental data.

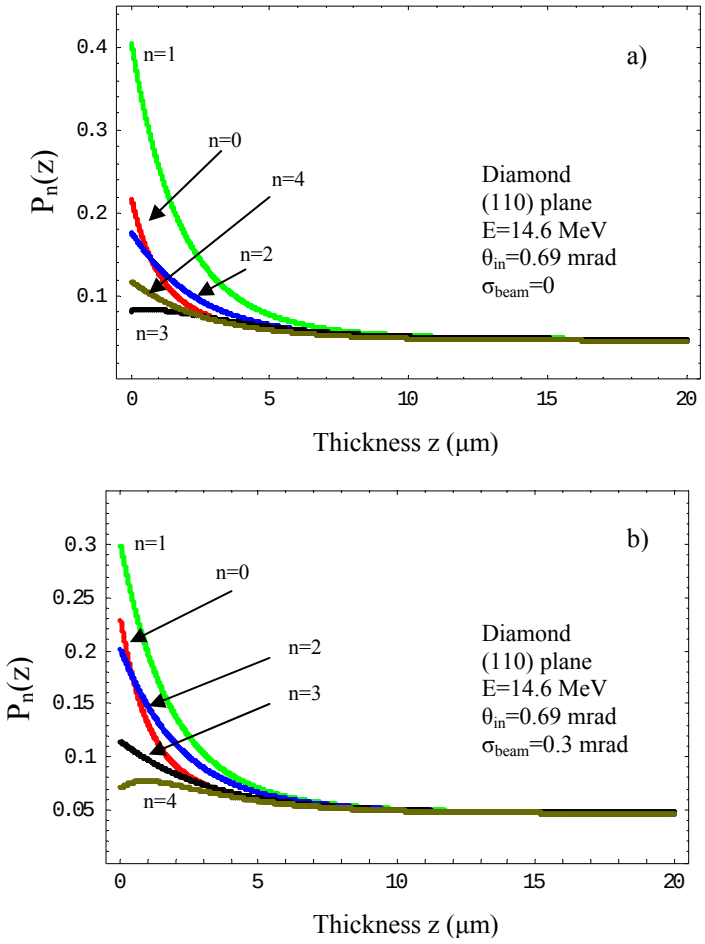

Fig. 1.13 Depth dependence of the occupation of states drawn versus the crystal thickness for 14.6 MeV electrons at an incidence angle of 0.69 mrad for zero beam divergence (a) and for a beam divergence of 0.3 mrad (b).

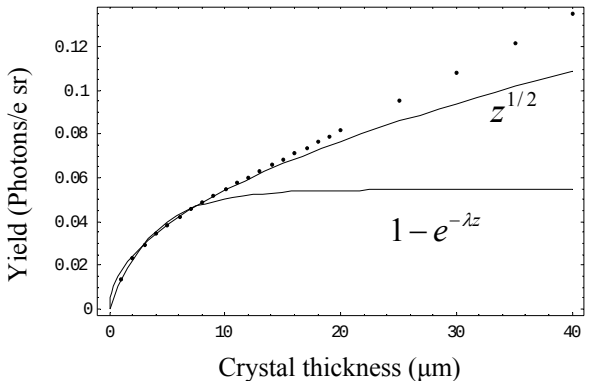

Fig. 1.14 Total CR photon yield from the 1→0 transition of 14.6 MeV electrons channeled in the (110) plane of diamond drawn versus the crystal thickness.

The experimental data obtained in Ref. [Kep89] for 17 MeV electrons channeled in Si crystals have been fitted to an integrated exponential as well as to a square-root function. The largely spread data did, however, not allow to distinguish between them, possibly because the beam divergence was too large. The data measured in Ref. [Kep91] for Si crystal thicknesses less than 500 μm at electron energies of 52.2 and 82.23 MeV can be approximated by an integrated exponential function.

The experimental results of Genz [Gen96] obtained for diamond crystals of thicknesses between 13 and 55 μm can also be fitted by an integrated exponential function, but recent measurements performed on a 200 μm thick diamond crystal [Rei99] did not merge with earlier measurements and, despite an empirically determined scaling factor of 3.45, could be interpreted only by a square-root-fit, which has been explained by the influence of multiple scattering.

From these works one can conclude, that the choice of one of the expressions given in Fig. 1.14 for the CR photon yield is connected with the interval of crystal thickness considered, where the initial population of bound states is influenced by the divergence of the electron beam. At small crystal thickness, the experimental data satisfy both expressions, but over a broader interval of crystal thickness the square-root function should be applied.

Note that only thermal scattering has been considered up to now. Although this is the main scattering process for thin crystals, at larger crystal thickness multiple scattering becomes important. As found above, equilibrium occupation is reached after a small penetration depth, but this does not mean that it holds over the entire crystal thickness because the channeled particles will be dechanneled, i.e., they will be scattered into the continuum and leave the channeling regime. Andersen already mentioned that for electrons of MeV energies the statistical equilibrium between channeling states and free states is quickly established [And83]. The depth dependence of the occupation of the low number of channeling states then may be obtained from random multiple scattering only, since a major fraction of beam particles populates states in the continuum where electron scattering dominates. In this case, it can be shown that the occupation of channeling states at the crystal depth z is proportional to $z^{-1/2}$.

In preparation of an application of CR as a tunable quasi-monochromatic X-ray source at ELBE, a series of CR measurements has been performed at electron energies between 14.6 and 34 MeV using diamond crystals of thicknesses between 42.5 and 500 μm. These experiments will be described in the following chapter. Simulations of the expected CR spectra have been carried out applying the mathematical instrument of the CR theory developed in the frame of this work.

For illustration, CR spectra calculated by means of Eq. (1.59) for channeling in the (110) plane of a 42.5 μm thick diamond crystal are shown in Figs. 1.15 and 1.16.

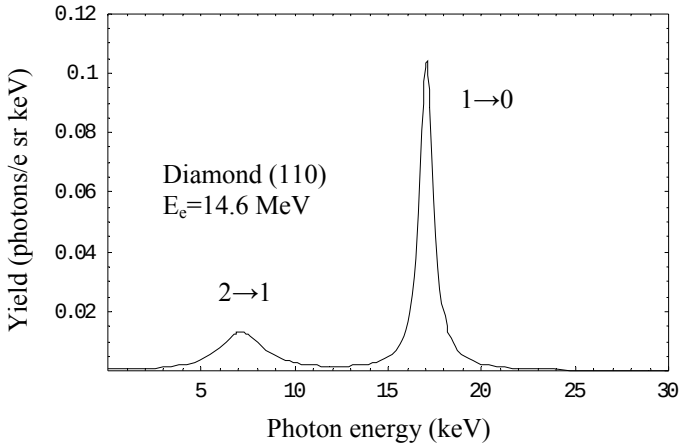

Fig. 1.15 Simulation of the CR spectrum for channeling of 14.6 MeV electrons in the (110) plane of a 42.5 μm thick diamond crystal.

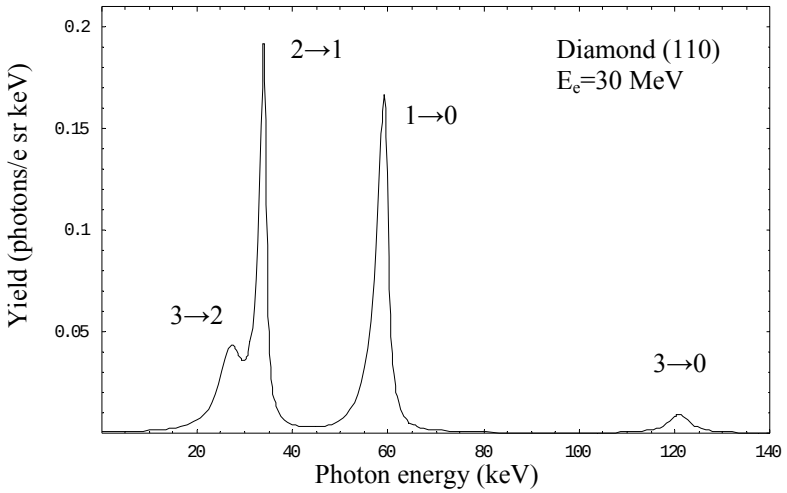

Fig. 1.16 Simulation of the CR spectrum for channeling of 30 MeV electrons in the (110) plane of a 42.5 μm thick diamond crystal.

1.10 Application

At some application of CR as an X-ray source, it is advantageous to use scaling laws which allow extrapolations of important parameters of CR such as, e.g., the CR photon energy, the CR line width or the CR photon yield to other electron beam energies.

As can be seen in Table 1.4, there is no explicit dependence of the coherence length on the electron energy, but according to Eq. (1.35) Γ_{coh} is proportional to γ^2. The number of bound states increases with increasing electron energy, but discrete states at planar channeling are only observed at electron energies up to about 100 MeV. The reason is that the spacing between the transverse energy levels in

the continuum potential decreases with increasing particle energy due to the relativistic mass $m\gamma$ contained in the Hamiltonian [see Eq. (1.11)]. As it is well known, the frequency of transverse oscillations of a channeled electron in its rest system is given by $\omega = \sqrt{k/M}$ for a harmonic potential. Due to $M = m\gamma$ its transverse energy $\hbar\omega$ is proportional to $\gamma^{-1/2}$. Therefore, the maximum CR photon energy observed at $\theta = 0$ scales such as $\sim\gamma^{3/2}$ [cf. Eq. (1.32)]. As a consequence, the relative CR line width, i. e., Γ/E_0 theoretically scales with the electron energy such as $\sim\gamma^{1/2}$, and the CR photon rate such as $\sim\gamma^{5/2}$.

The energy of the 1→0 transition at planar channeling along the (110) plane of diamond, calculated by means of the many-beam formalism, and the corresponding CR photon yield for a crystal thickness of 5 μm, however, scale with the electron energy such as $\sim\gamma^{1.73}$ (Fig. 1.17) and $\sim\gamma^{1.92}$ (Fig. 1.18), respectively, because the continuum potential of this plane is by far no harmonic one.

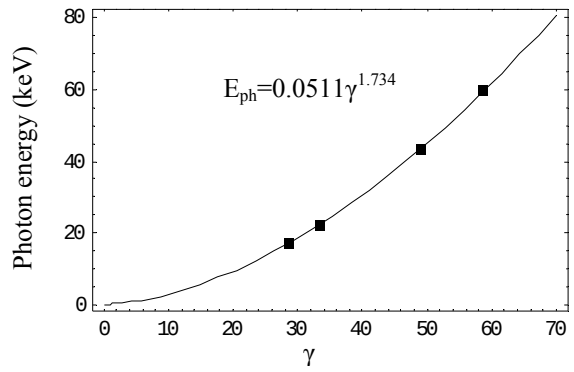

Fig. 1.17 Calculated CR photon energy for the 1→0 transition of electrons channeled in the (110) plane of diamond as a function of the electron energy (given in units of γ).

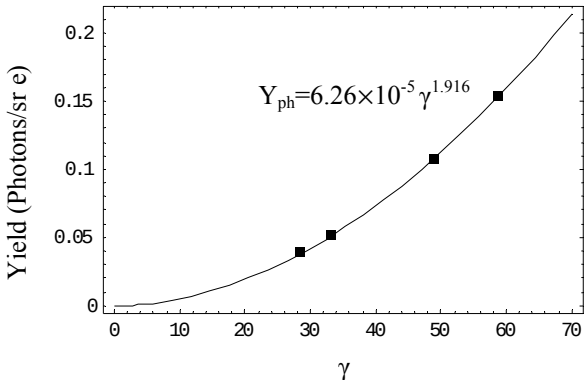

Fig. 1.18 Calculated CR photon yield for the 1→0 transition of electrons channeled in the (110) plane of a 5 μm thick diamond crystal as a function of the electron energy (given in units of γ).

The crystal thickness which is effective for CR production at channeling is limited due to the action of different scattering processes. As discussed above, thermal scattering is the main process for thin

crystals. Multiple scattering increasingly influences the occupation of transversely bound states in thicker crystals. Therefore, the equilibrium occupation becomes instable at larger crystal depth, and the CR photon yield follows a square-root function.

1.11 Summary

In this chapter, a detailed theoretical description of planar channeling for electron energies less than 100 MeV has been presented. Transverse transition energies of channeled electrons have been calculated numerically applying the many-beam formalism with the thermally averaged Doyle-Turner potential.

Processes which contribute to the broadening of the CR lines were investigated. Intrinsic CR line widths have been calculated using the method of the complex optical potential, which describes the incoherent scattering of channeled particles on the thermally vibrating crystal atoms. The influence of multiple scattering on the spectral distribution of CR, resulting in both a CR peak-energy shift towards smaller energy and an asymmetric CR line shape, could be successfully simulated by the convolution of the intrinsic Lorentzian CR line shape with a Gaussian-like distribution accounting for electron multiple scattering during channeling.

The variation of the occupation of channeling states with the penetration depth of the electrons into the crystal has been calculated for different incidence angles as well as angular divergences of the incoming electron beam.

Applying the developed mathematical instrument, CR spectra for the measurements at ELBE could be simulated for electron energies between 14.6 and 34 MeV and for thicknesses of the used diamond crystals between 42.5 and 500 μm.

Scaling laws for the dependence of important CR parameters on the electron beam energy have been deduced from theoretical calculations.

Chapter 2

Measurements of channeling radiation at ELBE

The realization of an intense quasi-monochromatic CR X-ray source requires an electron beam of high quality. The new generation of relatively compact superconducting electron accelerators such as ELBE, which are able to deliver brilliant electron beams, i.e., beams of high average current at low emittance, make allowance for this demand. In order to accomplish a CR source aimed at its application in biophysics research, a setup for preceding measurements of CR has been established at the electron beam of ELBE in 2003.

Although CR is a well-investigated phenomenon, specific features such as, e.g., the CR line width or the dependence of the CR yield on the crystal thickness were poorly known. Since diamond has earlier been found to be the most suitable single crystal for intense CR production [Gar91], diamond type IIa crystals of different thickness were used in the experiments. After a brief description of the radiation source ELBE [Elb06] and of the experimental setup for CR measurement, the following paragraphs give main attention to the method of CR data processing [Wag04, Wag05] and to the comparison of experimental data with the results of theoretical calculations presented in chapter 1 of this work.

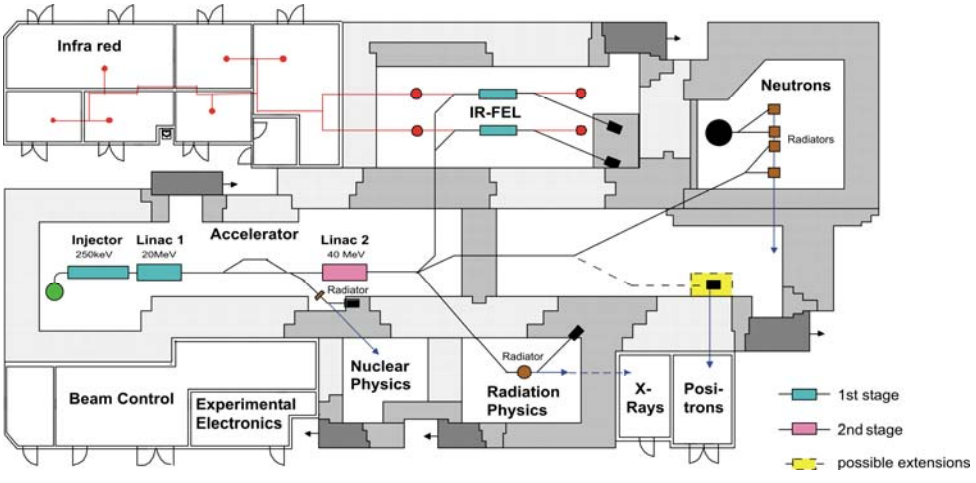

Fig. 2.1 Floor scheme of the radiation source ELBE.

2.1 Radiation source ELBE

The radiation source ELBE bases on a superconducting linear electron accelerator which operates at a frequency of 1.3 GHz and delivers beams with micropulse repetition rates of 260 (cw), 26 and 13 MHz. The beam energy can be set between about 6 and 35 MeV at a maximum average beam current of about 1 mA. The arrangement of the ELBE facility with the experiment areas is schematically shown in Fig. 2.1.

The accelerator consists of a pulsed thermionic DC electron gun, an injector stage pre-accelerating the electrons to 250 keV, two RF bunching sections forming micropulses of about 2 ps duration and four superconducting RF cavities operating at a temperature of 1.2 K. Via a switching magnet which controls the beam energy, the beam can be provided through different electron beam lines to the experiment caves, where it mainly serves for the production of secondary radiation such as bremsstrahlung (BS), X-rays, FIR radiation from a free-electron laser, neutrons and positrons.

In the radiation physics cave, where the setup for CR production is situated, the maximum available beam current is restricted to 200 μA for the reason of radiation protection. The limitation of the average current can be managed by introducing diaphragms of different aperture into the injector beam line. This method has the advantage that the transverse emittance of the electron beam can be diminished to values of about 3 π mm mrad (rms) at a beam divergence of the order of 0.1 mrad, a main requirement for an effective CR generation. The beam-energy spread amounts to 1.3×10^{-3}, and the beam energy can be tuned with an accuracy of about 200 keV.

2.2 Setup for CR measurement

After deflection of the electron beam from the accelerator hall into the radiation physics cave, it passes the UHV vacuum chamber positioned in a straight part of the beam line between the dipole magnets 1 and 2 (see Fig. 2.2). This chamber houses a 3-axes goniometer [Wag05b] used for the precise alignment of the diamond crystals with respect to the electron beam. After traversing the crystal target, the electron beam is deflected by the dipole magnet 2 into the beam dump.

Directly behind the crystal target, a secondary emission monitor (SEM) and a small Faraday cup can be moved into the beam line. The construction and operation of these devices which are applied for the accurate measurement of the beam current through the target are described in detail in Ref. [Neu07]. The method of beam transmission monitoring in a short geometry seems to be more suitable than the measurement of the beam transmission through the target into the beam dump, because the latter method is rather sensitive with respect to a stable beam setting. It should be mentioned that the transmission of the electron beam into the beam dump is incomplete due to electron scattering in the

target material. Especially for target thicknesses of several hundreds of µm, the transmission is reduced to only several percent.

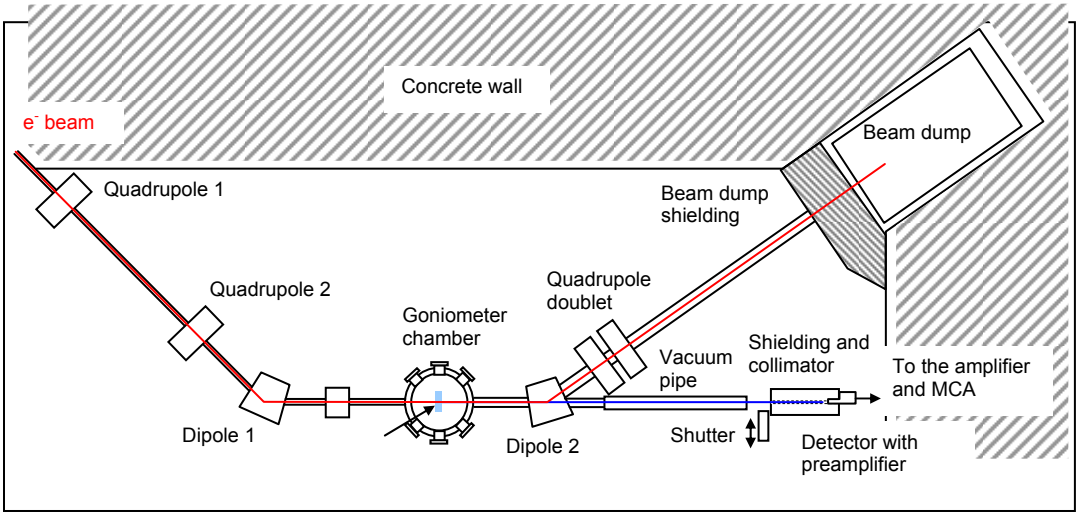

Fig. 2.2 Scheme of the radiation physic cave at ELBE.

The CR and BS generated in the crystal and emitted in direction of the passing electron beam has to penetrate a thin Be window (127 µm), which separates the UHV beam line from an auxiliary vacuum tube evacuated to 1.5 mbar. After traversing about 45 cm of air, the radiation is registered by an X-ray spectrometer. The materials positioned in the path between target and detector limit the lower registration threshold to about 5 keV. A massive Pb collimator with an entrance aperture of only 1 mm shields the detector from intense direct and background radiation and defines the solid angle for radiation measurement to 7.2×10^{-8} sr.

2.3 X-ray detectors

The CR as well as the accompanying BS has been registered by means of different solid state detectors. Silicon-PIN diodes of dimension 2.4×2.8 mm^2 (Amptek XR-100T) and cadmium telluride (CdTe) detectors of dimension 3×3 mm^2 (Amptek XR 100T-CdTe) have been used [Amp07]. Their different sensitive thicknesses (300 µm and 1 mm, respectively) defined the dynamic range for X-ray registration. Since the detectors are equipped with thin Be entrance windows (25 µm and 250 µm, respectively), the registration threshold also depends on the detector type, and radiation absorption in these windows has also to be taken into account.

X-rays incident to the detector interact with the Si, Cd and Te atoms via the photoelectric effect or via Compton scattering creating in the average one electron/hole pair per energy loss of 3.62 eV or 4.43 eV, respectively. Since the charge collection for events proceeding near to the rear contact of the

detector is more slowly than for events in the bulk material, false peaks and an additional background can occur in the measured spectrum. Since these events are characterized by a slower pulse rise-time, they can be excluded by activation of a rise-time-discrimination (RTD) circuit incorporated in the commercial preamplifier.

The most important properties of the detectors with respect to radiation measurement are their energy resolution and registration efficiency. ^{241}Am, ^{55}Fe, ^{133}Ba, and ^{210}Pb photon sources have been applied for the energy calibration of the detectors. The full width at half maximum (FWMH) of the Si-PIN diode amounted to (470±2) eV for the 13.93 keV line of ^{241}Am.

The registration efficiency can be estimated by accounting (i) for the probability of photon transmission through the Be window and (ii) for the probability of interaction with the detector material. The product of these probabilities reads

$$p = \exp(-\mu_{Be} t_{Be})[1 - \exp(-\mu_{\mathrm{det}} t_{\mathrm{det}})] \qquad (2.1)$$

where μ_{Be} and μ_{det} are the total attenuation coefficients of Be and of the detector material, respectively. The corresponding registration efficiencies as a function of the photon energy [Amp07] are shown in Fig. 2.3.

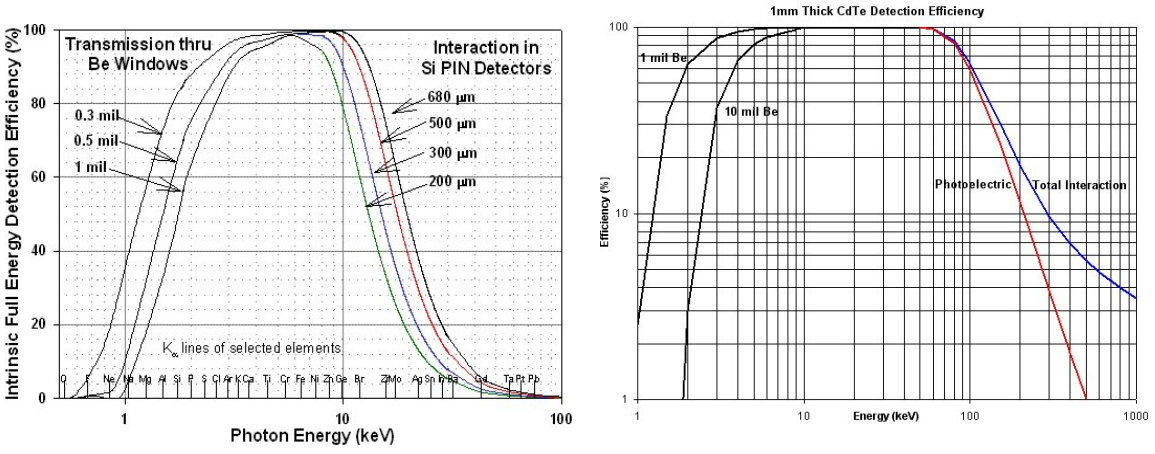

Fig. 2.3 Plots of the registration efficiency as a function of the photon energy for the Si-PIN diode (left panel) and for the CdTe detector (right panel).

At operation of the CdTe detector in the RTD regime, its registration efficiency was found to be significantly lower than expected for its dimensions (see Fig. 2.4). Since the effective thickness of the detector depends upon its charge transport properties and of the RTD setting, RTD has not been used for this 1 mm thick detector.

To explain the curves shown in Fig. 2.4, the following consideration is worthwhile. Usually, the registration efficiency of a detector is determined by the use of calibrated radiation sources in a well defined geometry. Since for the CR measurements the actual efficiency within an energy range of $0 \div 100$ keV is of interest, another method has been applied.

It is well known that for photon energies less than mc^2 the differential BS cross-section in forward direction is reciprocally proportional to the photon energy [Jac75]. Therefore, a channel-by-channel multiplication of some measured and energy-calibrated BS spectrum with the corresponding energy values, should result in a flat distribution. Each deviation from such a flat distribution points to a reduced registration efficiency, which may be caused by different processes such as, e.g., radiation absorption on the path from the source to the detector, nonlinearities of photon detection or incomplete energy absorption in the detector material. In the present measurement geometry (see Fig. 2.2), attenuation of low-energy photons occurs due to absorption in the crystal depth, in the Be window of the beam line, in the foil separating the auxiliary vacuum tube from atmosphere, along the path through air to the detector, and in the Be window of the detector. As already mentioned, absorption in these materials defines the lower registration threshold, but it also modifies the actual registration efficiency up to photon energies of about 10 keV due to a reduced radiation transmission. Otherwise, the diminished efficiency at higher photon energies is mainly connected with the finite detector thickness.

The total registration efficiency for the given experimental setup has been calculated in accordance with Eq. (2.1) and is drawn in Fig. 2.4 as a full line. The measured BS spectra, multiplied with the corresponding photon energy and scaled to the calculated curves, are also shown in Fig 2.4 for both detectors used. Note that two peculiarities can be realized. In the upper panel corresponding to the Si-PIN diode, additional photon peaks occur in the measured spectrum due to fluorescence from the Ag contacts of the diode. In the lower panel corresponding to the CdTe detector, deviations of the energy-multiplied BS spectra from the calculated one occur at the K-absorption edges of the detector materials Cd and Te.

For the CdTe detector, the registration efficiency is given with and without RTD. The observed difference between the two measurement regimes has also been proven by the use of a ^{241}Am source. The ratios of the counting rates registered in the RTD “off” and RTD “on” regime at the photon peak energies 17.67 keV, 26.34 keV and 59.54 keV of ^{241}Am were found to be 0.75, 0.62 and 0.54, respectively. Obviously, the difference is larger at higher photon energy what points to a reduced effective depth of this detector in the RTD regime.

Uncertainties of the effective depth of the used detectors needed an independent method for the more exact determination of this depth. Otherwise the calculation of the registration efficiency would fail. In the absence of calibrated sources, a single photon source which emits two lines of X-rays with a well known intensity ratio can be used. If these photon energies are large enough to avoid attenuation in the

Be window of the detector, the ratio of the counting rates should be

$$\frac{N_1}{N_2} = \frac{P_1(1-e^{-\mu_1 t})}{P_2(1-e^{-\mu_2 t})} \tag{2.2}$$

where P_1 and P_2 are the emission probabilities of the two lines, and μ_1 and μ_2 are the linear attenuation coefficients at the corresponding photon energies. The solution t of Eq. (2.2) is the effective detector thickness.

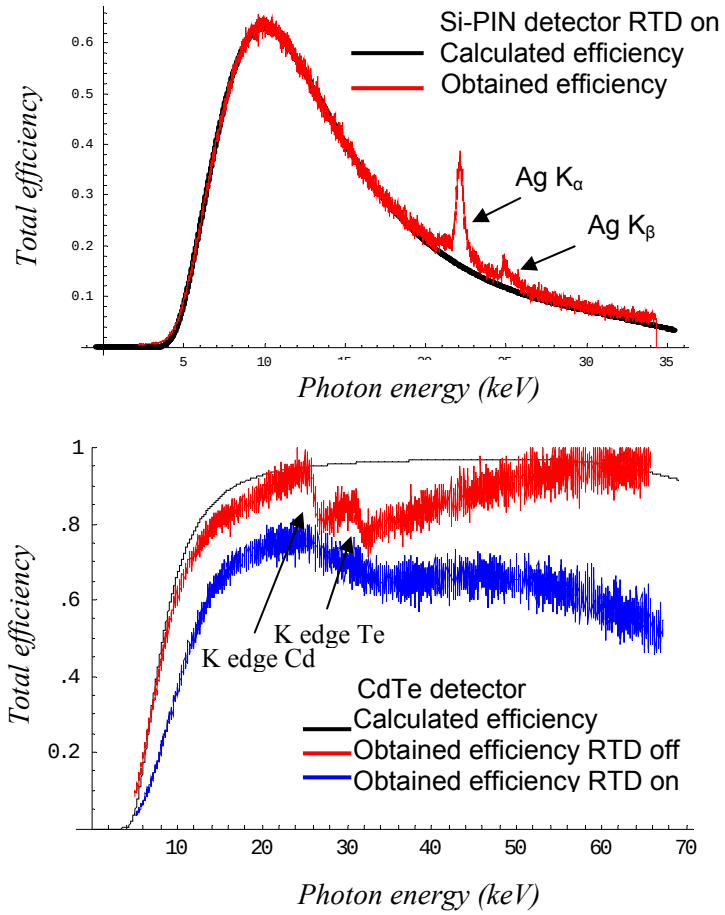

Fig. 2.4 Calculated total registration efficiencies (full lines) and efficiencies obtained from the energy-multiplied bremsstrahlung spectra. Upper panel: Si-PIN diode. Lower panel: CdTe detector in two operation regimes.

Equation (2.2) has also been applied for the determination of the effective depth of the Si-PIN diode using a ^{241}Am source. A value of 275 μm was found instead of 300 μm reported by the producer.

2.4 Diamond crystals

All diamond crystals utilized in the experiments are of type IIa and were cut normal to the [110] axis (x-cut). The crystal thicknesses measured by means of a submicron stylus profiler (VEECO DEKTAK 8) amount to (42.5 ± 4.0) µm, (102.2 ± 4.7) µm, (168 ± 3.9) µm and (500 ± 25) µm. The miscut angle and the orientation of the reciprocal lattice vectors of main crystal planes have been determined in previous X-ray diffraction measurements.

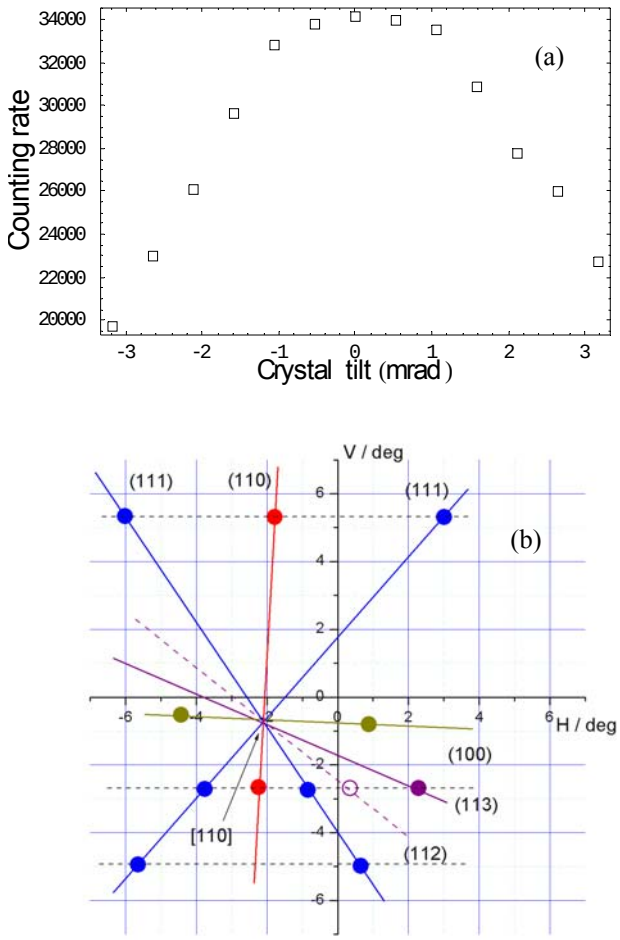

Fig. 2.5 Tilt-angle scan of a 42.5 µm thick diamond crystal registered near the (110) plane at an electron energy of 14.6 MeV (a). Crystal map constructed from a series of angular scans and the corresponding crystal planes (b). V and H denote the rotation and tilt angle in goniometer coordinates, respectively.

The exact alignment of the crystal with respect to the direction of the electron beam is achieved by means of angular scans. The crystal mounted to the goniometer is rotated or tilt around its vertical or horizontal axis, respectively, and the counting rate of registered radiation is draw versus the

goniometer coordinate. Maxima of the obtained distributions correspond to crystal positions where the channeling condition is fulfilled for a certain crystal plane as exemplarily shown in Fig. 2.5a for the (110) plane of a 42.5 μm thick diamond crystal. From a series of angular scans, the orientation of the crystal with respect to the electron beam can be reconstructed by mapping the found maxima in goniometer coordinates. With the help of such a crystal map (Fig. 2.5b), the channeling condition along the chosen plane can easily be set.

2.5 Measurements and data processing

Measurements of planar CR have been measured on diamond crystals at the electron energies 14.6, 17, 25, 30 and 34 MeV. The electron energy (E_e) was determined by means of beam deflection in the switching magnet of ELBE with a typical error of about 200 keV. One should notice that this method provides a value for the electron momentum p_e, whereus the relation $E_e^{\,2} = (p_e c)^2 + (m_e c^2)^2$ is valid for relativistic electrons. It follows $E_e = \frac{p_e c}{\beta} \approx p_e c$, where $\beta = \sqrt{1 - \frac{1}{\gamma^2}} \approx 0.999387 \div 0.999887$ for the above given values of the total electron energy E_e. Note that E_e differs from the kinetic electron energy $T_e \approx p_e c - m_e c^2$ by the rest energy of the electron mc^2.

Since CR is always accompanied with BS, this background has to be measured at a sufficiently misaligned crystal position and subtracted from the spectrum obtained in the aligned crystal position For that both spectra have to be normalized to the same number of incident electrons (see § 2.3).

In the frame of this work, a consistent procedure for CR data reduction has been developed and implemented into an interactive computer code based on the package Matematica 4.1. This program subsequently accomplishes the following steps of data reduction:

(i) Data input operations concerning the corresponding CR and BS spectra as well as the conditions given by the measurement geometry.

(ii) Normalization of the spectra to equal number of incident electrons (see § 2.3).

(iii) Correction of the normalized spectra for the total registration efficiency. The procedure described in § 2.4 is first executed for the BS spectrum, where self-absorption in the crystal is ignored. The result obtained for a 168 μm thick diamond crystal is illustrated in Fig. 2.6. The deviation of the energy-multiplied spectrum from a flat behavior at low photon energy reveals the effect of self-absorption of radiation in the crystal which depends on its thickness.

(iv) Correction for self-absorption of radiation in the crystal. The flat behavior of the energy-multiplied spectrum obtained in a broad interval of photon energy down to the registration threshold (Fig. 2.6) indicates the accuracy of the correction procedure.

(v) Reproduction of the real shapes of the BS as well as CR spectrum by dividing the normalized spectra by the obtained total registration efficiency. For illustration, normalized BS and CR spectra for (110) planar channeling of 17 MeV electrons in a 42.5 μm thick diamond crystal are shown in Fig. 2.7, where the two prominent peaks correspond to the transverse transitions 1→0 and 2→1 possible at this electron energy. The corresponding corrected BS and CR spectra are shown in Fig. 2.8. It should be mentioned that the corrected BS spectrum follows the known $1/E_x$ dependency.

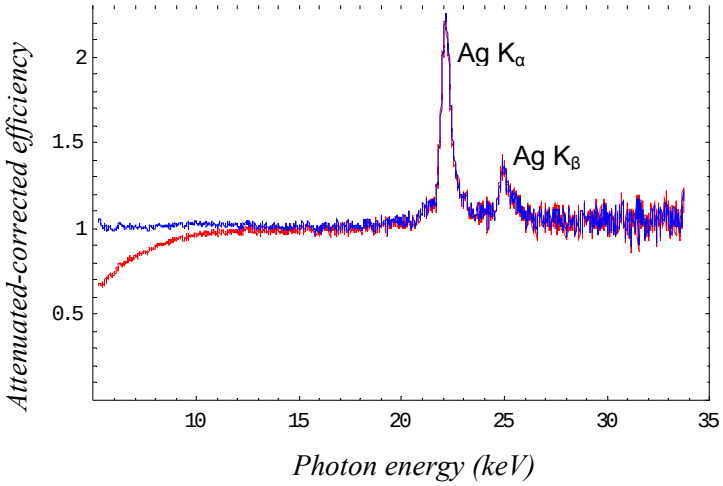

Fig. 2.6 Energy-multiplied spectrum of BS, corrected for detector efficiency, attenuation in window materials and self-absorption, normalized to a total efficiency of 100%, from a measurement with 14.6 MeV electrons traversing a randomly oriented, 168 μm thick diamond crystal (SI-PIN diode). Deviations from one occur at photon energies between 5 and about 13 keV due to exclusion of self-absorption from the correction procedure.

(vi) Subtraction of BS background. Since during electron channeling the production of BS is enhanced by a factor of about 1.3 ÷ 1.6, the corrected BS spectrum has to be normalized within a suitable interval of photon energy to the measured CR spectrum. This enhancement effect is caused by the prolonged time the channeled particle stays in close vicinity to the atoms of the channeling plane [Kum89]. Additionally to the CR lines, some background components may remain after subtraction of BS. Such components represent free-to-bound transitions.

(v) Accomplishment of a least-squares curve fit to the BS-subtracted CR spectrum by application of the Levenberg-Marquardt method for the minimization of the χ^2-function. For this procedure, every CR line is approximated by a spectral distribution of the form given by Eq. 1.50, possible additional peaks from free-to-bound transitions are modeled by Gaussians, and the remaining background is included by a low-order polynomial distribution. The values obtained from calculations of the CR

photon energies by means of the many-beam method (see chapter 1) can be used as starting parameters for the fit procedure. Simultaneously for all CR lines contained in a measured CR spectrum, one obtains a best value for the measured CR peak energy E_{exp}, the maximum CR energy E_0, the line width Γ_T, the asymmetry parameters α, the peak magnitude, and also the coefficients of the background function. It must be mentioned that due to multiple scattering the measured peak energy E_{exp} differs from the maximum energy E_0 by some δE.

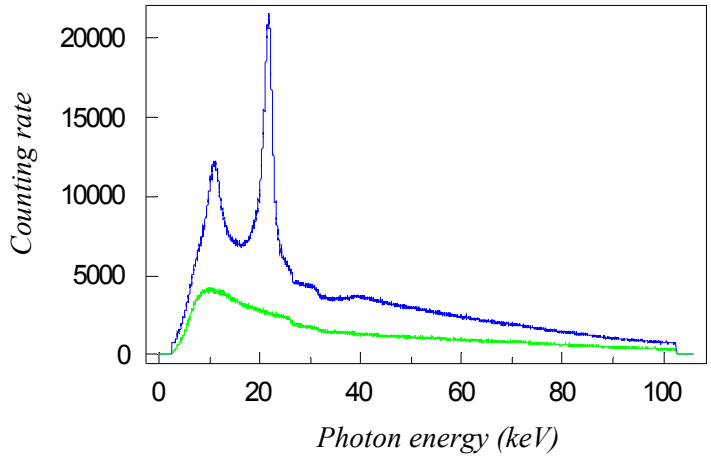

Fig. 2.7 Spectra of (110) planar CR (upper one) and BS (lower one) measured on a 42.5 μm thick diamond crystal at the electron energy of 17 MeV and normalized to equal number of incident electrons.

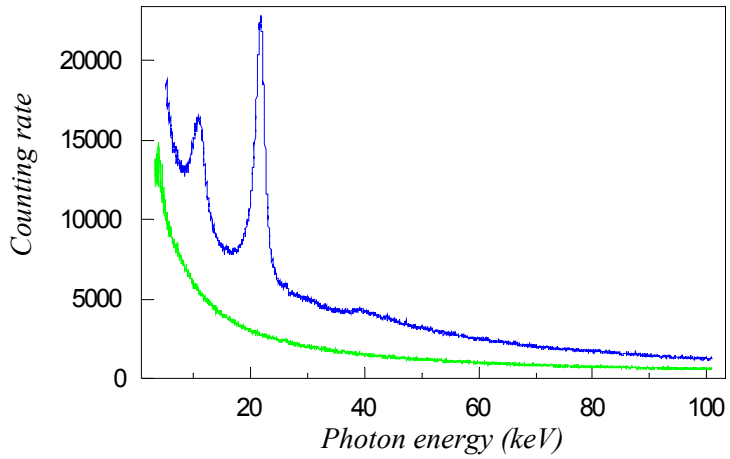

Fig. 2.8 Spectra of (110) planar CR (upper one) and BS (lower one) as shown in Fig. 2.7 but corrected for the total registration efficiency.

As an example, the CR line shapes obtained from the described fit procedure performed for three transitions of (110) planar CR observed at an electron energy of 30 MeV on a 168 μm thick diamond crystal are drawn in Fig. 2.9.

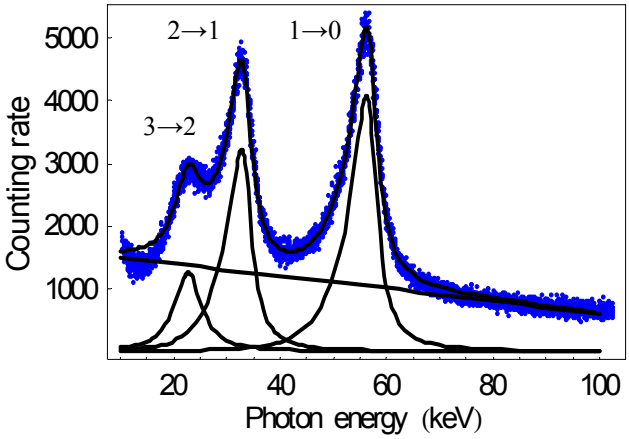

Fig. 2.9 Line shapes of three transitions of (110) planar CR registered on a 168 μm thick diamond crystal at the electron energy of 30 MeV.

In order to examine the influence of multiple scattering on the CR line shapes, the CR peaks have also been approximated by Voigt profiles, which represent convolutions of the intrinsic Lorentzians with Gaussians. Since a Voigt profile is a symmetric distribution, the fits to the measured CR lines involve some possible peak energy shifts but not the effect leading to an asymmetric line shape.

For illustration, the background corrected spectrum of (110) planar CR registered on a 168 μm thick diamond crystal at the electron energy of 17 MeV is shown in Fig. 2.10 together with two approximated Voigt profiles, while the same spectrum approximated by two asymmetric spectral distributions given by Eq. (1.50) is shown in Fig. 2.11.

To compare the quality of these two approximations of the CR line shapes, the weighted deviations between the measured and modeled spectral distributions (residuals) are shown in the lower panels of Figs. 2.10 and 2.11. The systematic deviations of the residuals from zero near the position of the prominent peak observed in the lower panel of Fig. 2.10 indicate a remarkable asymmetry of this CR line. It is obvious from Fig. 2.11 that the asymmetric line profile given by Eq. (1.50) nearly perfectly fits to the data because the corresponding residuals are spread uniformly around zero, thus providing confidence in the resulting values of the fit parameters.

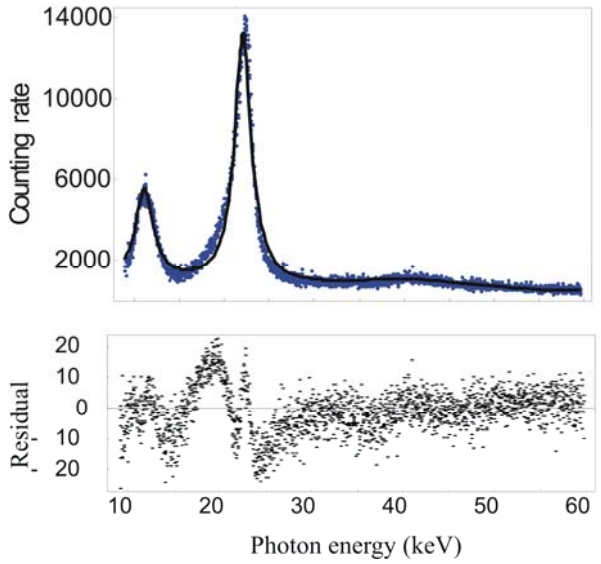

Fig. 2.10 Spectrum of (110) planar CR measured on a 168 μm thick diamond crystal at the electron energy of 17 MeV and approximated by two Voigt profiles. The lower panel shows the residuals between the measured and the approximated line shapes.

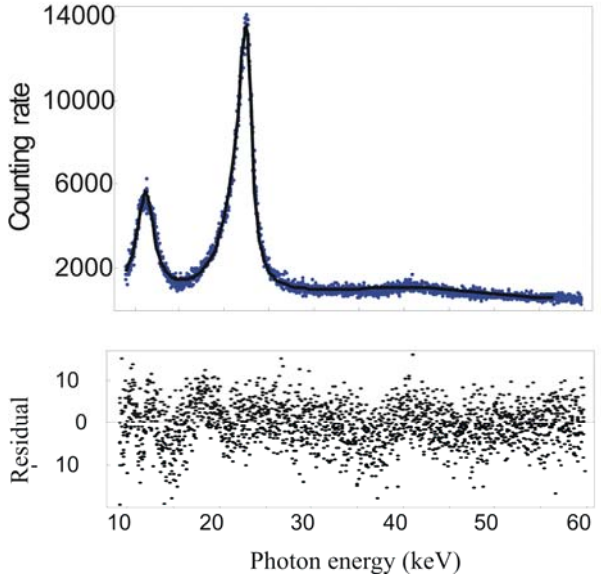

Fig. 2.11 The same spectrum as shown in Fig. 2.10 but approximated by two asymmetric spectral distributions given by Eq. (1.50). The lower panel shows the residuals between the measured and the approximated line shapes.

2.6 Results of CR measurements on diamond

The results of the data analysis performed for the CR measurements carried out at ELBE will be presented in this paragraph. They will also be compared with values obtained in many-beam calculations for the (100), (111) and (110) planes of diamond. In the subsequent figures, measured CR spectra are shown, which have been corrected as described in § 2.6, and the calculated CR photon energies are indicated by vertical lines of lengths chosen proportional to the relative transition rates obtained by the use of Eq. (1.60). The corresponding planar continuum potentials are drawn including the possible eigenvalues and Bloch bands.

2.6.1 The (100) plane

The (100) plane of diamond has a rather shallow potential (Fig. 2.12). At an electron energy of 14.6 MeV, only the two states with $n = 0$ and $n = 1$ are bound. Therefore, only one CR line corresponding to the transition 1→0 is observed. The line shape indicates that the second energy level already touches the continuum. The calculated transition energy well agrees with the measured CR photon energy.

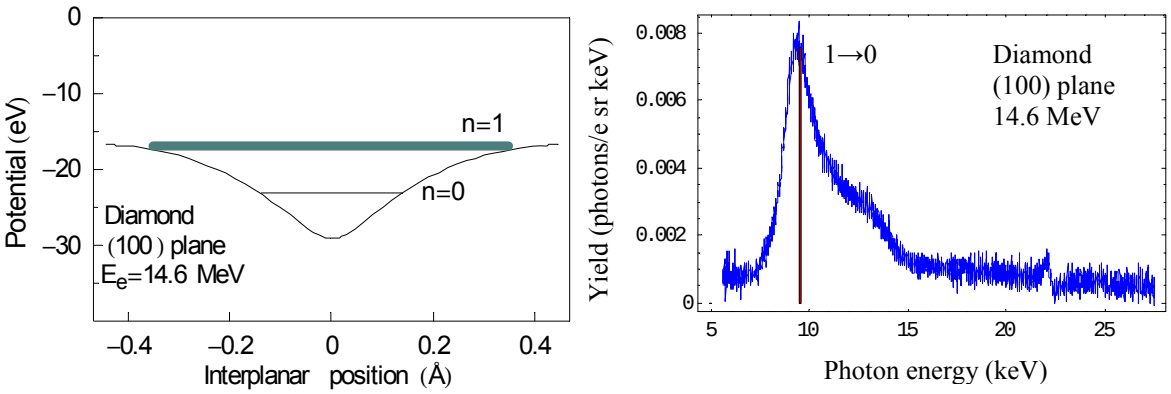

Fig. 2.12 Planar potential of the (100) plane of diamond and eigenvalues (Bloch bands) calculated for the electron energy of 14.6 MeV (left panel). Corresponding CR spectrum measured on a 42.5 µm thick crystal (right panel).

2.6.2 The (111) plane

Due to the unequally spaced crystal planes, the potential of the (111) plane of diamond is rather broad and has two minima. Only transitions between sufficiently spaced energy states are resolved as single CR lines in the spectrum of Fig. 2.13, whereus transitions between narrow bound states overlap. The much weaker transition 3→0, i.e. $\Delta n = 3$, is also observed. The agreement between calculated and measured CR photon energies is somewhat poorer than for the (100) plane. Possible reasons for a shift of measured CR peak positions towards lower energy were already discussed in Ref. [Kle85] and

attributed to non-spherical electron distributions of the atoms forming this plane.

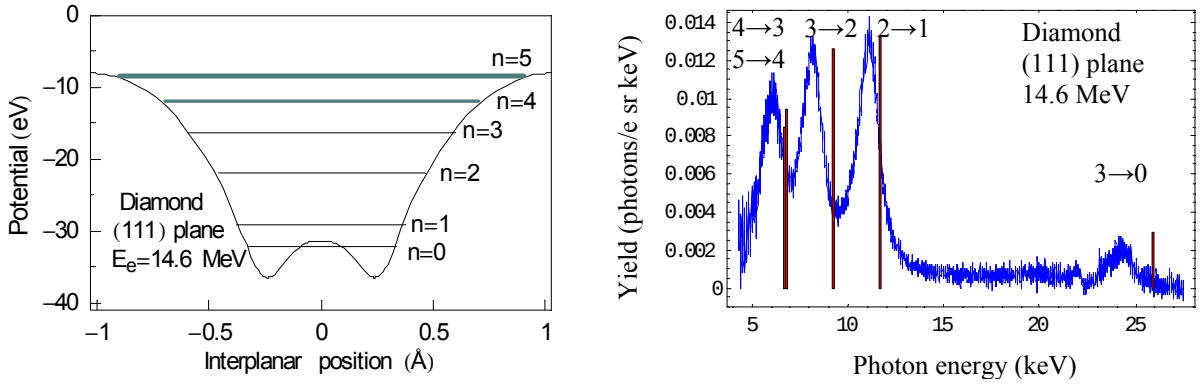

Fig. 2.13 Planar potential of the (111) plane of diamond and eigenvalues (Bloch bands) calculated for the electron energy of 14.6 MeV (left panel). Corresponding CR spectrum measured on a 42.5 μm thick crystal (right panel).

This leads to modified electron scattering form factors as well as Fourier coefficients of the planar potential (cf. chapter 1), and the potential becomes shallower. Consequently, the transition energies become slightly smaller. This effect has not been taken into account in the present calculations.

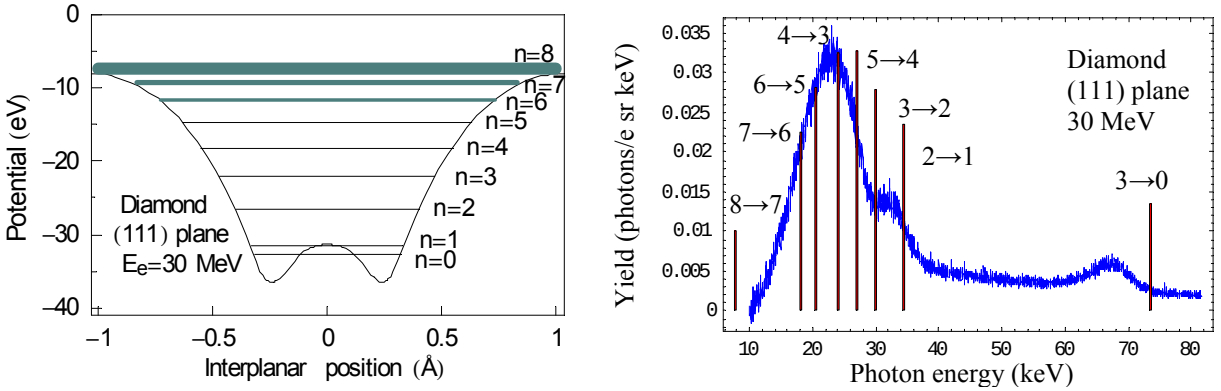

Fig. 2.14 Planar potential of the (111) plane of diamond and eigenvalues (Bloch bands) calculated for the electron energy of 30 MeV (left panel). Corresponding CR spectrum measured on a 42.5 μm thick crystal (right panel).

At the electron energy of 30 MeV (Fig. 2.14), a broad intense peak of CR is observed, which represents a superposition of a variety of possible transitions. Since the individual CR lines become broader at increasing beam energy, they cannot be resolved any longer.

2.6.3 The (110) plane

As the (100) plane, the (110) plane of diamond has a simple potential, but it is about twice deeper than that of (100) plane. For channeled electrons of energy 14.6 MeV, three well separated transverse states exist, and intense CR lines are observed from both the two possible transitions (Fig. 2.15).

For the electron energy of 30 MeV, a third CR line from the transition 3→2 occurs (Fig. 2.16). The CR photon energies are shifted to higher energy compared with the spectrum shown in Fig. 2.15 (cf. also Figs. 1.17 and 1.18), and due to the broader line widths, the CR lines from the higher transitions begin to overlap. The energy of the 3→0 transition amounts to 120.88 keV being out of the dynamic range set for the detector. The small deviations between the measured and the calculated CR photon energies may be caused by the effect of multiple scattering, but are most likely due to changed beam energy.

According to the theory of CR, the 1→0 transition of channeled electrons in the (110) plane is the most intense one found for diamond. Therefore, it should be most suitable to be used for some application of CR as an intense quasi-monochromatic X-ray source.

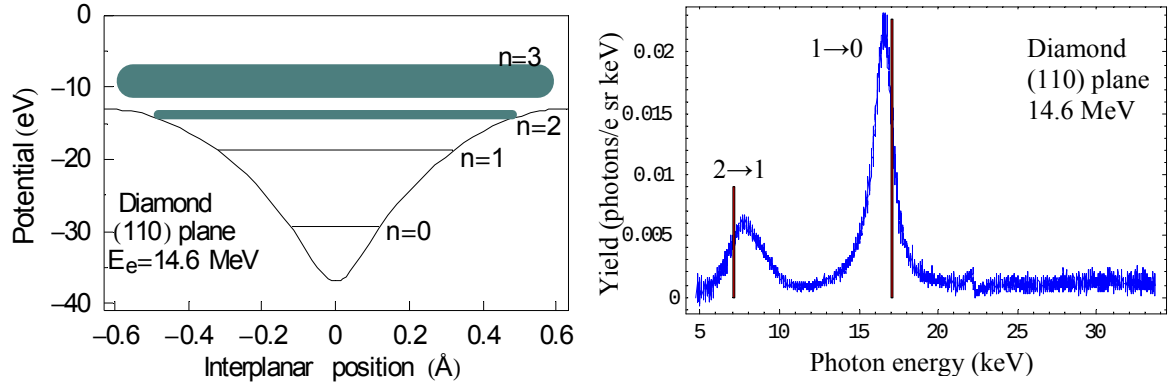

Fig. 2.15 Planar potential of the (110) plane of diamond and eigenvalues (Bloch bands) calculated for the electron energy of 14.6 MeV (left panel). Corresponding CR spectrum measured on a 42.5 μm thick crystal (right panel).

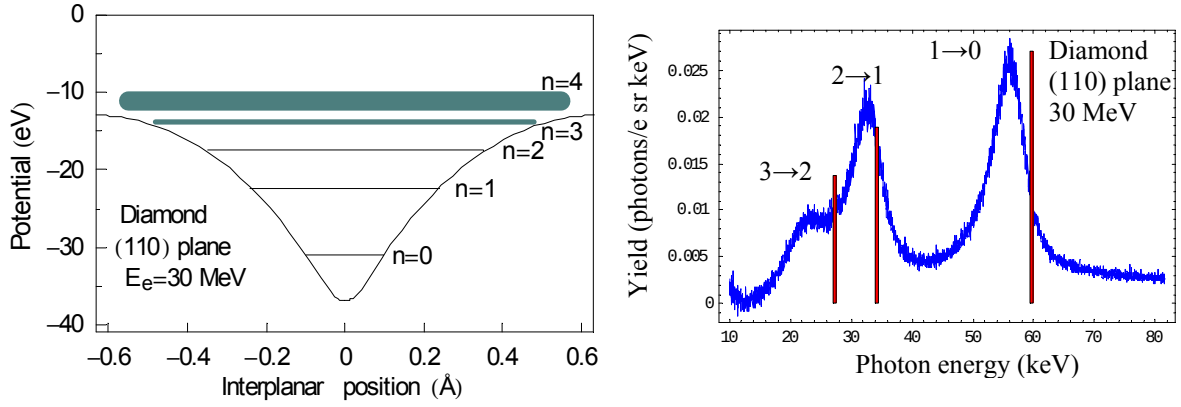

Fig. 2.16 The same as shown in Fig. 2.1 but for the electron energy of 30 MeV.

2.6.4 Asymmetry parameters

The values of the asymmetry parameter α resulting from the analysis of the performed CR measurements are presented in Tab. 2.1. The effective (rms) multiple-scattering angles $\Theta_{ms,ch}$ for electrons channeled in the (110) plane and generating CR by the transition 1→0 are listed in column 3 of Tab. 2.1. The mean multiple-scattering angles Θ_m for non-channeled electrons (i.e., for a misaligned crystal) have been calculated by the use of Eq. (1.47). The corresponding ratio $\Theta_{ms,ch} / \Theta_{ms}$ is given in column 4 of Tab. 2.1.

One can conclude that the asymmetry parameter does not change significantly with the electron energy. This is true for each crystal thickness considered. Consequently, the dependence $\Theta_{ms,ch} \sim 1/E_e$ holds as given by Eq. (1.47) for amorphous targets. The slightly higher value of α obtained for the crystal thickness of 500 μm at the electron energy of 30 MeV can be understood because, in this case, one observes a small overlap of the CR lines resulting from the transitions 1→0 and 2→1.

Table 2.1 Asymmetry parameters and mean multiple-scattering angles obtained by fits of asymmetric line profiles to the CR lines measured for the 1→0 transition of electrons channeled in (110) plane of diamond.

E_e (MeV)	α	$\Theta_{ms,ch}$ (mrad)	$\Theta_{ms,ch} / \Theta_{ms}$
42.5 μm			
14.6	0.172	6.03	0.55
17	0.177	5.32	0.56
30	0.168	2.87	0.54
34	0.175	2.60	0.56
102 μm			
17	0.211	6.33	0.41
30	0.216	3.69	0.42
168 μm			
14.6	0.246	8.62	0.36
17	0.230	6.91	0.33
30	0.226	3.84	0.33
500 μm			
14.6	0.278	9.73	0.22
17	0.281	8.46	0.22
30	0.311	5.31	0.24

The values obtained for the squared asymmetry parameter α^2 at the electron energy of 17 MeV are drawn versus the crystal thickness in Fig. 2.17. It is obvious that this dependence, which has for the first time been investigated in the frame of this work [Aza06], is not linear, as one would expect from Eq. (1.47), but can be described by a function of the form $\alpha^2 = sL^b$, where the coefficient s merges the ordinate scale and $b = 0.37$. This means that the multiple-scattering angle effective for CR observation increases more slowly with the crystal thickness than given by Eq. (1.47). Note that $\Theta_{ms,ch}$ is 1.5 ÷ 4 times larger than the critical angle for channeling along the (110) plane of diamond. Therefore, the observed shift of the CR photon energy, the line-broadening and the line asymmetry are caused by multiple scattering of channeled electrons within the channeling plane.

Since the values found for $\Theta_{ms,ch}$ are much less than $1/\gamma$, all transitions proceeding at $\Theta \leq \Theta_{ms,ch}$ contribute to the observed CR line and modify its shape as described by Eq. (1.50).

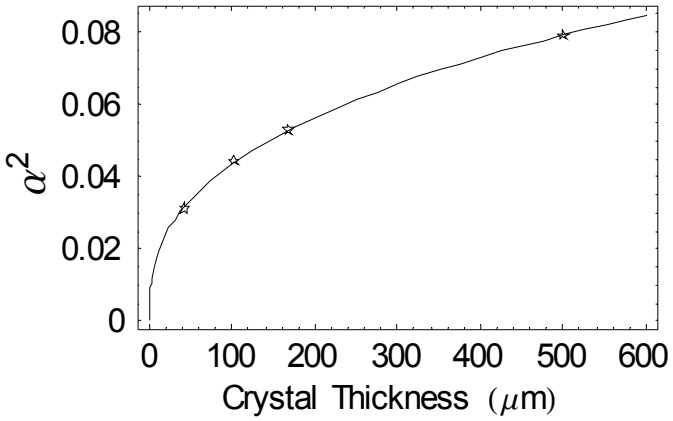

Fig. 2.17 Squared asymmetry parameter as function of the crystal thickness for electrons of energy 17 MeV channeled in the (110) plane of diamond.

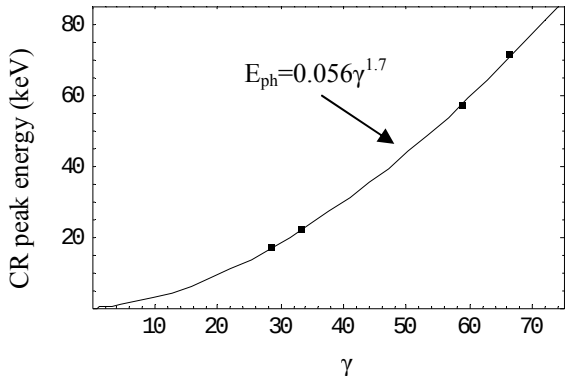

Fig. 2.18 Measured CR photon energy as function of the electron energy (given in units of γ) for the 1→0 transition of electrons channeled in the (110) plane of diamond.

Table 2.2 Measured and calculated CR photon energies of the 1→0 transition in the (110) plane of diamond. Since these values are congenerously afflicted with uncertainties and possible systematic deviations, errors are not given.

L (μm)	E_{exp} (keV)	E_0 (keV)	δE (keV)	δE / E_0	E_{calc} (keV)
14.6 MeV					
42.5	16.58	16.76	0.18	0.011	17.06
168	16.99	17.21	0.22	0.013	
500	16.47	16.75	0.28	0.017	
17 MeV					
42.5	21.72	21.96	0.24	0.011	22.23
102	21.42	21.70	0.28	0.012	
168	22.37	22.65	0.28	0.012	
500	21.38	21.68	0.30	0.014	
30 MeV					
42.5	56.19	56.87	0.68	0.012	59.49
102	56.72	57.71	0.99	0.017	
168	56.22	57.00	0.78	0.014	
500	55.06	56.61	1.55	0.027	
34 MeV					
42.5	70.02	70.96	0.94	0.013	73.78

2.6.5 Transition energies

Table 2.2 lists the CR photon energies E_{exp} obtained from the fits of asymmetric profiles to the experimental data, the maximum energies E_0 and the transition energies E_{calc} calculated for different crystal thicknesses L. Column 4 of Tab. 2.2 reveals that the shift of the CR photon energy δE caused by multiple scattering increases with increasing crystal thickness at a given electron energy, but it also increases with the electron energy at a given thickness.

The shift of the CR photon energy due to multiple scattering can be estimated by convolving the expression given by Eq. (1.45) with the one-dimensional multiple scattering distribution described by Eq. (1.46)

$$E_\gamma = \frac{1}{\sqrt{2\pi}\theta_{ms,ch}} \int_{-\infty}^{+\infty} e^{-\theta^2/2\theta_{ms,ch}^2} \frac{E_0}{1+\gamma^2\theta^2} d\theta . \tag{2.3}$$

After changing the variable Θ in Eq. (2.3) to $\phi = \theta/\sqrt{2}\theta_{ms,ch}$, the relative shift of the CR photon energy due to multiple scattering reads

$$\frac{\delta E}{E_0} = \frac{1}{\sqrt{\pi}} \int \frac{e^{-\phi^2}}{1+2\gamma^2\theta_{ms,ch}^2\phi^2} d\phi - 1 . \tag{2.4}$$

As came out (see Tab. 2.1), the asymmetry parameter, being defined as $\alpha = \gamma\theta_{ms,ch}$, does not depend on γ for a fixed crystal thickness because $\theta_{ms,ch} \sim 1/\gamma$. Therefore, the relative shift of the CR photon energy $\delta E/E_0$ should also not vary with the electron energy. Within certain accuracy, this is confirmed by the values given in column 5 of Tab. 2.2. Note that the maximum photon energy E_0 is also a fit parameter, which is modified by the actual shift of the CR photon energy due to multiple scattering. Hence, the difference between E_0 and E_{calc} can only result from some difference between the actual electron energy and that defined by the beam tuning. The relative discrepancy amounted to 2.3% at 14.6 MeV and to 5.1% at 34 MeV, corresponding to values of 0.36 MeV and 1.73 MeV, respectively.

It was explained in chapter 1, the CR photon energy for the 1→0 transition of electrons channeled in the (110) plane of diamond scales with the electron energy such as $E_0 \sim \gamma^c$. The exponent c has been defined by a least-squares fit to the measured CR photon energies. The obtained value amounts to 1.700 ± 0.016 (Fig. 2.18) and is very close to the value 1.73 found from calculations performed on the base of the Doyle-Turner potential. However, both values are far from 1.5 which corresponds to a harmonic potential.

2.6.6 CR line widths

The contributions to the residual CR line widths, as calculated in accordance with chapter 1, are listed in Tab. 2.3 for the crystal thickness of 42.5 μm. The partial widths due to Doppler broadening Γ_{Dopp}, resulting from the effect of multiple scattering during channeling, are calculated by means of Eq. (1.48) using the values for $\Theta_{ms,ch}$ given in Tab. 2.1. The total CR line width Γ_{calc} evaluated by means of Eq. (1.49) is given in column 6 of Tab. 2.3. The residual line widths Γ_{exp} (FWHM), obtained from the approximation of asymmetric profiles to the measured CR lines, and the values of Γ_T, resulting from this fit procedure, are listed in Tab. 2.4.

As an effect of multiple scattering, the total line width considerably increases with increasing crystal thickness at a given electron energy, while Γ_T has been found to be rather constant. Such behavior can be expected, if the leading term of Γ_T is that given by Eq. (1.35). The increase of Γ_T with increasing

electron energy for a given crystal thickness is more pronounced than that of Γ_{Dopp}. The experimental line widths are larger than those estimated by Eq. (1.49), because the quadratic additive of the partial widths underestimates the width obtained by the convolution given by Eq. (1.50). Otherwise, the values of Γ_{exp} are slightly smaller than those resulting from the summation $\Gamma_T + \Gamma_{Dopp}$.

After a small correction for the detector resolution and the Bloch-wave broadening, the values of Γ_T obtained from the fit procedure also allow an estimation of the coherence length [see Eq. (1.35)]. A comparison between calculated and experimentally found coherence lengths is given in Tab. 2.5, where the data of Ref. [Gen96] obtained at electron energies of 5.2 and 9 MeV and those of Ref. [Gou88] obtained at 53.2 and 80.3 MeV are adjoined.

From the values given in columns 3 and 4 of Tab. 2.5 one can conclude that the coherence length relating to the 1→0 transition of (110) planar CR is nearly independent on the electron energy and in the average amounts to (0.64 ± 0.04) μm.

Following the arguments of Ref. [Gou88] that thermal scattering is not localized, a mean value of (1.28 ± 0.02) μm has been estimated for the coherence length at room temperature of the two most tightly bound channeling states in the (110) plane of diamond.

The comparison of the values given in columns 2 and 4 of Tab. 2.5 reveals that the coherence lengths calculated by means of the optical potential method are about 1.5 times larger than the observed ones. Although thermal scattering dominates during channeling in diamond crystals, incoherent scattering of the channeled electrons on the electrons of the crystal atoms should also contribute, especially for those particles occupying the low lying tightly bound channeling states. According to Ref. [Bur84], the relation between these two scattering mechanisms is roughly 4 : 1 at an electron energy of 54 MeV, and this ratio should slightly decrease with decreasing electron energy.

Table 2.3 Partial and residual line widths as calculated for the 1→0 transition of (110) planar CR generated in a 42.5 μm thick diamond crystal.

E_e (MeV)	Γ_{coh} (keV)	Γ_{Bloch} (keV)	Γ_{Dopp} (keV)	Γ_{det} (keV)	Γ_{calc} (keV)
14.6	0.29	0.26	0.50	0.47	0.87
17	0.41	0.17	0.69	0.49	0.95
30	1.51	0.02	1.61	0.60	2.29
34	2.01	0.01	2.15	0.63	3.01

Table 2.4. Measured and calculated line widths of CR from the 1→0 transition in the (110) plane of diamond.

L (μm)	Γ_{exp} (keV)	Γ_T (keV)	Γ_{Dopp} (keV)	Γ_{calc} (keV)
14.6 MeV				
42.5	1.51	1.09	0.50	0.87
168	1.80	1.07	1.02	1.25
500	2.20	1.31	1.30	1.48
17 MeV				
42.5	2.00	1.45	0.69	0.95
102	2.19	1.45	0.98	1.18
168	2.47	1.44	1.16	1.39
500	2.77	1.26	1.74	1.90
30 MeV				
42.5	5.88	4.25	1.61	2.29
102	7.94	5.75	2.67	3.13
168	6.12	3.94	2.89	3.32
500	11.98	7.99	5.53	5.77
34 MeV				
42.5	7.84	6.00	2.15	3.01

Table 2.5. Coherence lengths l_{calc} calculated for the 1→0 transition of (110) planar CR by means of the optical potential method. The values l_{ref} are taken from Refs. [Gou88, Gen96]. The values given in columns 4÷7 have been estimated from the measurements performed on diamond crystals of thicknesses 42.5, 102, 168 and 500 μm.

E_e (MeV)	l_{calc} (μm)	l_{ref} (μm)	$l_{42.5}$ (μm)	l_{102} (μm)	l_{168} (μm)	l_{500} (μm)
5.2		0.64				
9.0		0.68				
14.6	1.11		0.68		0.69	0.54
17	1.06		0.66	0.65	0.65	0.76
30	0.90		0.65	0.48	0.70	0.34
34	0.87		0.59			
53.2		0.59				
80.3		0.62				

2.6.7 CR photon yields

The CR photon yields Y_{exp} obtained from the fits of asymmetric profiles to the measured CR lines from the 1→0 transition of electrons channeled in the (110) plane of diamond crystals of different thickness and the values calculated as described in chapter 1 are listed in Tab. 2.6.

The total errors of the photon yields are determined by the statistical errors obtained in the fit procedure, by uncertainties of the electron energy and of the beam current, by the tolerances of the crystal thicknesses, and by the error of the solid angle of CR registration. While the statistical errors are negligible, the typical value estimated for the accuracy of the measured CR photon yields amounts to about 20%. Indeed, if the crystal thickness of thinner crystals can usually be determined with lower accuracy than that of thicker crystals, the error of the measurement of the number of electrons, which transmitted the crystal behaves reversely [cf. Neu07]. Independently from the crystal thickness, the remaining components contributing to the total error of the CR photon yields are of the same order for all electron energies.

The CR photon yields obtained in the measurements performed at the electron energy of 14.6 MeV are shown in Fig. 2.19 as a function of the crystal thickness z. The curve drawn through the experimental values represents a least-squares fit of a model function $a\sqrt{z}$ to the data. It can be concluded that multiple scattering obviously governs the CR photon yield at crystal thicknesses between 42.5 and 500 μm. If thermal scattering leads to equilibrium occupation of channeling states within the first 5 ÷ 10 μm of traversed crystal depth (see § 1.9.2), one may assume that, in the case of diamond, multiple scattering determines the CR photon yields even starting from a much smaller crystal depth (cf. Ref. [Gen96]).

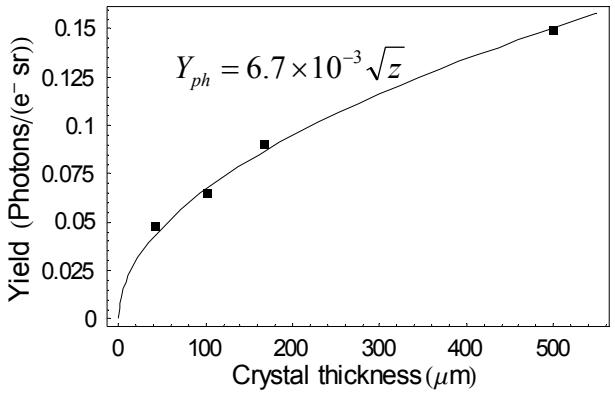

Fig. 2.19 Measured CR photon yield as function of the crystal thickness for the 1→0 transition of 14.6 MeV electrons channeled in the (110) plane of diamond.

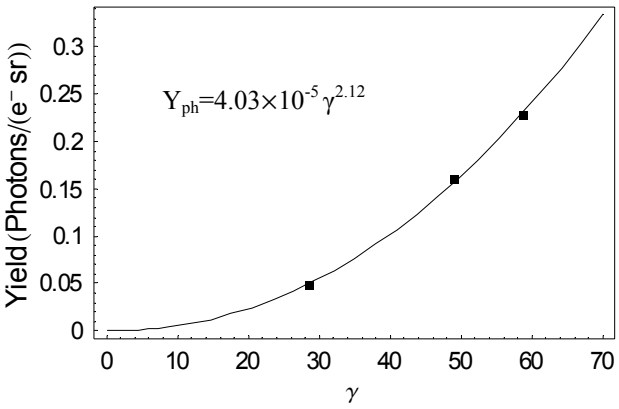

Fig. 2.20 Measured CR photon yield as function of the electron energy (given in units of γ) for the 1→0 transition in the (110) plane of a 42.5 μm thick diamond crystal.

Table 2.6 Measured and calculated photon yields for the 1→0 transition of (110) planar CR generated in diamond crystals of thicknesses 42.5, 102, 168 and 500 μm.

L (μm)	Y_{exp} (photons/e sr)	Y_{calc} (photons/e sr)
14.6 MeV		
42.5	0.048	0.112
102	0.065	0.173
168	0.090	0.223
500	0.149	0.384
17 MeV		
42.5	0.059	0.148
102	0.09	0.230
168	0.13	0.295
500	0.30	0.509
25 MeV		
42.5	0.159	0.318
30 MeV		
42.5	0.229	0.448
102	0.406	0.693
168	0.52	0.890
500	1.012	1.535

The CR photon yields obtained for the 1→0 transition in the (110) plane of a 42.5 μm thick diamond crystal are shown as a function of the electron energy in Fig. 2.20. The curve drawn through the experimental values represents a least-squares fit of a model function $b\gamma^c$ to the data. The exponent c was found to be 2.12 ± 0.09. This value is smaller then the value of 5/2, which can be determined for a harmonic potential, but it is remarkably larger than the value of 1.92 obtained from a calculation on the base of the Doyle-Turner potential for the very small crystal thickness of 5 μm (see Fig. 1.18).

2.7 Conclusions from the CR measurements

For electron energies between about 15 and 35 MeV, the transition energies calculated by means of the many-beam formalism using the Doyle-Turner potential are generally in good agreement with the measured CR photon energies for channeling in the (100) and (110) planes of diamond. The number of bound states in the broader potential of the (111) plane is larger. This fact leads to an overlap of CR lines from a variety of possible transitions at higher electron energy what complicates a detailed analysis. At the electron energy of 14.6 MeV, where several CR lines can be resolved, the calculated transition energies are, however, remarkably larger than the CR photon energies observed. Probably, as discussed in Ref. [Kle85], the reason for this discrepancy is the non-spherical electron distribution of the atoms positioned in this crystal plane.

The theoretical calculations as well as the measurements reveal that the 1→0 transition of electrons channeled in the (110) plane is the most intense one in diamond. Hence, this transition is most suitable for the application of planar CR as an intense quasi-monochromatic X-ray source. Therefore, the investigations concerning the line shape and photon yield presented in the preceding paragraphs have been focused to this CR line.

The analysis of different line-broadening mechanisms contributing to the total width of a registered CR line showed that multiple scattering increasingly affects its spectral shape with increasing crystal thickness. For the first time, the influence of multiple scattering within the channeling plane has been investigated systematically for relatively large variations of the crystal thickness and the electron energy as well [Aza06]. The method of fitting a convolution of an intrinsic Lorentzian line shape with a Gaussian-like distribution accounting for multiple scattering to the registered spectral distributions of CR provided a consistent picture of the consequences of the line-broadening mechanisms.

It could be shown that the mean value of the multiple-scattering angle effective for the observation of planar CR in forward direction is weaker than earlier assumed and calculated from multiple-scattering in an amorphous target. The ratio $\Theta_{ms,ch} / \Theta_{ms}$ decreases with increasing crystal thickness and does not depend on the electron energy. Since the angle $\Theta_{ms,ch}$ depends in the same manner on the electron energy as Θ_{ms} valid for an amorphous target does, the underlying scattering mechanism seems to be

the same in both cases. At increasing crystal thickness it should, however, become less probable that the electrons remain in the channeling condition after a certain number of scattering events. Since in terms of an occupation length, the electrons are dechanneled, the mean multiple scattering angle, which is effective for CR observation and the formation of the residual CR line shape, is smaller than calculated by means of Eq. (1.47).

It must be mentioned that the formal application of Eq. (1.47) in Ref. [Kep91] allowed a satisfactory interpretation of the measured spectra of planar CR generated in Si crystals. However, in this work only crystal thicknesses between 10 and 20 μm have been considered. Furthermore, the results obtained in the present work could not confirm those found in Ref. [Gou88], where (at that time) a somewhat simplified method had to be applied because the measured spectra were rather complex. The statement $\Theta_{ms,ch} = 0.3 \times \Theta_{ms}$ made in Ref. [Cho99] has also no general validity.

The asymptotic behavior of channeled electrons in thick crystals has been theoretically investigated in Ref. [Ogn94]. The calculation of CR spectra measured by other authors, however, made several assumptions necessary, where that of an uniform line-broadening principally differs from the aproach applied in the present work. As has been shown, multiple scattering causes a remarkable CR line-broadening as well as a small shift of the CR photon peaks towards lower energy. Hence, the residual width of a planar CR line is modified by multiple scattering what is ignored in Eq. (5) of Ref. [Ogn94]. Since the comparison of calculated spectra with measured ones has been made in Ref. [Ogn94] for the rather large electron energy of 54 MeV, the intrinsic line width there dominates, and the effect of multiple scattering becomes relatively weaker and can be easily overseen.

As expected, the residual line width of planar CR is described neither by a linear [Bur84] nor by a quadratic [Net94] additive of the contributing partial widths, because it results from the convolution of different distribution functions. This basic idea expressed in Refs. [Gou88] and [Cho99] has in the present work been consequentially applied for the processing of the measured CR data, because the observed CR line shapes were asymmetric to a remarkable degree. Note also that Eq. (4.64) of Ref. [Cho99] is very similar to Eq. (1.50), but nevertheless it is incorrect and does not converge if used in a fit procedure for the approximation of measured CR lines.

The line-broadening of planar CR due to multiple scattering amounts to 1 ÷ 2 keV, even for diamond crystals of relatively large thickness. Compared with the line-broadening, the peak-energy shift is much smaller. Concerning the application of CR as a quasi-monochromatic X-ray source, this turns to be an advantageous precondition for the use of thicker crystals for intense CR production [Rei99, Wag05].

Since the applied method automatically provides realistic approximations for the intrinsic line width of CR, coherence lengths relating to the considered CR transition could be deduced and were found to be in good agreement with the results of earlier investigations [Gou88, Gen96]. This supports the

conclusion that the coherence length of tightly bound channeling states is to a high degree insensitive to the electron energy.

Certain uncertainties in earlier investigations of the CR photon yield (cf. Ref. [Kep89]) did not allow confident conclusions about the dependence of the CR photon yield on the crystal thickness. Later measurements performed on diamond crystals of a thickness up to 55 μm at electron energies of 5.2 and 9 MeV [Net94, Gen96] yield experimental values which differ by a factor of 20 for the both electron energies, while the scaling of the CR photon yield with the electron energy claimed to be such as $\sim\gamma^{5/2}$ results in a factor of only four. In these experiments, the electron current has been determined by the transmission through the crystal into a Faraday cup situated inside the beam dump. At low electron energy, the actual transmission is, however, considerably smaller than 100%. It has been concluded that for the electron energies considered the CR intensities depend on the crystal thickness such as $I \propto (1-e^{-\lambda z})$. The occupation length $1/\lambda$ has been determined to be 17.5 μm and 27.6 μm for 5.2 MeV and 9 MeV electrons, respectively.

In subsequent measurements of CR yields performed at electron energies of 9 and 10 MeV on diamond crystals of thickness 42 and 204 μm [Rei99], the obtained values were smaller by a factor of 3.45 compared with the former measurements [Net94]. Impurities of the used diamond crystals have been made responsible for such a discrepancy. After empirical scaling of the CR yields found in Ref. [Rei99] to the results published earlier in Ref. [Gen96], a dependence of the CR photon yield on the crystal thickness such as has been deduced for crystal thicknesses between 13 and 204 μm and explained by the effect of multiple scattering. On this limited data base, an optimal crystal thickness of even 1 mm has been extracted for maximum CR yield from the 1→0 transition of 20 MeV electrons channeled in the (110) plane of diamond. Such a large value, however, follows only from an extrapolations to a higher electron energy and with the assumption that the increase of the CR photon yield in accordance with its proportionality to $z^{1/2}$ is solely limited by self-absorption in the crystal.

A serious resume of this brief review of earlier published results of investigations of the dependence of the CR photon yield on the electron energy as well as on the crystal thickness can only state that confident absolute values of CR yields were not yet been available up to now.

Therefore, the systematic study of the mentioned dependences performed in the frame of this work on diamond crystals of type IIa can by all means be understood as a substantial contribution to a more complete and confident knowledge of important features of planar CR. Since the experimental data obtained in the CR measurements at ELBE cover the interval of electron energy between about 15 and 35 MeV and a range of crystal thickness between about 40 and 500 μm, it nevertheless seems to be worthwhile to limit all conclusions made to the investigated intervals of the given parameters.

For example, it has been found that the measured CR photon yields are lower by a factor of about two compared with the calculated values. In agreement with the theory of CR, the CR photon yields measured for channeling in the (110) plane of diamond scale with the electron energy such as $\sim\gamma^{2.12}$,

and with the crystal thickness as $\sim z^{1/2}$. Extrapolations of these trends out of the above mentioned intervals would have the character of theoretical prediction, because they would include the assumption that all effects which may influence the CR emission are exactly described.

Finally, one can conclude that the scaling laws extracted from the measured CR data are of advantage for estimating main parameters of a non-conventional X-ray source based on the production of CR on diamond crystals.

Chapter 3

Planar channeling radiation from electrons channeled in quartz

3.1 Introduction

Channeling radiation emitted from electrons of medium energy has mainly been studied on monoatomic crystals such as diamond [Gou82, Rei99], Si [Gou88, And80, Kep92], Ge [Par83, Cho99], and on metals (e.g. Be, Ni, Sb, W [And83, Gar91, Bus77]). Binary or polyatomic crystals (e.g. LiH [Gar91], LiF [Ber82, Swe84], GaAs, ruby [Fre96]) have scarcely been utilized.

Most of the above mentioned crystals are characterized by a cubic lattice. In such crystals, intense CR is observed from planes with small indices such as (100), (110) and (111). A unique feature of CR has been observed on the binary crystal of LiF [Swe84]. Its halite structure leads to mixed as well as segregate planes, where the former ones consist of Li and F ions, and the latter ones are built from only one sort of ions. Since channeling along crystal planes is governed by the continuum potential, CR emitted by relativistic charged particles channeled in mixed planes resembles that from particles channeled in planes of monatomic crystals. The continuum potential of segregate planes of binary crystals, however, has usually two dips of different strength formed by one or the other sort of crystal atoms, respectively. Consequently, the CR spectrum can contain a mixture of CR lines originating from transverse transitions of channeled electrons between states localized in the different potential wells. This effect has first been observed in Ref. [Swe84].

There are several applications of CR which forced the interest in studying CR emission on single crystals:

(i) CR provides a method for characterizing of crystal properties such as, e.g., different sorts of crystal defects, impurities [Kum89], thermal vibration amplitudes of the crystal atoms [Kep91] etc.

(ii) CR provides a method for characterizing of properties of the channeled particles, e.g., their energy or energy spread.

(iii) CR can be applied for the production of intense quasi-monochromatic X-rays [Gen90, Gar91, Gen96].

A further perspective of CR, recently widely discussed in a series of theoretical works, is connected with the principal possibility to stimulate the CR emission by means of ultrasonic waves excited in the crystal. The non-uniform charge distribution within the unit cell of a quartz (SiO_2) single crystal causes certain structural asymmetries which make quartz a piezoelectric. By the use of the reverse piezoelectric effect, the excitation of longitudinal ultrasonic vibrations of GHz frequencies in the quartz crystal should, therefore, be practicable. The stimulation of CR emission is predicted to proceed via local modulations of the extremely strong (≈ 100 GeV/m) crystal potential. Theoretical studies of this process have been published in Refs. [Bar80, Mkr86, Mkr87, Mkr88, Ded94, Ave97, Gri00a÷c, Gri01a÷e, Gri03a÷b, Ava06a÷b]. Different effects induced by the influence of ultrasound (US) on CR emission are predicted, e.g., CR line splitting, modulation of the CR spectrum, and even a possible amplification of the CR intensity at US frequencies near to a well defined resonance region.

These predictions motivated the experimental investigation of CR emission especially on quartz crystals, because they are easily available commercially. The first experiments were performed at ultra-relativistic electron energy [Ava88, Ava90]. Recent calculations [Avao6a÷b], however, consider lower electron energies in the MeV region.

The implementation of US for a dedicated stimulation of CR in quartz crystals at medium electron energies, however, needs in a detailed knowledge of the properties of CR generated in the undisturbed crystal. The spectrometry of CR on quartz provides information about the suitability of different crystal planes for US impact.

Up to now, the generation of CR in quartz at medium electron energies has not been studied. In the frame of the present work, calculations of planar continuum potentials, transverse transition energies, CR line widths and CR intensities for medium-energy electrons channeled in different planes of quartz have for the first time been carried out [Aza07]. First such CR measurements on quartz have been performed at ELBE [Wag07]. The results of these investigations as well as a comparison of the theoretical and experimental data are presented in the following paragraphs.

3.2 Quartz single crystal

The stoichiometry of SiO_2 causes a fluorite structure of an α-quartz single crystal (Fig. 3.1a). The unit cell of its lattice contains three Si and six O atoms (Fig. 3.1b). The hexagonal lattice is defined by the two primitive vectors $\vec{a}_1$, $\vec{a}_2$ of equal length opening an angle of 120°, and the third coordinate is given by the vector $\vec{c}$ perpendicular to both the others (Fig. 3.1c). In Cartesian coordinates, these vectors are expressed such as

$$\vec{a}_1 = a(\frac{\sqrt{3}}{2}\hat{x} - \frac{1}{2}\hat{y}), \quad \vec{a}_2 = a\hat{y}, \quad \vec{c}_3 = c\hat{z} \tag{3.1}$$

with a = 4.913 Å and c = 5.405 Å at room temperature. The hexagonal coordinates of the atoms in the unit cell are given by

$$\begin{aligned} &Si:(-u,-u,1/3);(u,0,0),(0,u,\frac{2}{3}) \\ &O:(x,y,z);(y-x,-x,z+\frac{1}{3});(-y,x-y,z+\frac{2}{3});(x-y,-y,-z);(y,x,\frac{2}{3}-z);(-x,y-x,\frac{1}{3}-z) \end{aligned} \tag{3.2}$$

with u = 0.465, x = 0.415, y = 0.272, and z = 0.12. The primitive vectors in the reciprocal lattice read

$$\vec{b}_1 = \frac{2\pi}{a}\frac{2}{\sqrt{3}}\hat{x}; \vec{b}_2 = \frac{2\pi}{a}(\frac{1}{\sqrt{3}}\hat{x}+\hat{y}); \vec{b}_3 = \frac{2\pi}{c}\hat{z}\ . \tag{3.3}$$

With these conventions, a crystal plane in a hexagonal lattice is defined by four indices (*hkil*) where (*h*,*k*,*l*) are Miller indices and $i = -(h+k)$. The interplanar distance d_p is then given by

$$\frac{1}{d_p{}^2} = \frac{4}{3}\left(\frac{h^2+hk+k^2}{a^2}\right)+\frac{l^2}{c^2}\,. \tag{3.4}$$

Because of the asymmetry of the quartz single crystal, the planes given by the indices (*hkil*) and (*khil*) have the same interplanar distance, but they have different planar potentials due to different positions of the Si and O atoms in these planes.

Since for channeling the depth and shape of the planar potential as well as the interplanar distance are important, a larger number of bound states can be localized in a deeper potential well, but a large interplanar distance together with a narrow potential well lead to poor initial population of transverse states in this plane. This interplay is very pronounced for quartz and enables the observation of CR even from planes with indices larger than one. The large variety of crystal planes in quartz is illustrated in Fig. 3.2 which shows the zone of the x-cut axis $[2\bar{1}\bar{1}0]$.

3.3 Many-beam calculations for crystal planes of quartz

The Fourier coefficients of the continuum potential were, as in the case of diamond, calculated using the Doyle-Turner approach. The coefficients a_i and b_i in Eq. (1.30) [Doy68] are listed in Tab. 3.1 for the Si and O atoms.

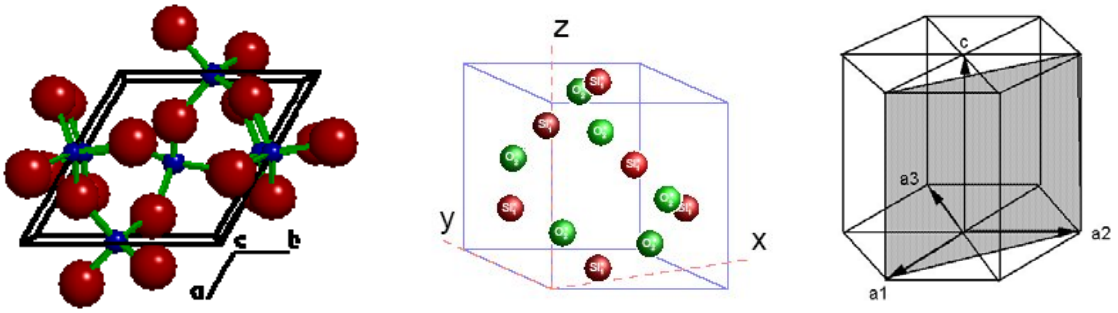

(a) (b) (c)

Fig. 3.1 Tetrahedral structure of an α-quartz single crystal (a). The small spheres represent the Si atoms and the large spheres the O atoms. Unit cell of the quartz crystal (b). Hexagonal structure of quartz with the primitive vectors a_1, a_2, a_3 and c (c).

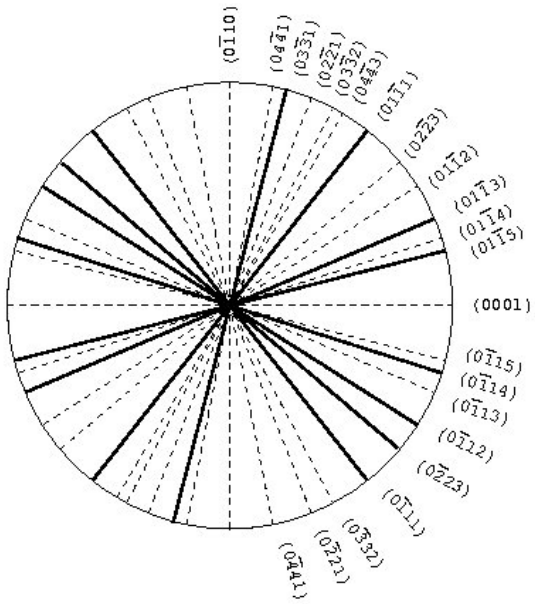

Fig. 3.2 Zone of crystal planes perpendicular to the axis $[2\bar{1}\bar{1}0]$.

Table 3.1 Values of the coefficients a_i and b_i for the Si and O atoms in quartz

	a_1(Å)	a_2(Å)	a_3(Å)	a_4(Å)
Si	2.1293	2.5333	0.8349	0.3216
O	0.4548	0.9173	0.4719	0.1384
	b_1(Å^2)	b_2(Å^2)	b_3(Å^2)	b_4(Å^2)
Si	57.7748	16.4756	2.8796	0.3860
O	23.7803	7.6220	2.1440	0.2959

Note that the continuum potential is given by a linear combination of the atomic potentials of the Si and O atoms in the unit cell. The thermal vibrations of the crystal atoms are taken into account by the corresponding Debye-Waller factors $M_j(\vec{g}) = \frac{1}{2} g^2 \langle u_j^2 \rangle$. Since the mean-squared vibration amplitudes $\langle u_j^2 \rangle$ are different for the Si and O atoms of a quartz crystal, the values given for room temperature in Ref. [Smi63] and amounting to 0.00507 Å^2 and 0.00886 Å^2, respectively, have been adopted.

For illustration, the shapes of the continuum potentials calculated for the $(0\bar{2}23)$ and $(01\bar{1}0)$ planes of quartz are shown in Fig. 3.3. The eigenvalues and Bloch bands correspond to the energy of the channeled electrons of 32 MeV. The potential of the mixed plane $(0\bar{2}23)$ is formed by a combination of Si and O atomic potentials (Fig. 3.3a). The potential of the $(01\bar{1}0)$ plane shows alternating segregate potential wells, where the deep ones are formed by Si atoms, and the smaller modulations are caused by the O atoms (Fig. 3.3b). When the strengths of the potentials presented in Fig. 3.3 are comparable, the interplanar distances of these two planes differ considerably and amount to 1.375 Å and 4.255 Å, respectively.

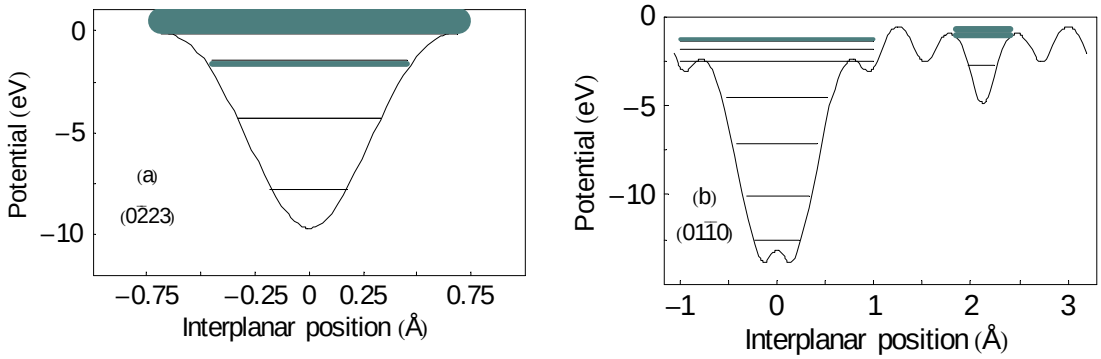

Fig. 3.3 Calculated planar potentials, eigenvalues and Bloch bands for 32 MeV electrons channeled in the $(0\bar{2}23)$ *plane (a) and in the* $(01\bar{1}0)$ *plane (b) of quartz.*

The probability densities of the first three bound states in the $(0\bar{2}23)$ and in the $(01\bar{1}0)$ plane of quartz are drawn in Fig. 3.4. From the present calculations one should expect that the intensities of CR generated in these two planes will differ remarkably. The initial populations (i.e., those at the crystal depth z = 0) of the first three bound states in the $(0\bar{2}23)$ and $(01\bar{1}0)$ planes of quartz are shown in Fig. 3.5. Note that the initial population of states in the $(01\bar{1}0)$ plane is considerably smaller than

that of states in the $(0\bar{2}23)$ plane. This effect is caused by the larger interplanar spacing in the $(01\bar{1}0)$ plane.

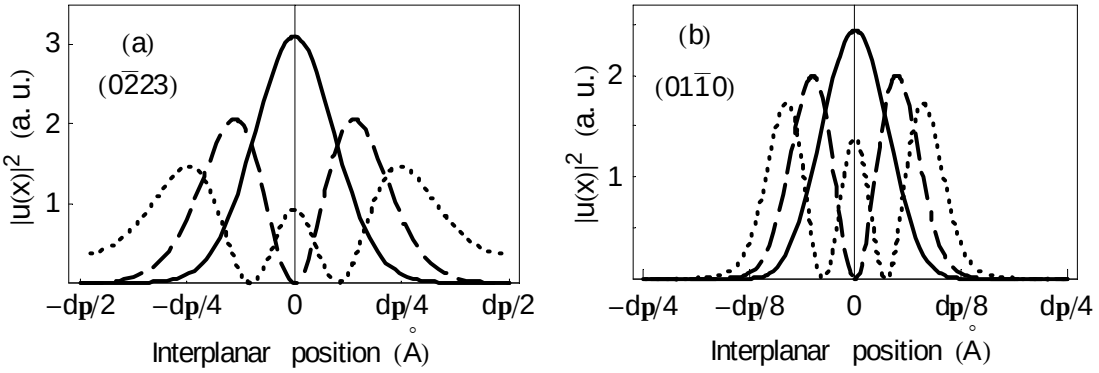

Fig. 3.4 Probability densities of the first three bound states calculated for 32 MeV electrons channeled in the $(0\bar{2}23)$ *plane (a) and in the* $(01\bar{1}0)$ *plane (b) of quartz (n = 0 – full line, n = 1 – dashed line, n = 2 – dotted line).*

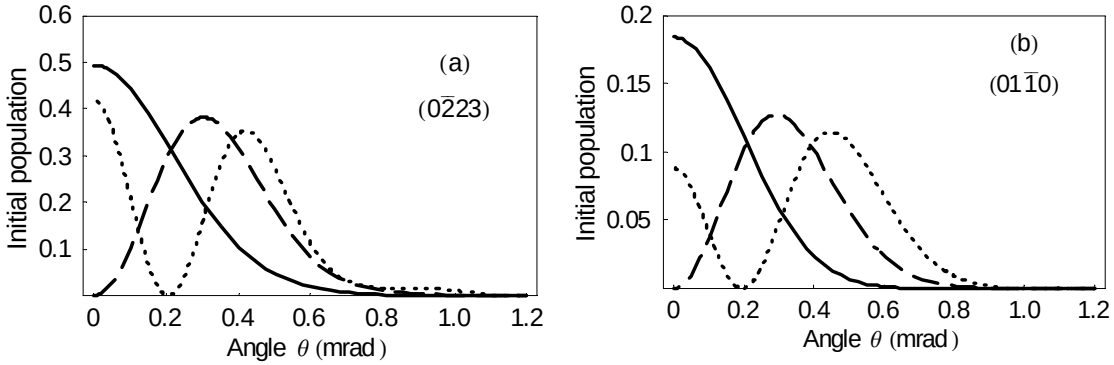

Fig. 3.5 Initial populations calculated for the first three bound states in the $(0\bar{2}23)$ *plane (a) and in the* $(01\bar{1}0)$ *plane (b) of quartz.*

3.4 Measurements of planar CR generated in quartz

Measurements of planar CR out of different crystal planes of quartz have for the first time been carried out at ELBE [Wag07]. The parameters of the electron beam, the experimental setup and the procedures of data reduction and analysis were the same as already described in chapter 2 of this work. Two x-cut quartz crystals of diameter 20 mm and of thicknesses (200 ± 4) μm and (500 ± 5) μm were available for the measurements.

Before mounting the crystals to the goniometer, stereographic projections of the reciprocal lattice vectors have been generated by means of dedicated x-ray diffraction measurements. The knowledge of

the orientation of crystal planes with respect to the crystal surface is of particular advantage in the case of quartz crystals. As illustrated in Fig. 3.2, there are many narrow planes, and the assignment of registered CR to a definite crystal plane is more difficult than on diamond crystals.

For illustration, spectra of planar CR and BS normalized to the same number of incident 34 MeV electrons and representing a measurement of channeling in the $(01\bar{1}1)$ plane of a 200 μm thick quartz crystal are shown in Fig. 3.6. The same spectra but corrected for the total registration efficiency (see § 2.6) are shown in Fig. 3.7.

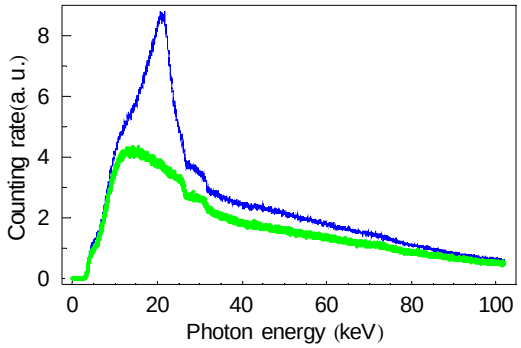

Fig. 3.6 Spectra of $(01\bar{1}1)$ *planar CR (upper one) and BS (lower one) measured at the electron energy of 34 MeV on a 200 μm thick quartz crystal.*

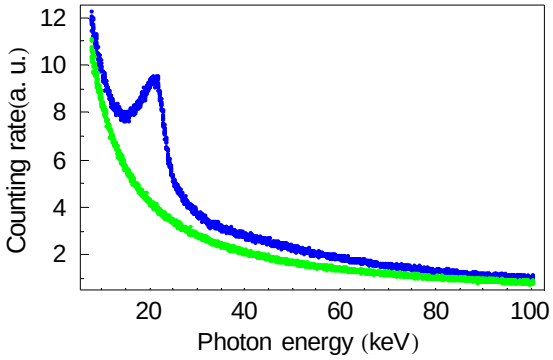

Fig. 3.7 The same spectra as shown in Fig 3.6 but corrected for the total registration efficiency.

The following figures represent background-subtracted spectra of planar CR obtained for 17, 25 and 32 MeV electrons channeled in different planes of quartz. For comparison with the calculations, the corresponding continuum potentials, eigenvalues and Bloch bands are shown aside. The relative orientation of these planes can be found in Fig. 3.2. The calculated transition energies are again indicated in the spectra by vertical lines, the lengths of which are chosen proportional to the values determined by means of Eq. (1.60) assuming equilibrium population of the states.

A first family of planes being accessible for CR measurement on an x-cut quartz crystal is given by the Miller indices $h = 0$, $k = 1$, $l = 0,1,2,\ldots$ (see Figs. 3.8 ÷ 3.11). With increasing value of the index l, the

planar potential simplifies and becomes shallower. As a result, the number of bound states quickly decreases. Therefore, the CR lines from single transitions in the $(01\bar{1}0)$ plane and in the $(01\bar{1}1)$ plane cannot be resolved but superimpose and form broad CR peaks.

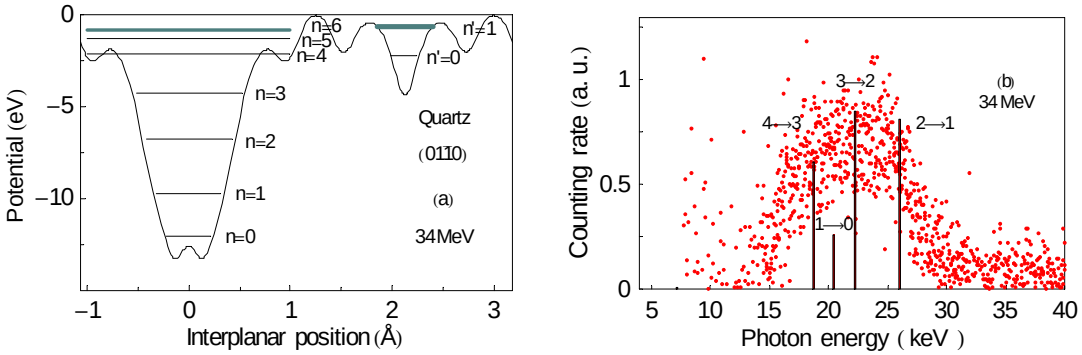

Fig. 3.8 Planar potential of the $(01\bar{1}0)$ *plane of quartz (a) and measured CR spectrum for 34 MeV electrons (b) at a crystal thickness of 500 μm.*

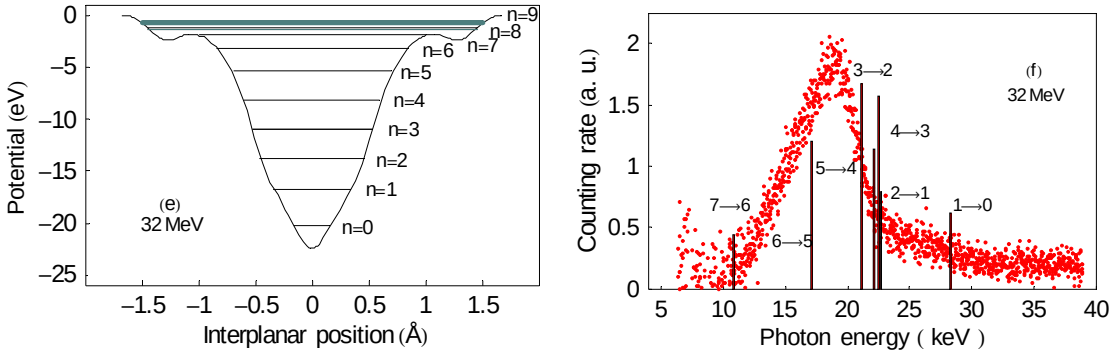

Fig. 3.9 Planar potential of the $(01\bar{1}1)$ *plane of quartz (e) and measured CR spectrum for 32 MeV electrons (f) at a crystal thickness of 200 μm.*

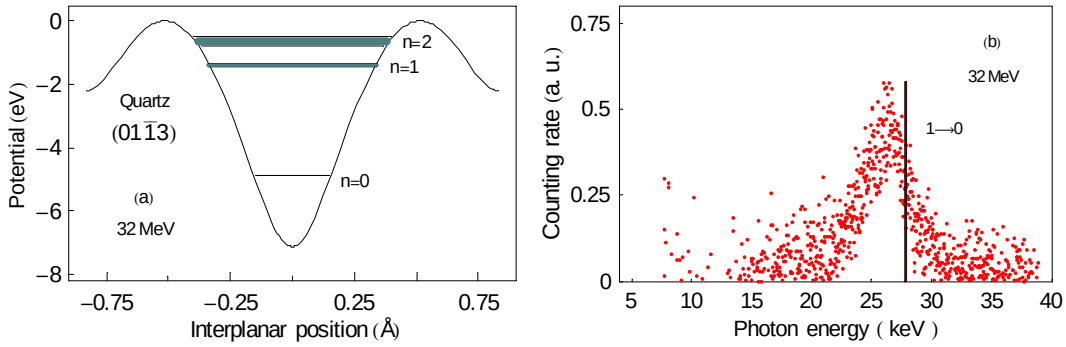

Fig. 3.10 Planar potential of the $(01\bar{1}3)$ *plane of quartz (a) and measured CR spectrum for 32 MeV electrons (b) at a crystal thickness of 200 μm.*

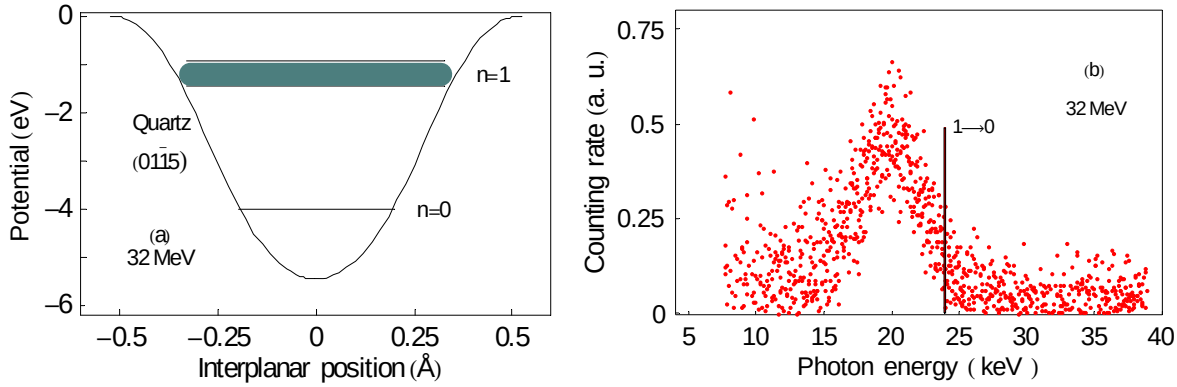

Fig. 3.11 Planar potential of the $(01\bar{1}5)$ *plane of quartz (a) and measured CR spectrum for 32 MeV electrons (b) at a crystal thickness of 200 μm.*

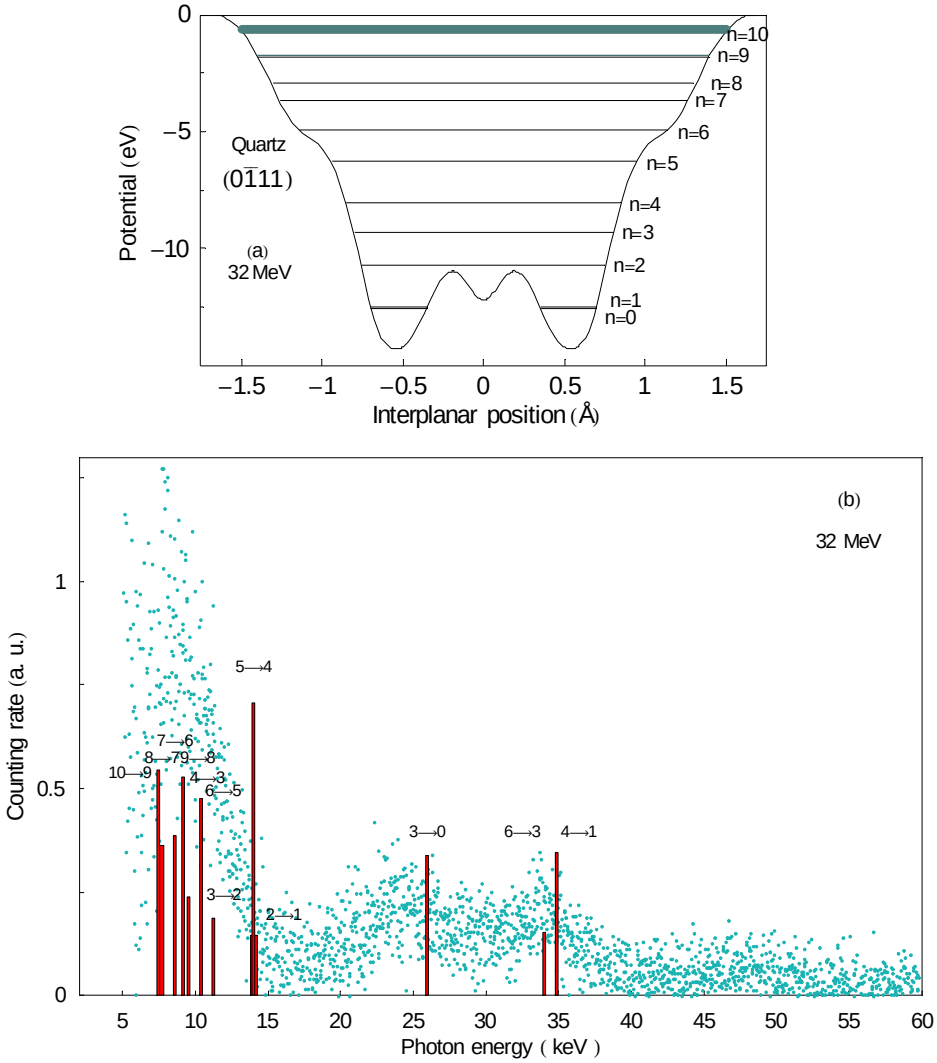

Fig. 3.12. Planar potential of the $(0\bar{1}11)$ *plane of quartz (a) and measured CR spectrum for 32 MeV electrons (b) at a crystal thickness of 200 μm.*

Small deviations between measured and calculated energies may be caused by slight remaining misalignment of the crystal although multiple scattering also leads to shifts of the CR photon energy towards lower values.

In general, the properties of CR observed for another family of planes given by the Miller indices $h = 0$, $k = -1$, $l = 0, 1, 2,\ldots$ (Figs. 3.12 ÷ 3.15) are similar. Note that the $(0\,\bar{1}\,10)$ and $(01\,\bar{1}\,0)$ planes are parallel in a hexagonal lattice. However, compared with the family of planes considered before, the tilt of planes at $l \neq 0$ goes reversely in the second family.

The $(0\,\bar{1}\,11)$ plane is of special interest (Fig. 3.12). Here the Si and O atoms causing the local minima and bents of the planar potential are located narrower to the central position of this plane than it is the case, e.g., in $(01\,\bar{1}\,0)$ plane (see Fig. 3.8a). Therefore, the continuum potential of the $(0\,\bar{1}\,11)$ plane has a broad shape, while the $(01\,\bar{1}\,0)$ plane consists of parallel segregate planes. The broader the potential well is, the larger is the number of bound states and the more CR lines contribute to the CR spectrum observed. As in the $(01\,\bar{1}\,1)$ plane (see Fig. 3.9), the CR lines corresponding to transitions with $\Delta n = 1$ cannot be resolved. However, more energetic transitions with $\Delta n = 3$ lead to two bumps observed in the CR spectrum.

The present measurements manifest a further difference between the two families of planes considered. Namely, for $k = 1$, CR is observed in planes with odd indices l. Otherwise, for $k = -1$, CR is observed in planes with even indices $l > 1$. This effect another time reveals the asymmetry of the quartz crystal. Generally, the planes out of which CR has not been observed have narrow potentials of small depth (< 5 eV).

The trend to shallower potentials with increasing index l exists in both families of planes. Indeed, the tilt of these planes with respect to the primitive vector $\vec{c}$ increases with l, and the planes approach the basis plane (0001) of the hexagonal lattice (see Fig. 3.2). The planar potential of the (0001) plane has also a small depth. In addition to that, the interplanar distance of the (0001) plane is large (5.405 Å). Therefore, CR from this plane could not be observed. Note also that at small photon energies the corrections for self-absorption in the crystal are large diminishing the reliability of the data at these energies considerably, although the registration threshold amounted to about 5 keV.

On the other hand, the somewhat more complicate crystal structure of the binary quartz crystal (compared with cubic crystals such as, e.g., diamond, Si or Ge) allows for planes with relatively large indices, which have rather deep potentials and out of which CR can be observed. The continuum potential of the $(0\bar{2}23)$ plane and CR spectra measured from channeled electrons of energies 17, 25 and 32 MeV are shown in Fig 3.15. At the electron energy of 17 MeV, only the two states with $n = 0$ and $n = 1$ are bound, and the one CR line from corresponding transition $1 \rightarrow 0$ is observed. Electrons of energies 25 and 32 MeV can populate three well separated transversal states in the $(0\bar{2}23)$ plane and

produce rather intense CR lines corresponding to the two possible transitions. In such a case, the scanning procedure for the alignment of the crystal plane with respect to the electron beam can be carried out distinctively for maximum population of a chosen initial state. Therefore, the calculated and measured energies of the observed CR lines agree nearly perfectly (Fig. 3.15).

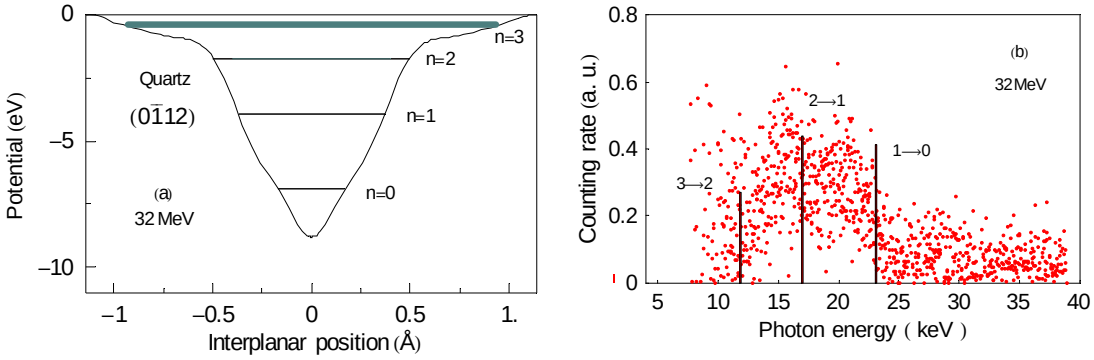

Fig. 3.13 Planar potential of the $(0\bar{1}12)$ *plane of quartz (a) and measured CR spectrum for 32 MeV electrons (b) at a crystal thickness of 200 μm.*

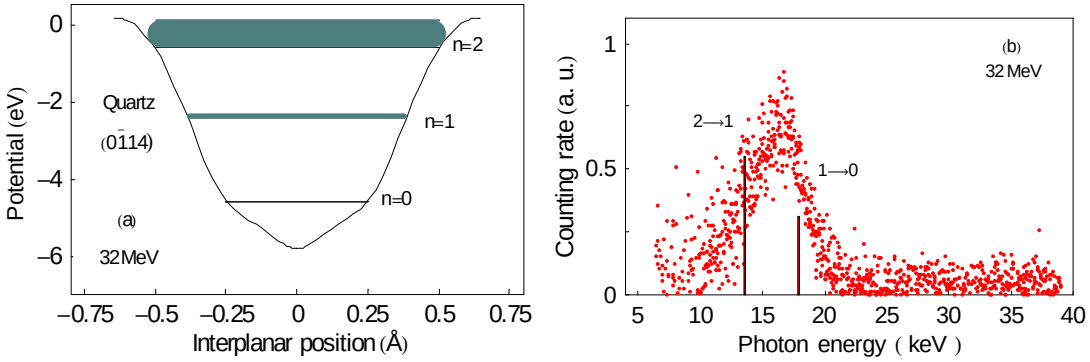

Fig. 3.14 Planar potential of the $(0\bar{1}14)$ *plane of quartz (a) and measured CR spectrum for 32 MeV electrons (b) at a crystal thickness of 200 μm.*

The photon energy of the 1→0 transition scales as $\gamma^{1.7}$ with the electron energy which is similar to the diamond crystal. Another example for observation of CR from a plane with large indices is demonstrated in Fig. 3.16. At electron energy of 32 MeV, there are only three bound states inside the potential affording the transitions 1→0 and 2→1 which have been resolved (Fig. 3.16b).

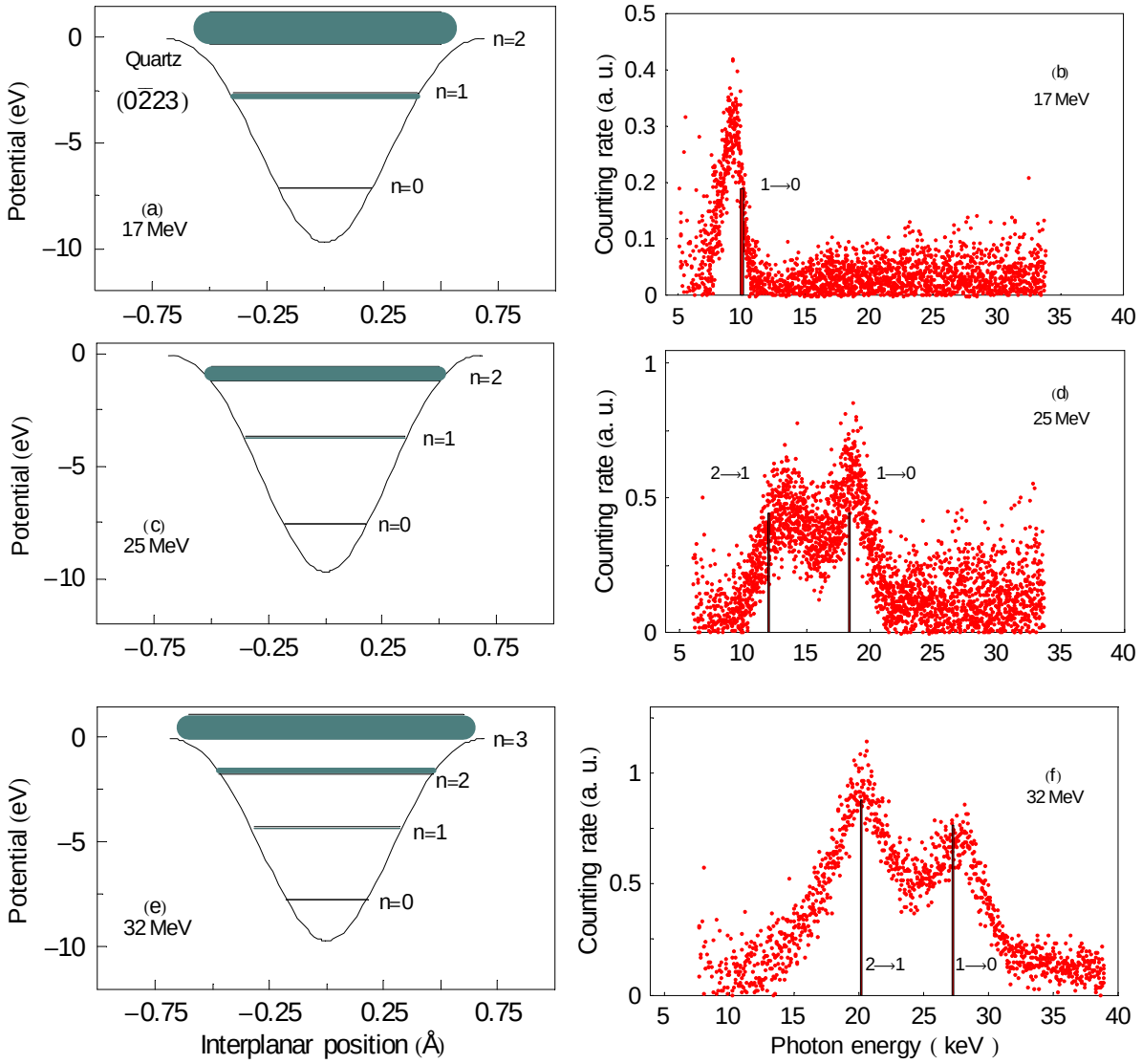

Fig. 3.15 Planar potential of the $(0\bar{2}23)$ *plane of quartz and eigenvalues and Bloch bands calculated for channeled electrons of energy 17 MeV (a), 25 MeV (c), 32 MeV (e) and the corresponding CR spectra (b), (d), (f), respectively, measured at a crystal thickness of 200 μm.*

3.5 Results of CR measurements on quartz

The experimental values obtained for the CR photon energies, line widths and yields of separated transitions of channeled electrons of different energy in different crystal planes of quartz are presented in this paragraph and will be compared with the results of many-beam calculations.

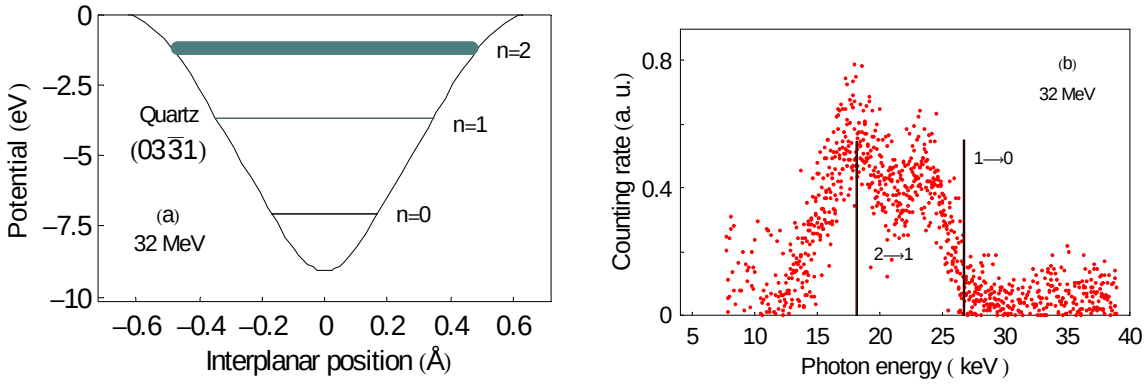

Fig. 3.16 Planar potential of the $(03\bar{3}1)$ *plane of quartz (a) and measured CR spectrum for 32 MeV electrons (b) at a crystal thickness of 200 µm.*

3.5.1 Transition energies

The photon energies of several CR lines separated in the corresponding spectra are compared with calculated transition energies in Tab. 3.2. The errors given in column 4 of Tab. 3.2 reflect only the accuracy of the fit procedures performed for approximation of Lorentzians to the experimental data.

Table 3.2 Measured and calculated energies of separated CR lines from planar electron channeling in quartz.

E_e (MeV)	Plane	Transition	Measured energy (keV)	Calculated energy (keV)
17	$(0\bar{2}23)$	1→0	9.20±0.02	10.04
		2→1	—	4.99
25	$(0\bar{2}23)$	1→0	18.53±0.04	18.42
		2→1	13.44±0.05	12.08
32	$(0\bar{2}23)$	1→0	27.52±0.04	27.26
		2→1	20.21±0.03	20.16
32	$(0\bar{1}11)$	3→0	24.57±0.15	25.91
		4→1	33.65±0.14	34.87
32	$(0\bar{1}12)$	1→0	20.59±0.16	23.11
		2→1	15.60±0.15	16.99
		3→2	—	11.88
32	$(01\bar{1}3)$	1→0	26.03±0.03	27.83
		2→1	—	4.23
32	$(01\bar{1}5)$	1→0	19.80±0.04	23.95
32	$(03\bar{3}1)$	1→0	23.44±0.06	26.73
		2→1	17.87±0.06	18.09

The uncertainty of the measured CR photon energies, however, is mainly determined by the accuracy of the energy tuning of the electron beam that was evaluated to be less than 1.5 %. Therefore, taking the scaling of the CR photon energy with the electron energy into account, the accuracy of the measured energies should not be better than about 2.5 %, i.e., the absolute errors amount to values between 0.4 and 0.6 keV. Remaining small discrepancies may be attributed to slight crystal misalignment during the measurements, to the effect of multiple scattering, and also to the imperfectness of the quartz crystals used.

3.5.2 CR line widths

As explained in chapter 1, the CR line shape registered in a CR measurement is governed by several line-broadening mechanisms. In the case of quartz, the intrinsic CR line width dominates the total line width to a higher degree than in diamond crystals because of the lower Debye temperature (≈1000 K). The imaginary part of the complex potential of the $(0\bar{2}23)$ plane is shown in Fig. 3.17 for 32 MeV electrons. A comparison of Fig. 3.17 with, e.g., Fig. 1.7 valid for diamond reveals that the imaginary part of the continuum potential of quartz is not strongly located at the channeling plane and it is broader. Therefore, the coherence lengths for quartz crystals are much smaller than for diamond.

Table 3.3 Partial contributions to the total CR line widths calculated by the many-beam formalism and measured line widths for electrons channeled in different planes of quartz.

E_e (MeV)	Plane	Transition	Γ_{in} (keV)	Γ_{Bloch} (keV)	Γ_{Dop} (keV)	Γ_{det} (keV)	Calculated line width (keV)	Observed line width (keV)
17	$(0\bar{2}23)$	1→0	0.92	0.64	0.60	0.50	1.37	1.62±0.05
		2→1	0.59	4.15	0.30	0.50	4.23	—
25	$(0\bar{2}23)$	1→0	2.09	0.31	1.10	0.50	2.43	3.38±0.13
		2→1	1.47	3.27	0.72	0.50	3.69	3.28±0.15
32	$(0\bar{2}23)$	1→0	3.27	0.15	1.63	0.50	3.90	4.65±0.12
		2→1	2.67	2.27	1.21	0.50	3.74	4.88±0.10
32	$(0\bar{1}12)$	1→0	2.88	0.00	1.38	0.50	3.23	4.23±0.55
		2→1	1.99	0.05	1.02	0.50	2.29	5.01±0.47
		3→2	1.81	1.75	0.71	0.50	2.66	—
32	$(01\bar{1}3)$	1→0	3.13	0.72	1.67	0.50	3.65	4.85±0.10
		2→1	2.21	2.99	0.25	0.50	3.76	—
32	$(01\bar{1}5)$	1→0	2.97	4.31	1.43	0.50	5.45	5.02±0.11
32	$(03\bar{3}1)$	1→0	3.29	0.22	1.60	0.50	3.70	3.65±0.22
		2→1	2.55	2.76	1.08	0.50	3.94	4.88±0.19

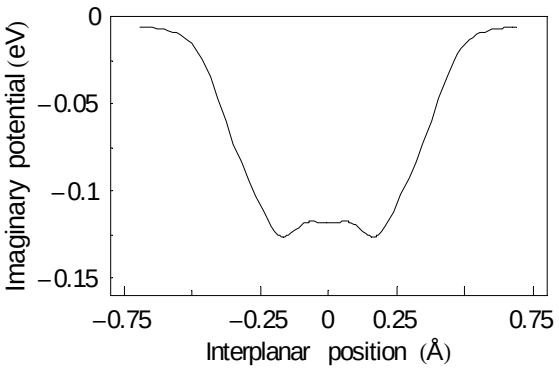

Fig. 3.17 Imaginary part of the complex potential of the $(0\bar{2}23)$ *plane of quartz calculated for the electron energy of 32 MeV.*

The partial contributions to the total CR line width Γ_{tot} are listed in Tab. 3.3 for a 200 μm thick quartz crystal. The Doppler broadening is calculated by mean of Eq. (1.48). As discussed in chapter 1, the mean multiple-scattering angle may be found by a peak shape analysis of measured CR lines. In the case of quartz, the statistics of the measured CR peaks as well as the overlap of CR lines prevent an application of this method. Therefore, the mean multiple scattering angle could be deduced for the $(0\bar{2}23)$ plane only. The obtained value amounts to about $(0.3 \div 0.5) \times \theta_{ms}$, where θ_{ms} means the root-mean- squared multiple-scattering angle for non-channeled electrons.

The coherence length is the main source of CR line-broadening for transitions between tightly bound states. Otherwise, for transitions from states located near to the top of the continuum potential, the main contribution to the total line width results from Bloch wave broadening. The total line width given in column 8 of Tab. 3.3 is a quadratic additive of all partial contributions. Nevertheless, the observed values of the CR line with are in a reasonable agreement with the calculated ones, but they are consistently larger.

3.5.3 CR photon yields

According to Eq. (1.59) the photon yield of CR is proportional to the integral of the occupation function $P_i(z)$ along the crystal depth z. This depth dependence has been determined for the $(0\bar{2}23)$ plane of quartz and the electron energy of 32 MeV by solving the system of coupled differential equations given in Eq. (1.63) numerically for δz = 0.01 μm. The occupation of bound states as function of the crystal depth is shown in Fig. 3.18 for an electron beam with an angular divergence of σ_{beam} = 0.3 mrad incident to the quartz crystal under an angle θ = 0.3 mrad.

In order to investigate the variation of the CR yield with the crystal thickness, a numerical integration has been performed for the transitions 1→0 and 2→1 (Figs. 3.19 and 3.20).

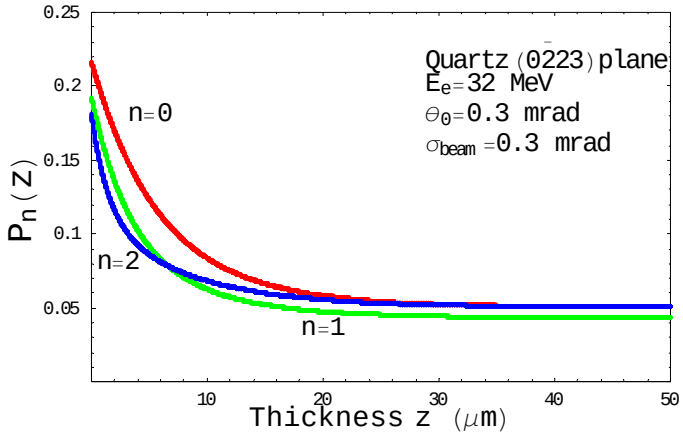

Fig. 3.18 Occupation of bound states in the $(0\bar{2}23)$ *plane of quartz as function of the crystal thickness at an electron beam divergence of 0.3 mrad and for the incidence angle of 0.3 mrad.*

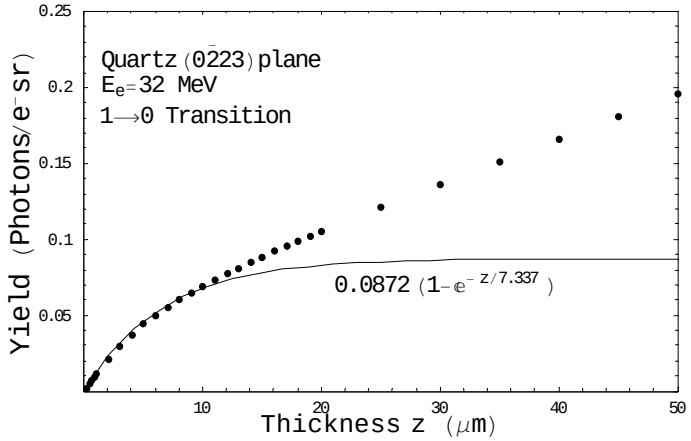

Fig. 3.19 Total CR photon yield for the 1⟶0 transition in the $(0\bar{2}23)$ *plane of quartz as function of the crystal thickness for 32 MeV electrons. The dots represent calculated values. The line corresponds to an exponential decay of the occupation probability.*

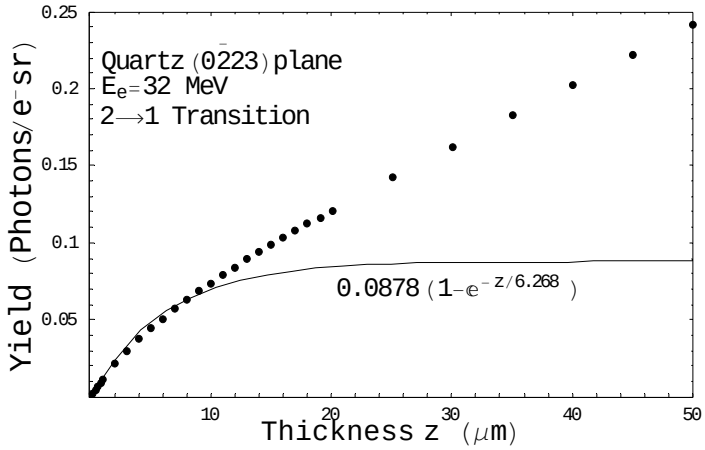

Fig. 3.20 The same as shown in Fig 3.19. but for the 2⟶1 transition.

As has been found for diamond, the occupation of bound states quickly decreases with increasing crystal depth and reaches equilibrium near to a penetration depth of 20 μm (see Fig. 3.18). Therefore, the calculated CR yields further on change linearly (see Figs. 3.19 and 3.20). However, due to multiple scattering, the equilibrium occupation of states can actually not survive, and the channeled electrons will successively be dechanneled.

The calculated CR photon yields have been approximated at small crystal thicknesses by a curve representing the function $P_n(0)(1-e^{-z/l_{occ}})$, where the occupation length l_{occ} was found to amount to 7.337 μm and 6.268 μm for the initial states with n = 1 and n = 2, respectively.

The CR photon yields obtained for resolved CR lines and for different planes in quartz are listed in Tab. 3.4. and compared with values estimated by the use of corresponding functions as drawn in Figs. 3.19 and 3.20. Surprisingly, the measured and estimated yields mostly agree with acceptable accuracy. It is obvious from Figs. 3.19 and 3.20, that a direct comparison of measured and calculated CR photon yields should be performed for real crystal thicknesses being less than 20 μm. The found reasonable agreement between measured and estimated yields probably points at the fact that in-plane multiple scattering plays for quartz a less role than for diamond. The de-population of states proceeds similar to an exponential decay with a short occupation length.

Table 3.4 Calculated and measured yields of CR from 32 MeV electrons channeled in quartz.

E_e (Me	Plane	Transition (i→f)	$P_i(0)$	l_{occ}^{calc} (μm)	$d^2N_{i\to f}/d\Omega dz^{calc}$ $(photons/e^- sr)$	$Yield^{exp}$ $(photons/e^- sr)$
32	$(0\bar{2}23)$	1→0	0.087	7.34	0.087	0.122
		2→1	0.088	6.27	0.088	0.081
32	$(0\bar{1}12)$	1→0	0.125	5.91	0.036	0.032
		2→1	0.118	5.97	0.036	0.045
32	$(01\bar{1}5)$	1→0	0.245	7.06	0.075	0.069
32	$(01\bar{1}3)$	1→0	0.173	6.38	0.075	0.069
32	$(03\bar{3}1)$	1→0	0.195	7.75	0.098	0.041
		2→1	0.184	6.84	0.081	0.075

3.6 Conclusions

Planar CR generated by electrons of medium energies in different crystal planes of quartz has for the first time been measured and analyzed. The hexagonal structure of α-quartz provides a variety of crystal planes which are very close to each other. Compared with the diamond structure, this feature complicates the mapping of planes and the assignment of relevant indices to observed CR spectra. The

calculations of the planar continuum potentials as well as the corresponding channeling states by means of the many-beam formalism considerably facilitated the identification of the measured CR data.

The analysis of different line-broadening mechanisms contributing to the total CR line width has been investigated for CR line separated in the measured spectra. The intrinsic CR line widths were estimated by the use of the complex optical potential. Compared with diamond, the imaginary parts of the planar potentials of quartz are broader. Therefore, the intrinsic CR line widths are nearly two times larger than those found for diamond and dominate for the tightly bound states. The values of transition energies and line widths obtained from many-beam calculations are in reasonable agreement with measured values.

The occupation functions of bound states have been calculated by solving the system of coupled differential equations numerically. It has been found that equilibrium occupation of bound states is reached in quartz at a penetration depth of nearly 20 μm. Since the thickness of the quartz crystal amounted to 200 μm, accurate adjustment between experimental and theoretical CR yields was not possible.

Reminding the suggestion to stimulate CR emission by US excited in the crystal, the CR data obtained in the present work for quartz are of fundamental interest for a dedicated evaluation of the effect of US and the choice of suitable crystal planes. The relatively large crystal thickness used for the CR measurements was also chosen in view of such investigations.

Chapter 4

Resonator cavity

4.1 Introduction

In order to investigate the influence of US on CR emission, acoustic vibrations have to be excited in the quartz single crystal by means of ultrasonic waves propagating through the crystal. From Refs. [Gri00a÷c, Gri01a÷e, Gri03a÷b, Ava06a÷b], and also from the results of CR measurements on quartz described in chapter 3 of this work, it is clear that US frequencies in the GHz region are necessary. A brief survey of electromagnetic cavity resonators and its application for the generation of ultrasonic waves in a piezoelectric crystal will be given in the present chapter.

Cavity resonators are metallic enclosures that can trap electromagnetic high-frequency fields. The boundary conditions at the cavity walls force the field to be exit only at certain quantized resonant frequencies.

The source-free Maxwell equations read

$$\begin{aligned} \vec{\nabla} \times \vec{E} + \partial \vec{B} / \partial t &= 0 \\ \vec{\nabla} \times \vec{H} - \partial \vec{D} / \partial t &= 0 \\ \vec{\nabla} \cdot \vec{B} &= 0 \\ \vec{\nabla} \cdot \vec{D} &= 0 \end{aligned} \tag{4.1}$$

with $\vec{D} = \varepsilon \vec{E}$ and $\vec{B} = \mu \vec{H}$. For radio-frequency (RF) cavities, a classification can be made with respect to the resonance modes. With the conditions

$$\begin{aligned} E_z = 0, H_Z \neq 0 \quad & \text{TE modes} \\ E_z \neq 0, H_z = 0 \quad & \text{TM modes} \end{aligned} \tag{4.2}$$

transverse electric (TE) or transverse magnetic (TM) modes are defined in accordance with the longitudinal field components.

In our case, the so called accelerating mode of a cylindrically symmetric cavity is of interest. In TM mode, the radial (r) and longitudinal (z) components of the magnetic field and the azimuthal component (φ) of the electric field vanish. If one assumes

$$H_\phi(r,z,t) = H_\phi(r,z)\cos\omega t \tag{4.3}$$

and defines the wave number $k = w/c$, then the Maxwell equations in cylindrically symmetric geometry can be written in the form

$$\frac{\partial}{\partial r}\left[\frac{1}{r}\frac{\partial}{\partial r}(rH_\varphi(z,r))\right] + \frac{\partial^2 H_\phi(z,r)}{\partial z^2} + K^2 H_\phi(z,r) = 0 \tag{4.4}$$

$$E_r(z,r,t) = -\frac{1}{K}\frac{\partial H_\phi(z,r)}{\partial z}\sin\omega t \tag{4.5}$$

$$E_z(z,r,t) = \frac{1}{Kr}\frac{\partial}{\partial r}(rH_\phi(z,r))\sin\omega t. \tag{4.6}$$

Here Eq. (4.4) is the Helmholtz eigenvalue equation, and the other two equations define the components of the electric field. The Helmholtz equation is an elliptic partial differential equation. Hence, the same type of boundary conditions are required for its solution as for the generalized Poisson equation. Namely, *Φ(x)* or its derivative must be specified at all boundary positions, but not both at the same position. The Helmholtz equation can be solved analytically for simple geometries or numerically for complex geometries.

4.2 Pillbox cavity

A pillbox resonator (Fig. 4.1) is a cylindrical cavity, for which analytical solutions of the Helmholtz equation can be deduced, and the resonant frequency, stored energy, quality factor, etc. can be defined.

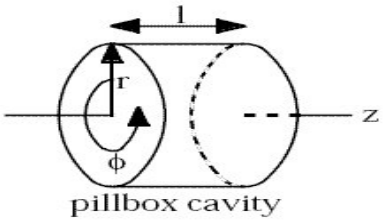

Fig. 4.1 Pillbox cavity

The accelerating modes TM_{mni} for the pillbox cavity are denoted by three subscripts, where m is the number of full periods in azimuth φ , n is the number of radial zeros of the field, and i is the number of half–period variations in the z direction.

The analytical solutions of the Helmholtz equation for TM_{mni} read

$$E_z(r,z,t,\phi) = E_\circ J_m(\frac{x_{mn}}{a}r)e^{i\omega t}\cos(m\phi)\cos(k_z z) \tag{4.7}$$

$$H_\phi(r,z,t,\phi) = H_\circ J'_m(\frac{x_{mn}}{a}r)e^{i\omega t}\cos(m\phi)\cos(k_z z) \tag{4.8}$$

where $k_z = i\pi/l$, i ≥ 0, x_{mn} are roots of the Bessel function, and a and l denote the radius and the length of the cavity, respectively. The resonant frequency is given by

$$\gamma_0 = c\sqrt{(\frac{x_{mn}}{2\pi a})^2 + \frac{1}{4}(\frac{i}{l})^2} \quad . \tag{4.9}$$

Several TM_{mni} and TE_{mni} modes of a pillbox cavity are shown in Fig. 4.2.

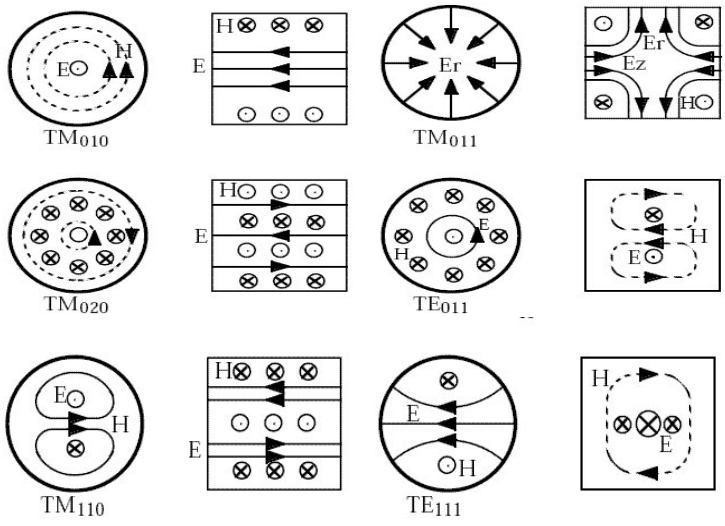

Fig. 4.2 TM_{mni} and TE_{mni} modes of a pillbox cavity

The dependence of the resonance frequency f_r on the diameter and the length of a pillbox cavity are shown in Fig. 4.3 for TM_{mni} modes.

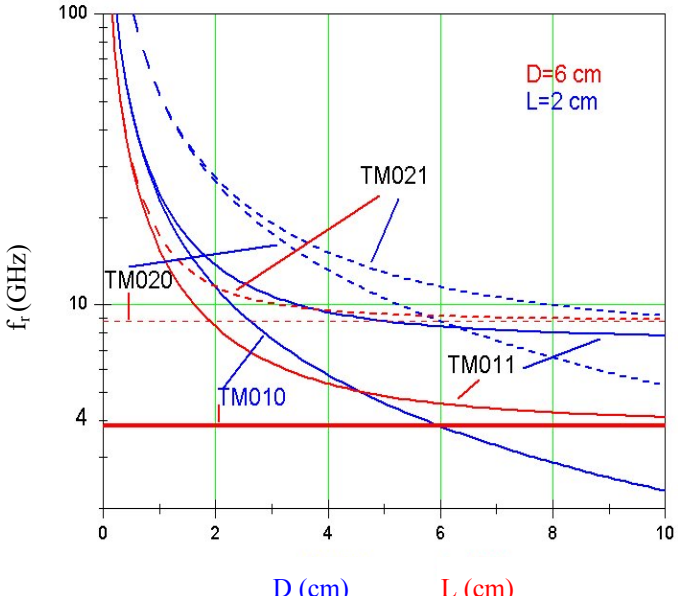

Fig. 4.3 Resonance frequency of the pillbox cavity as function of the diameter D (blue curves with L=2 cm) and length L (red curves and D=6 cm) for different TM_{mni} modes.

For the calculation of the field distribution in a pillbox, the program package Superfish [Bil03] has been applied. Depending on the given boundary conditions, the solutions of the Helmholtz equation for a definite cavity are either TM_{mni} or TE_{mni} modes. The program Superfish provides plots of the electric field, calculates the quality factor, the power losses in the walls of the cavity, and the sensitivity of the eigenfrequencies to small perturbations of the structure of the cavity.

For the excitation of longitudinal acoustic waves in the piezoelectric quartz crystal, only the TM_{0n0} modes are of interest. At these modes, the r and φ components of the electric field are zero. The electric field is always directed parallel to z, and the resonance frequency depends only on the radius of the cavity. The electric field, being directed perpendicular to the surface of a piezoelectric crystal positioned inside the pillbox cavity, excites longitudinal acoustic vibrations in the crystal.

For illustration, the output from the program Superfish is shown in Figs. 4.4 ÷ 4.9 for a cylindrical cavity and for different modes, where the arrows indicate the magnitude and direction of the electric field. In Figs. 4.8 and 4.9, the field distribution is shown for a coaxial cavity without and with a quartz crystal, respectively. Here an electric field exists only in the volume V' at the end of the coaxial hollow pipe near to the crystal surface, and in the remaining volume V of the cavity the electric field is nearly equal to zero. The strength of the electric field is stronger than for the other configurations. Therefore, this geometry has

been chosen for the prototype of a resonator cavity to be used in first experimental investigations of the influence of US on CR emission in quartz.

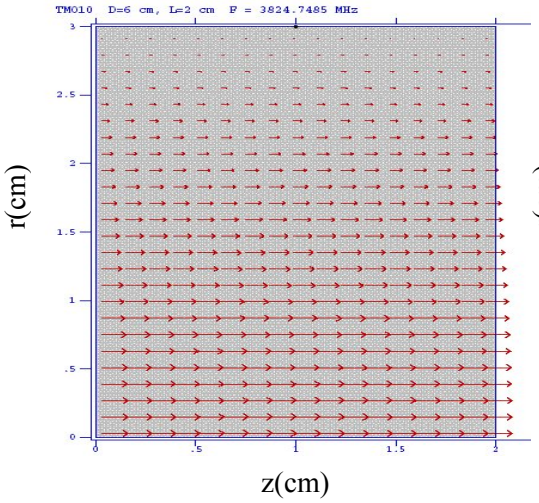

Fig. 4.4 TM010 mode , f=3824.4785 MHz.

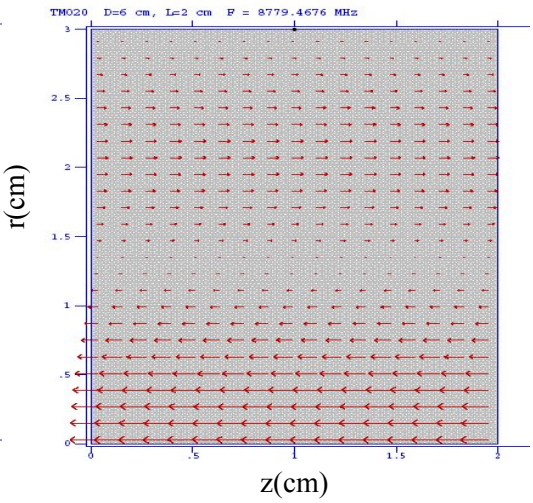

Fig. 4.5 TM020 mode , f=8779.4676 MHz.

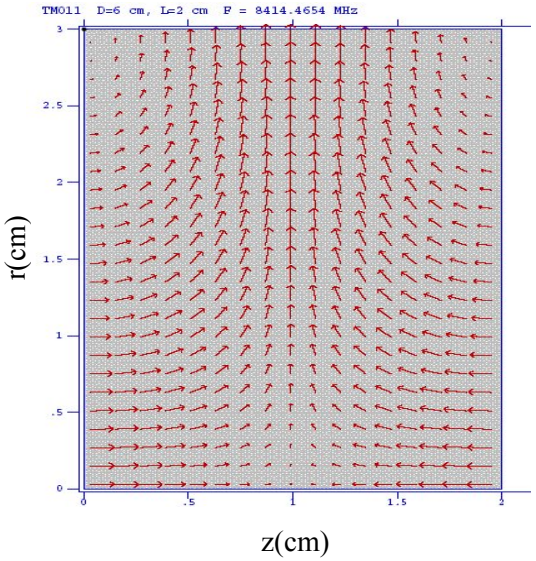

Fig. 4.6 TM011 mode , f=8414.4654 MHz.

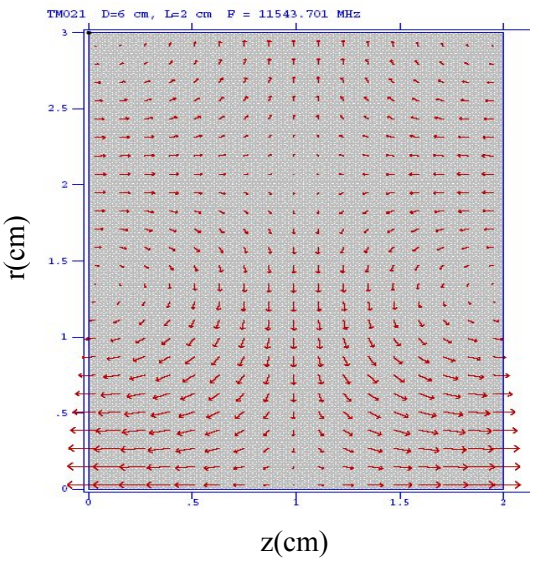

Fig. 4.7 TM021 mode , f=13763.7400 MHz.

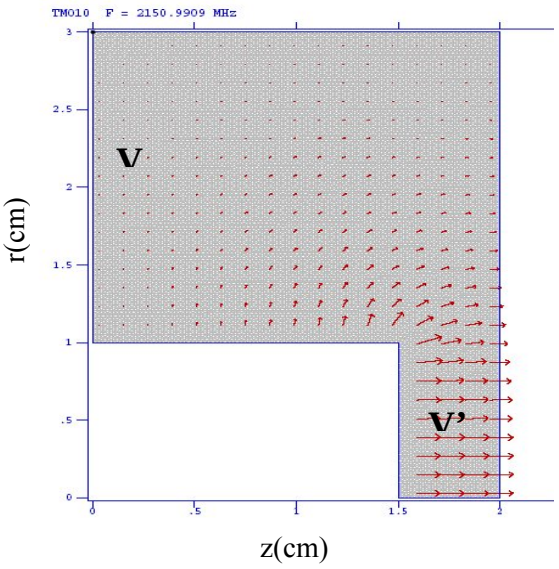

Fig. 4.8 Coaxial cavity without quartz crystal, f=2150.9909 MHz.

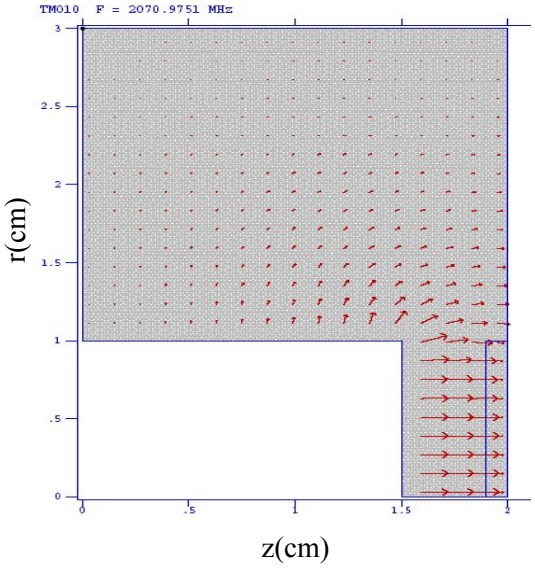

Fig. 4.9 Coaxial cavity with quartz crystal, f=2070.9751 MHz.

Chapter 5

Influence of ultrasound on planar channeling radiation

This chapter is devoted to the evaluation of the influence of US on planar CR from electrons channeled in the piezoelectric quartz crystal.

The quantum mechanical description of CR under the influence of ultrasonic waves excited in a single crystal has been considered in Refs. [Bar80, Mkr86, Mkr88, Ded94, Ave97, Gri00a÷c, Gri01a÷e, Gri03a÷b]. In the framework of the perturbation theory it has been shown that resonance effects are possible, if the frequency of US approaches values corresponding to some difference between transversely bound states in the planar continuum potential.

The perturbation theory is, however, not applicable at resonance. Therefore, theoretical methods from the non-linear optics have been adopted in Ref. [Ava06a] and applied in Ref. [Ava06b] for the description of CR emitted by 20 MeV electrons channeled in a vibrating quartz crystal. These calculations, performed for the $(01\bar{1}1)$, $(01\bar{1}0)$ and $(0\bar{1}11)$ planes of quartz, predict a spectral redistribution of CR emitted under the influence of resonant US.

In the following paragraphs, both above mentioned theoretical approaches will be applied for the calculation of US-influenced CR generated in different planes of quartz, aiming at the deduction of prerequisites for experimental investigations. Further on, the setup and the results of a first measurement of CR with US excitation of the quartz crystal will be presented, which has been carried out at ELBE.

5.1 Perturbation theory

In Ref. [Gri03b] a standing acoustic wave is assumed to be excited in the crystal along the direction of the relativistic motion of the channeled particle (z-axis). The planar transverse potential

$$\bar{V}(x,z) = \langle V(x) \rangle \Lambda(z) \tag{5.1}$$

is modulated by the factor $\Lambda(z) \cong 1 + 2\sum_{m=1,2,..}(-1)^m J_m(mk_s a^*)\cos\left[m\left(k_s z + \varphi\right)\right]$, where $\langle V(x)\rangle$ is the undisturbed continuum potential of the plane considered, $a^* = a\sin(\omega_s t)$, $J_m(z)$ denotes the Bessel function, and k_s is the wave number of US. According to Eq. (5.1), the factor Λ does not dependent on the crystal parameters. The wave function of a channeled particle is then determined by a two dimensional Schrödinger equation

$$\frac{-\hbar^2}{2m\gamma}\left(\frac{d^2}{dx^2}+\frac{d^2}{dz^2}\right)\psi(x,z)+\overline{V}(x,z)\psi(x,z)=E\psi(x,z)\,. \tag{5.2}$$

This equation describes the quantum states of the channeled particle in the ultrasonic field, where the variables x and z in the wave function $\psi(x,z)$ are not separable. Therefore, an accurate solution of Eq. (5.2) is difficult, and some approximations have to be made. In accordance with the perturbation theory, the wave function $\psi(x,z)$ can be expanded into a series of orthogonal functions $U_{kn}(x)$ of the non-disturbed system (i.e., in the absence of US)

$$\psi(x,z)=\sum_{kn}C_{kn}(z)U_{kn}(x)\,. \tag{5.3}$$

The coefficients $C_{kn}(z)$ are calculated in Ref. [Gri01e]. In a linear approximation, the wave function of the channeled particle represents a superposition of three plane waves with the phases $(p_z - v\hbar k_s)z/\hbar$, $v=0,\pm 1$. The interaction of the channeled relativistic charged particle with the standing ultrasonic wave excited in the crystal leads to the splitting of the projection of its momentum in channeling direction into three components: $p_z-\hbar k_s$, p_z, $p_z+\hbar k_s$. The term $\hbar k_s$ denotes the momentum associated with an acoustic phonon. The Doppler formula for the frequency of CR photons [cf. Eq. (1.58)] emitted in the presence of US takes the form

$$\hbar\omega=\frac{\left(\varepsilon_i-\varepsilon_f-v\hbar c k_s\right)}{\left(1-\beta\cos\theta\right)},\ v=0,\pm 1 \tag{5.4}$$

Theoretical considerations of the influence of US on CR [Gri01e] predict additional radiative transitions, which may lead to an amplification of the total CR intensity. It has been shown in Ref. [Gri01e] that a resonance effect can take place, if the frequency of US approaches some critical value. This value corresponds to the energy difference between the bound states *i* and *f* of transverse motion of the channeled particle, i. e., $k_s=\left|\varepsilon_i-\varepsilon_f\right|/\hbar c$. The frequency of US necessary for resonance reads

$$\nu_n^* = \frac{V_s}{c}\frac{\left|\varepsilon_f - \varepsilon_i\right|}{h} \tag{5.5}$$

where V_s is the velocity of US inside the crystal. Values calculated for the resonance frequency of US for planar channeling of 30 MeV electrons in selected planes of quartz are listed in Tab. 5.1.

Table 5.1 Calculated resonance frequencies for 30 MeV electrons channeled in selected planes of quartz.

Plane	Transition	Frequency of US (GHz)
$(01\bar{1}1)$	1→0	15.26
$(0\bar{2}23)$	1→0	14.33
	2→1	9.62
$(01\bar{1}5)$	1→0	12.44

In Ref. [Gri01c] two types of transitions of channeled electrons are indicated, namely direct transitions given by $n_i - n_f > 0$ and inverse transitions given by $n_i - n_f < 0$ for $v = -1$ [cf. Eq. (5.4)]. It has been shown that the impact of US on direct radiative transitions of channeled electrons is negligibly small, but for inverse transitions some resonance effect can occur. In the simplest case of resonance, three transversely bound states of the channeled electron are involved (see Fig. 5.1). Note that resonance for inverse transitions occurs when $\hbar k_s \to \varepsilon_3 - \varepsilon_1$. Therefore, the resonance frequency increases in this case by nearly a factor of two.

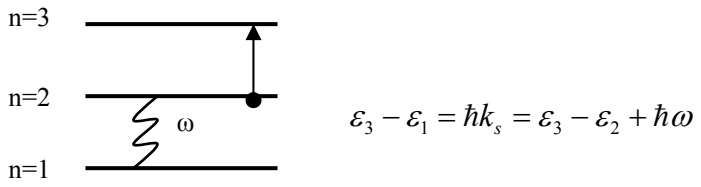

Fig. 5.1 The channeled electron in the state n=2 absorbs the energy $\hbar k_s$ of an US phonon, fulfills the inverse transition 2→3 and emits a CR photon of energy $\hbar\omega$.

5.2 Non-linear optics method

The effect of a driving external electric field on the spectrum of spontaneous radiation emission from a simple physical system has been developed in Refs. [Mol69, Mol70]. It has been shown that the external field splits the Lorentzian line shape observed for spontaneous emission of the undisturbed system into several components. This method has been adopted in Ref. [Ava06a÷b] for the description of CR emitted under the influence of US.

The details of the non-linear optics method are out of the scope of this work, but results obtained by formal application of this method for the calculation of the spectrum of CR in the presence of US will be presented in the following.

The spectral distribution of CR photons emitted in forward direction for a crystal momentum $k = 0$ is given by Eq. (1.59). In order to include the crystal momentum k into Eq. (1.59), the integration over all Bloch momenta in the first Brillouin zone is performed

$$\frac{d^2N_{CR}(i\to f)}{d\Omega_\gamma dE_\gamma}=\frac{\alpha\lambda_c^2}{\pi\hbar c}2\gamma^2\int_{-g/2}^{g/2}dk(E_{ki}-E_{kf})\left|\left\langle\psi_{kf}\left|\frac{d}{dx}\right|\psi_{ki}\right\rangle\right|^2\times \\ \int_0^L dze^{-\mu_{(E_\gamma)}(L-z)}\beta_i(k,z)\times\frac{1}{\pi}\frac{\Gamma_{fi}/2}{(\Gamma_{fi}/2)^2+(E-E_{k0})^2} \tag{5.6}$$

where, unlike Eq. 1.59, the Doppler broadening can be neglected, because for a quartz crystal the condition $\gamma^2\theta^2_{ms,ch}\ll 1$ is valid. The occupation of the initial state i at the crystal depth z is described by the function $\beta_i(k,z)$. Both the integrals over the Bloch momenta and over the crystal thickness L have been taken numerically.

According to Ref. [Ava06b], the spectral distribution of CR at the resonance condition $\hbar k_s=\left|\varepsilon_i-\varepsilon_f\right|$ is given by

$$\frac{d^2N_{CR}(i\to f)}{d\Omega_\gamma dE_\gamma}=\frac{\alpha\lambda_c^2}{\pi\hbar c}2\gamma^2\int_{-g/2}^{g/2}dk(E_{ki}-E_{kf})\left|\left\langle\psi_{kf}\left|\frac{d}{dx}\right|\psi_{ki}\right\rangle\right|^2\times \\ \int_0^L dze^{-\mu_{(E_\gamma)}(L-z)}\sum_{i=1}^{3}C_i\frac{1}{\pi}\frac{\Gamma_{fi}/2}{(\Gamma_{fi}/2)^2+(E-W_i)^2} \tag{5.7}$$

where the following conventions have been made:

$$C_1 = \frac{2R^2}{\Omega^2}\overline{\beta}(z) + \frac{R^2\Delta^2}{\Omega^4}\mathrm{B}$$

$$C_2 = \frac{(\Omega+\Delta)^2}{4\Omega^2}\overline{\beta}(z) - \frac{R^2(\Omega+\Delta)^2\Delta}{2\Omega^4}\mathrm{B}$$

$$C_3 = \frac{(\Omega-\Delta)^2}{4\Omega^2}\overline{\beta}(z) + \frac{R^2(\Omega-\Delta)^2\Delta}{2\Omega^4}\mathrm{B}$$

$$\mathrm{B} = (\beta_{kf}^0 - \beta_{ki}^0)(1-\cos\Omega z)\exp(-k_{II}z)$$

$$\overline{\beta}(z) = \rho_k^0 + \left[\beta_{ki}^0 - \rho_k^0 + \frac{2R^2}{\Omega^2}(\beta_{kf}^0 - \beta_{ki}^0)(1-\cos\Omega z)\right]\exp(-k_{II}z)$$

$$R = e\varepsilon_0\left\langle\psi_{kf}\left|p_x\right|\psi_{ki}\right\rangle/(m\omega_0^k)$$

$$\Omega = \sqrt{\Delta^2 + 4R^2}$$

$$\varepsilon_0 = 4V_0X_0/ed^2$$

$$\Delta = W - E_0^k$$

$$W = \hbar k_s$$

$$W_1 = W\ ; W_2 = W - \Omega\ ; W_3 = W + \Omega$$

Here X_0 denotes the magnitude of transverse deformation of the planes by US, β_{ki}^0 and β_{kf}^0 are the initial populations of the states *ki* and *kf*, respectively, and ρ_k^0 and k_{II} are parameters used for the approximation of the occupation function $\beta(z)$ without crystal deformation

$$\beta(z) = \rho_k^0 + \left[\beta_{ki}^0 - \rho_k^0\right]\exp(-k_{II}z)\,. \tag{5.8}$$

For $R \to 0$, i.e., when the crystal deformation $X_0 \to 0$, Eq. (5.7) approaches Eq. (5.6). The effect of US consists in the splitting of the undisturbed Lorentzian line shape of CR into three components. One component is centered at the usual CR energy, the two other ones have lower magnitude and form satellite lines positioned symmetrically to both sides from the main CR line, shifted by the amount of the saturation parameter Ω. Each of these three Lorentzians has the line width Γ_T characteristic for spontaneous CR emission.

The spectral distribution of CR from the transition 1→0 of 9 MeV electrons channeled in the (110) plane of a 13 μm thick diamond crystal has been calculated in Ref. [Ava06a] for various assumed values of the ratio of the deformation magnitude to half the interplanar distance. Note that this is a formal model calculation to compare the obtained results with experimental spectra measured in Ref. [Gen96]. Since diamond is no piezoelectric crystal, the excitation of ultrasonic vibrations in this crystal is not possible by means of external electromagnetic RF fields as described in chapter 4 of this work, and no other method has been specified which could be applied to deform a diamond crystal. It

could, however, been demonstrated by these calculations that the assumed crystal deformation leads to a modification of the emitted CR spectrum.

Another somewhat more realistic example concerns the spectral distribution of CR from the transition 6→5 of 20 MeV electrons channeled in the $(0\,\bar{1}\,1)$ plane of quartz [Ava06a]. It has been shown that the distance between the satellite lines and the main CR line increases with increasing magnitude of deformation, but the total number of emitted CR photons varies insignificantly. It has been concluded in Ref. [Ava06a] that some influence of the crystal deformation on the spectral distribution of CR generated by electrons channeled in quartz could not so clearly been demonstrated as has been done in the case of diamond.

The CR line splitting caused by the effect of US is associated with the sinusoidal modulation of the occupation function of the initial state *i* due to the coupling with the driving field. According to Eq. (5.7) the CR rate should increase, if the initial population of the final state *f* considered for some assumed transition is larger than that of the initial state *i*. In order to prove this hypothesis, numerical calculations have been carried out in this work for the effect of US on the spectral distribution of CR from the 1→0 transition of 30 MeV electrons channeled in the $(01\,\bar{1}\,5)$ plane of quartz. As has been shown in chapter 3, there are only two bound transversal states in this plane at the energy of the channeled electrons considered. Moreover, the initial state for the 1→0 transition is rather close to the top of the planar continuum potential. Therefore, the initial state *i* is characterized by a rather broad Bloch band. The depth dependence of the occupation function of this state is shown in Fig 5.2 for different values of *k*. As can be seen in this figure, equilibrium occupation of transversal states is reached after a penetrating depth of about 10 μm. Therefore, some redistribution of the CR spectrum due to US impact should be observed, if the crystal thickness is of the same order of magnitude.

For illustration of the results of the preformed calculations, the spectral distribution of CR from the 1→0 transition of 20 MeV electrons channeled in the $(01\,\bar{1}\,5)$ plane of quartz at resonant US impact is shown in Fig. 5.3 for Bloch momenta $k = 0.1g$. As can be seen, the crystal deformation due to US results in a splitting of the main CR line. For the estimation of the full effect of US, the spectral distribution of CR obtained at resonance has to be integrated over all Bloch momenta *k*. If the strength of the driving field is assumed to be large enough, every Lorentzian CR line corresponding to some Bloch momentum *k* will be split into three Lorentzians, and the resulting spectral distribution observed for CR out of the $(01\,\bar{1}\,5)$ plane of quartz is more complicate (Fig. 5.4).

Due to the larger interplanar distances and the broader continuum potentials of the $(01\,\bar{1}\,1)$ and $(0\,\bar{1}\,1\,1)$ planes of quartz (see chapter 3), a larger number of CR lines contribute and superimpose in the observed CR spectrum. When the effect of US on CR out of these planes should principally be the same as discussed for the $(01\,\bar{1}\,5)$ plane, its observation and interpretation should be more difficult.

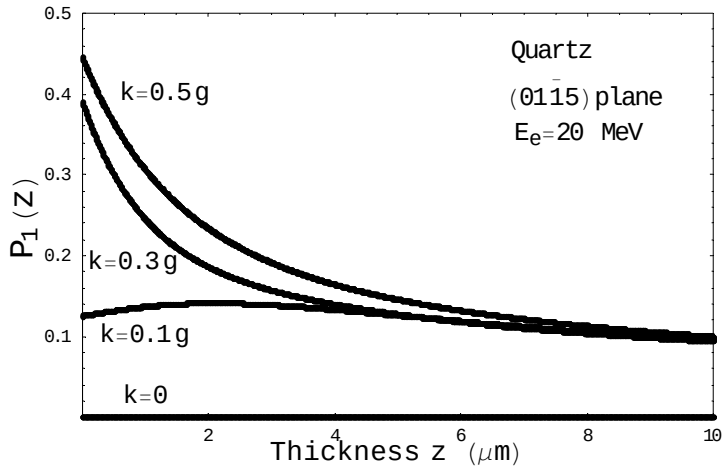

Fig. 5.2 Depth dependence of the occupation function of the state n=1 calculated for different values of the Bloch momentum k for channeling of 20 MeV electrons in the $(01\bar{1}5)$ *plane of quartz.*

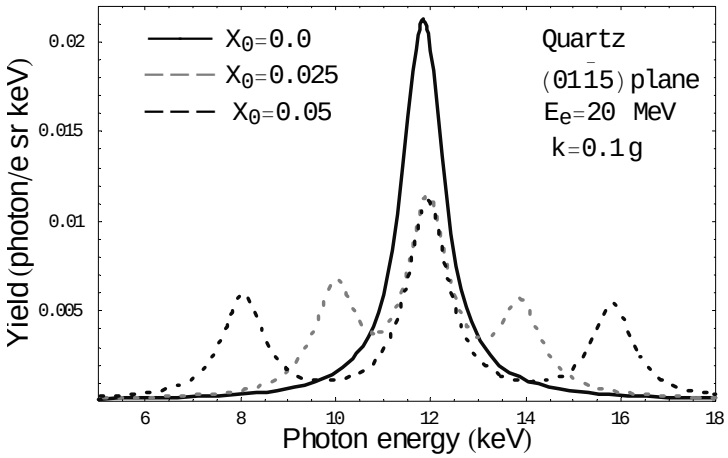

Fig. 5.3 Spectral distribution of CR from 20 MeV electrons channeled in the $(01\bar{1}5)$ *plane of a 20 μm thick quartz crystal calculated for a Bloch momentum k=0.1g and values of the relative deformation* $X_0 = 0,\ 0.025$ *and* 0.05.

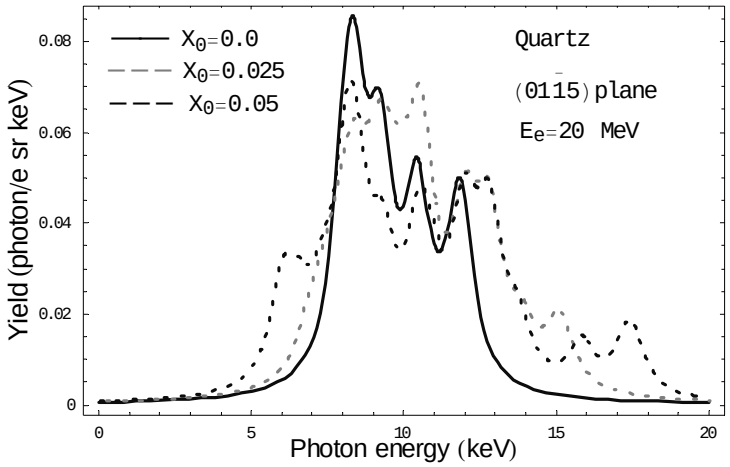

Fig. 5.4 Spectral distribution of CR from 20 MeV electrons channeled in the $(01\bar{1}5)$ *plane of a 20 μm thick quartz crystal calculated for the entire interval of Bloch momenta –g/2 ≤ k ≤ g/2 and values of the relative deformation* $X_0 = 0,\ 0.025$ *and* 0.05 *at resonant US impact.*

5.3 Experimental investigation of the influence of US on CR

In a first series of experiments performed at the electron beam of the radiation source ELBE, the influence of non-resonant US on the CR generated in different planes of a 500 μm thick quartz crystal should be investigated. A coaxial cavity designed for a resonance frequency of 2.5 GHz has been constructed (see chapter 4) and carefully matched to the small-band RF amplifier which delivered a maximum output power of 20 W. Since the calculated *Q*-value of the cavity amounted to 4000, the input frequency had to be tuned carefully by means of a stabilized RF signal generator.

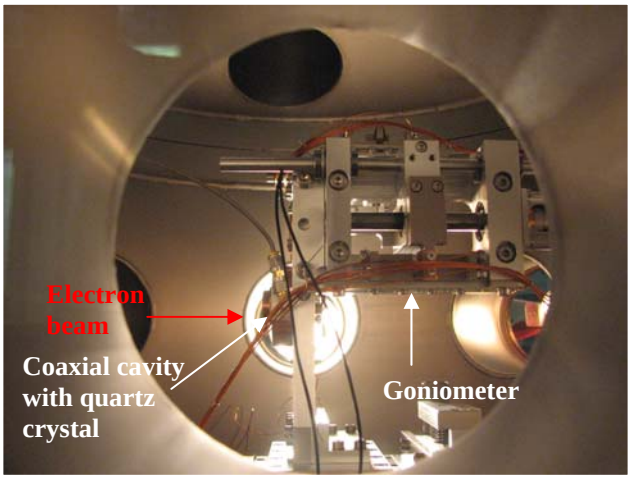

Fig. 5.5 Experimental setup for the generation of ultrasonic vibrations in the quartz crystal.

A photograph of the goniometer with mounted cavity is shown in Fig. 5.5. The electron beam enters the coaxial cavity (cf. Fig. 4.9) from the left side through an entrance pipe of diameter 15 mm and a hole of diameter 5 mm. The quartz crystal positioned inside the cavity is elastically pressed on the Cu cap of the resonator, where another hole of diameter 5 mm is left as beam exit. The gap between the entrance hole and the surface of the crystal is variable within certain limits for tuning the cavity to the chosen resonance frequency. The RF waves were magnetically coupled into the resonator by means of a loop fed through its cylindrical surface. In this type of cavity, a strong electric field exists only in the mentioned gap, which actually amounted to $\approx$1.5 mm.

The RF power dissipated to the walls of the cavity leads to some heating-up of the crystal during resonator operation, where the contribution from energy losses of the beam inside the crystal can be neglected at average beam currents of several tens of nA used in the measurements. Therefore, the actual temperature of the cavity has been measured during the experiments by means of a thermoelectric sensor. Within a typical measurement time of 1800 s, the temperature of the cavity increased by about 30 K.

Spectra of planar CR registered from 30 MeV electrons channeled in the $(01\bar{1}1)$ plane of a 500 μm thick quartz crystal with and without excitation of ultrasonic vibrations of frequency 2.5 GHz and the corresponding BS spectrum are shown in Fig. 5.6. Background-subtracted and efficiency-corrected CR spectra measured for channeling in the $(01\bar{1}1)$, $(01\bar{1}5)$ and $(0\bar{2}23)$ planes of this quartz crystal with and without US excitation are shown in Figs. 5.7, 5.8 and 5.9.

It is inherent in all these figures that the CR rate decreases in the presence of non-resonant ultrasonic waves proceeding through the crystal. This means that the occupation lengths of the initial states contributing to the observed radiative transitions are effectively shortened due to the impact of US. Such an effect can be interpreted by the action of an additional scattering mechanism introduced by the US. If thermal scattering is an incoherent interaction with phonons of the crystal lattice, the observed behavior of CR in the presence of non-resonant US might be of similar nature.

The microbunches of the electron beam, having the duration of about 2 ps at a repetition rate of 13 MHz, pass the crystal within about 1.5 ps. Due to their relativistic velocity, the electrons of a microbunch channeled in some plane practically interact with a frozen deformed crystal potential. However, there is no phase correlation with the ultrasonic waves generated in the crystal. Therefore, the observed spectra represent some average over all possible phase relations between the pulsed electron beam and the US. In other words, coherence between the incoming plane waves of electrons and the US waves in the crystal persists for every single microbunch only, but it is lost for the sequence of microbunches.

The high-frequency vibrations in the crystal lattice are commonly referred to phonons, where thermal phonons are characterized by Gaussian distributions with respect to their vibration frequencies. The

ultrasonic vibrations induced in the crystal lattice by the action of the external electric RF field can also be understood as phonons propagating through the crystal. For a 500 μm thick crystal, the damping of the US wave is of the order of 30%. Reflection of the US wave from the rear surface of the crystal leads to a superposition of the damped induced and reflected US waves in the crystal. A formal calculation of the number of US wave lengths fitting at a frequency of 2.5 GHz into the crystal thickness gives the number of 211.5, if the velocity of sound is assumed to be 5.12×10^3 ms^{-1} in an *x*-cut crystal. Taking the thickness tolerance of the crystal and the exact value of the RF frequency into account, it is obvious, that the condition for a damped standing longitudinal US wave in the crystal is at most fulfilled accidentally or locally. Hence, the US field in the crystal is formed by the interfering damped US waves propagating in both directions, where there is generally no fixed phase correlation. Standing waves can be excited in a quartz crystal in the MHz frequency region, known as the eigenfrequencies of vibrating quartz crystals in a resonant circuit. At GHz frequencies of the exciting external electric field, a mechanical disturbance generated at the surface of the quartz crystal via the reverse piezoelectric effect propagates through the crystal as a damped US wave. Hence, the resulting US field in the crystal is time-dependent. Therefore, the effect on the CR emission observed for non-resonant US excited in the crystal might, to some degree, be understood as caused by a quasi-temperature.

One must also keep in mind that the frequency of 2.5 GHz is far from the resonance frequencies given for some crystal planes in Tab. 5.1. As has been shown in Ref. [Gri03b], the resonance between CR and US frequencies is characterized as a parametric one. This means that in the denominator of Eq. (5.5) occurs an additional parameter j which can take the integer values $j = 1,2,3,\ldots$ However, it is clear that the resonance effect will be less for values $j > 1$.

If the temperature of some crystal increases, the depth of the planar continuum potential is diminished [And83, Gar90]. Therefore, the energy difference between transversally bound states slightly degreases, and so the energy of the emitted CR photons does. The peak positions of all CR lines observed with US are shifted towards lower energy compared with the positions registered without US. However, as many-beam calculations with an assumed higher crystal temperature, i.e., larger mean-squared vibration amplitudes of the crystal atoms, showed, the observed shifts cannot be explained with the slight rise of the temperature of the resonator (20 ÷ 30 K) during the measurements with US. Hence, the effect is not caused by the increase of the temperature of the resonator. The local temperature of the vibrating crystal, however, could not be measured. At higher crystal temperature, thermal scattering increases, the occupation lengths shorten, and the CR rate falls, as observed in the measurements with US. Consequently, to exclude some temperature effects, cooling of resonator and crystal is highly desirable, because operation of the cavity in vacuum enables only some heat transport via the holder of the resonator to the mechanics of the goniometer.

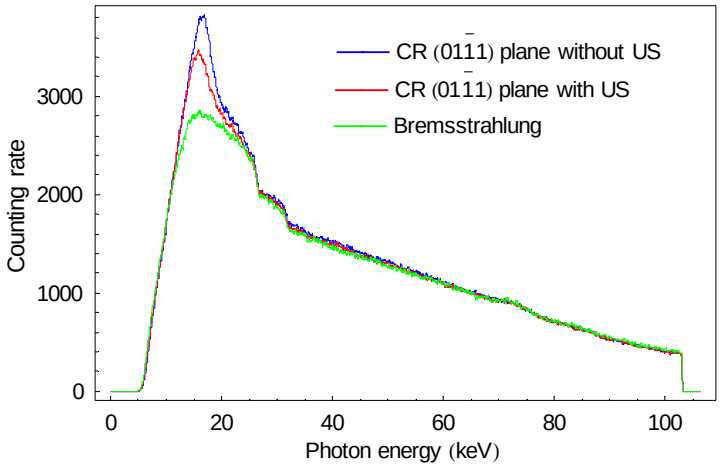

Fig. 5.6 Spectra of CR emitted by 30 MeV electrons channeled in the $(01\bar{1}1)$ *plane of a 500 μm thick quartz crystal without (upper one) and with (lower one) US of frequency 2.5 GHz excited in the crystal and the corresponding BS spectrum.*

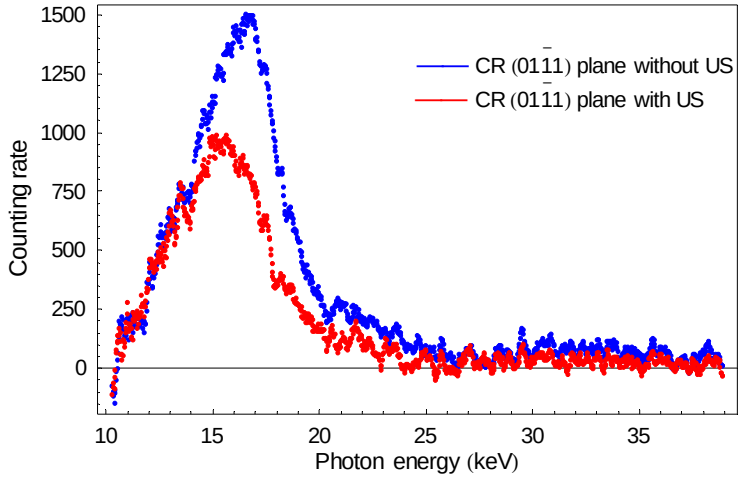

Fig. 5.7 Background-subtracted and efficiency-corrected spectra CR from 30 MeV electrons channeled in the $(01\bar{1}1)$ *plane of a 500 μm thick quartz crystal without (upper one) and with (lower one) US of frequency 2.5 GHz excited in the crystal.*

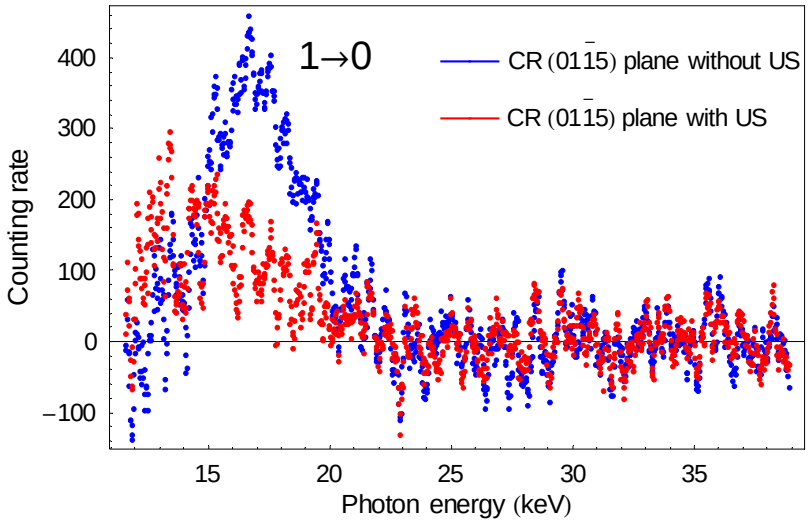

Fig. 5.8 Analogous to Fig. 5.7 but for channeling in the $(01\bar{1}5)$ *plane of quartz.*

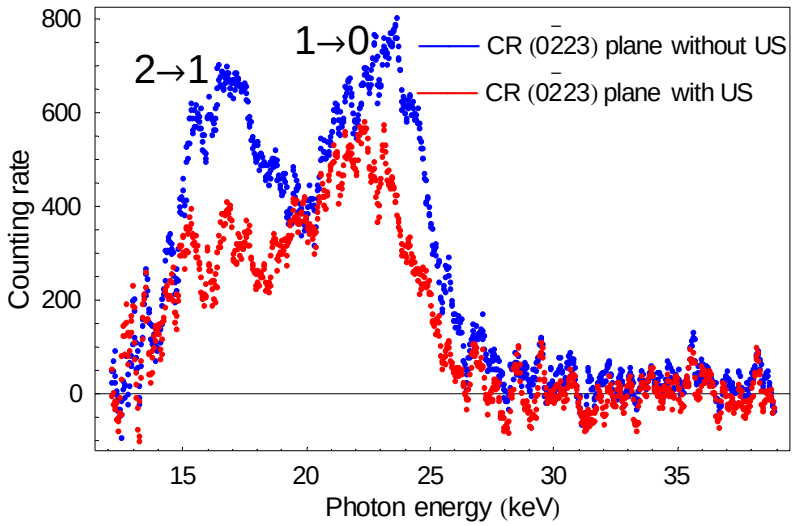

Fig. 5.9 Analogous to Fig. 5.7 but for channeling in the $(0\bar{2}23)$ *plan of quartz.*

5.4 Conclusions

Two different theoretical approaches to planar CR emission influenced by ultrasonic waves excited in the crystal are available and have been applied in this work for numerical calculations of CR line splitting and modulation of the CR photon spectra for channeling of electrons in different crystal planes of quartz. The resonance frequencies of US vibrations evaluated for transitions resolved in the measured CR spectra (see chapter 3) take values near to or higher than 10 GHz. Although the perturbation theory predicts a parametric character of the resonance, the effect should be diminished remarkably for integer-divided values of the resonance frequency.

On the base of the non-linear optics theory, spectral distributions of planar CR expected for channeling of 20 MeV electrons in the $(01\bar{1}5)$ plane of a 20 μm thick quartz crystal have been calculated at resonant influence of US and for various values of the relative deformation of the crystal lattice. The integration performed over the entire interval of Bloch momenta changes the resulting spectral distribution of CR substantially. In general, the deformations of the crystal lattice caused by the influence of resonant US leads to specified modifications of the CR spectrum.

First experimental investigations of the influence of non-resonant US on the CR emission from 30 MeV electrons channeled in different crystal planes of quartz have been carried out at the radiation source ELBE. A coaxial cavity for the excitation of ultrasonic waves of frequency 2.5 GHz has been designed, constructed and applied in the measurements.

It has been expected and was found experimentally that the excitation of US vibrations in the quartz crystal leads for all planes considered to a decreased CR emission rate. Small shifts observed for the CR photon energies have been discussed as probably caused by an additional scattering mechanism involved due to ultrasonic vibrations of the crystal lattice, because they could not be reproduced by an assumed higher temperature of the crystal. Nevertheless, confident measurements need cooling of the used cavities.

Since the resonance frequency of the used cavity was still far from satisfying the resonance condition for dedicated transverse transitions of channeled electrons, the measured spectra could principally not demonstrate the calculated modifications of the spectral distribution of CR. Enhancement of CR emission by the influence of US is predicted for much higher US frequencies.

In continuation of the present investigations, the applied technique has to be modified for reaching larger US frequencies, but it seems to be a challenging task to design a resonant cavity which operates at frequencies near to or even larger then 10 GHz. Therefore, concluding from the performed measurements, it is suggested to carry out similar CR measurements for dedicated crystal planes of quartz with US excitation at frequencies of several GHz but at several times higher electron energy. The quantum character of CR emission should, however, be preserved yet to enable a detailed interpretation of the influence of US on the measured CR spectra.

Summary

In the fall of 2006, an intense tunable quasi-monochromatic X-ray source based on electron CR came into operation at the radiation source ELBE. This source provides photon fluxes up to about 10^{11} s^{-1} at photon energies between 10 and 100 keV within a bandwidth of 10% and is to be applied in radiobiological investigations. Although research in radiation physics concentrated on CR after its theoretical prediction in 1976, and feasibility studies for a non-conventional X-ray source followed at the beginning of the 1990ies, such a project had not been put into practice. Part of the present work aimed at laying the foundations for the built up of an intense CR source at ELBE.

This concerns theoretical as well as experimental investigations of CR emission from diamond crystals found to be most suited for intense CR production. Based on the many-beam formalism of CR, a computer code has been developed and applied for the calculation of planar continuum potentials, transversely bound channeling states, transition energies, CR line widths and photon yields.

Measurements of planar CR have been performed at the electron beam of ELBE within an energy range between 14 and 34 MeV and for thicknesses of the diamond crystals between 42.5 and 500 μm. The newly developed program for data processing incorporates correction procedures for the registration efficiency of the detectors, self-absorption in the crystal, radiation attenuation in window materials, background subtraction and the approximation of asymmetric CR line profiles to the measured data. Absolute CR photon yields have for the first time been obtained for the above given ranges of electron energy and crystal thickness. The comparison with calculations performed show a reasonable agreement.

The square-root dependence of the planar CR photon yield on the thickness of diamond crystals, which has been concluded from an earlier work, has been confirmed. A systematic quantitative investigation of the influence of the crystal thickness on the CR line shape has for the first time been performed. The mean-squared multiple-scattering angle effective for planar CR observed in forward direction has been found to be weaker as assumed from scattering in amorphous targets. This finding justified the application of thicker diamond crystals in a CR X-ray source for optimization of the CR intensity. Scaling laws deduced from the measured CR data are of advantage for the operation of a CR source.

The second part of this thesis deals with the possibility of stimulation of CR emission by means of ultrasonic vibrations excited in a piezoelectric single crystal. From theoretical calculations, certain modifications of the CR spectrum emitted under the influence of US and probable amplification of the CR intensity are predicted.

The developed mathematical instrument, successfully tested in the preceding experiments on diamond crystals, has been applied for corresponding calculations of the CR emission from electrons channeled in different planes of the binary hexagonal piezoelectric quartz crystal. Since the knowledge of the CR spectra generated on undisturbed quartz crystals is a necessary precondition for some investigation of the influence of US, planar CR has for the first time been measured at medium electron energies for a variety of planes in quartz. As a consequence of the hexagonal structure of this crystal, relative intense CR could be registered even out of planes with indices larger than one.

The CR data obtained in the present work for quartz are of fundamental interest for a dedicated evaluation of the effect of US on CR and for the choice of crystal planes suitable for experimental investigations. Two different theoretical approaches to planar CR emission influenced by US were available and have been applied in this work for relevant calculations. On the base of the non-linear optics method, occupation functions and spectral distributions of planar CR have been calculated for channeling of 20 MeV electrons in the $(01\bar{1}5)$ plane of a 20 μm thick quartz crystal at resonant influence of US. The resonance frequencies have been deduced from the measurements of CR spectra performed on quartz. It has been shown that the deformation of the crystal lattice caused by the action of resonant US may lead to a remarkable modification of the CR spectrum.

First experimental investigations of the influence of US on CR started at ELBE aimed at the study of the effect of non-resonant ultrasonic vibrations excited in a 500 μm thick quartz crystal. A coaxial cavity with a resonance frequency of 2.5 GHz has been designed, constructed and applied in a series of CR measurements carried out at the electron energy of 30 MeV. The excitation of non-resonant US in the quartz crystal led to a decreased CR emission rate for all planes investigated. Such effect may be caused by an additional scattering mechanism which is involved by the periodic deformation of the crystal lattice and resembles thermal scattering. Since the frequency of the used cavity was still far from satisfying the resonance condition for dedicated transverse transitions of electrons channeled in crystal planes of quartz, the calculated modification of the spectral distribution of CR could principally not yet be demonstrated experimentally.

In continuation of these investigations, the technique applied for the excitation of US in quartz should be modified to reach US frequencies near to 10 GHz. Another, probably more effective way might consist in performing measurements at US frequencies of several GHz but at a several times larger electron energy. The quantum character of CR emission should, however, still be conserved.

References

[Alg79] M.J. Alguard, R.L. Swent, R.H. Pantell, B.L. Berman, S.D. Bloom, S. Datz, Phys. Rev. Lett. **42**, 1148 (1979).

[Amp07] Amptek Inc., Bedford, USA, www.amptek.com (2007)

[And77] J.U. Andersen, S.K. Andersen, W.M. Augustyniak, Kong. Danske. Vid. Selsk. Mat. Fys. Medd. **10**, 39 (1977).

[And80] J.U. Andersen, E. Lægsgaard, Phys. Rev. Lett. **44**, 1079 (1980).

[And83] J.U. Andersen, E. Bonderup, E. Lægsgaard, A.H. Sørensen, Phys. Scr. **28**, 308 (1983).

[Atk82] M. Atkinson, J.F. Back, P.J. Bussey, P. Christensen, J.A. Ellison, R.J. Ellison, K.R. Eriksen, D. Giddings, R.E. Hughes-Jones, B.B. Marsh, D. Mercer, F.E. Meyer, S.P. Møller, D. Newton, P. Pavlopoulos, P.H. Sharp, R. Stensgaard, M. Suffert, E. Uggerhøj, Phys. Lett. **110**B, 162 (1982).

[Ava88] R.O. Avakyan, A.E. Avetisyan, V.A. Gyurdzhyan, K.R. Dallakyan, S.R. Taroyan, A.R. Mkrtchyan, R.A. Gasparyan, R.G. Gabrielyan, A.R. Mkrtchyan, R.P Vardapetyan, Pis'ma Zh. Eksp. Teor. Fiz **48**, 577 (1988).

[Ava90] R.O. Avakyan, A.E. Avetissyan, A.V. Aharonyan, R.A. Asaturyan, R.B. Bakhshetsyan, E,M, Boyakhchyan, R.P Vardapetyan, R.G. Gabrielyan, K.R. Dallakyan, H.S. Kizogyan, L.A. Kocharyan, E.M. Matevossyan, R.M. Mirzoyan, A.G. Mkrtchyan, A.R. Mkrtchyan, A.Kh. Mkhittaryan,R.Ts. Sarkissyan, Yu.Z. Sukiassyan, S.P. Taroyan, O.A. Unanyan, G.M. Elbakyan, Nucl. Instrum. Meth. B **48**, 266 (1990).

[Ava06a] R.O. Avakian, K.A. Ispirian, V.J. Yaralov, Nucl. Instrum. Meth. B **252**, 20 (2006).

[Ava06b] R.O. Avakian, K.A. Ispirian, V.J. Yaralov, Nucl. Instrum. Meth. B **252**, 26 (2006).

[Ave97] H.K. Avetissian, K.Z. Hatsagortsian, G.F. Mkrtchian, Kh.V. Sedrakian, Phys. Rev. A **56**, 4121 (1997).

[Aza06] B.Azadegan, W. Wagner, J. Pawelke, Phys. Rev. B **74**, 045209 (2006).

[Aza07] B.Azadegan, W. Wagner, J. Pawelke, L.Sh. Grigoryan, in *Proc. Internat. Conf. on Charged and Neutral Particles Channeling Phenomena, Frascati, Italy (2006*) ed. S. B. Dabagov (SPIE, vol. **6634**, Bellingham, 2007).

[Bar80] V.G. Baryshevsky, I.Ya. Dubovskaya, A.O. Grubich, Phys. Lett. **77A**, 61 (1980).

[Ber82] B.L. Berman, S. Datz, R.W. Fearick, J.O. Kephart, R.H. Pantell, H. Park, R.L. Swent, Phys. Rev. Lett. **49**, 474 (1982).

[Bil03] J.H. Billen, L.M. Young, *Poisson Superfish Codes* (Los Alamos National Laboratory, 2003).

[Bir82] D.M. Bird, B.F. Buxton, Proc. Roy. Soc. London, Ser. A **379**, 459 (1982).

[Bur84] A.F. Burenkov, Yu.I. Dudchik, F.F. Komarov, Radiat. Effects **83**, 241 (1984).

[Bus97] G. Buschhorn, E. Dietrich, W. Kufner, M. Rzepka, H. Genz, H.-D, Gräf, P. Hoffmann-Staschek, U. Nething, A. Richter, Phys. Rev. B 55, 6196 (1997).

[Cho99] K. Chouffani, H. Überall, H. Genz, P. Hoffmann-Staschek, U. Nething, A. Richter, Nucl. Instrum. Meth. B **152**, 479 (1999).

[Cho99a] K. Chouffani, H. Überall., Phys. Status Solidi B **213**, 107 (1999).

[Ded94] G.V. Dedkov, Phys. Status Solidi B **184**, 535 (1994).

[Doy68] P.A. Doyle, P.S. Turner, Acta Crystallogr., Sect. A: Cryst. Phys., Diffr., Theor. Gen. Crystallogr. **24**, 390 (1968).

[Eid04] S. Eidelman, et al., Phys. Lett. B **592**, 246 (2004).

[Elb06] Radiation source ELBE, Forschungszentrum Dresden-Rossendorf, http://www.fzd.de (2007).

[Fre96] J. Freudenberger, H. Genz, L. Groening, P. Hoffmann-Staschek, W. Knüpfer, V.L. Morokhovskii, V.V. Morokhovskii, U. Nething, A. Richter, J.P.F. Sellschop, Nucl. Instrum. Meth. B **119**, 123 (1996).

[Gar90] C.K. Gary, A.S. Fisher, R.H. Pantell, J. Harris, M.A. Piestrup, Phys. Rev. B **42**, 7 (1990).

[Gar91] C.K. Gary, R.H. Pantell, M. Özcan, M.A. Piestrup, D.G. Boyers, J. Appl. Phys. **70**, 2995 (1991).

[Gen90] H. Genz, H.-D. Gräf, P. Hoffmann, W. Lotz, U. Nething, A. Richter, H. Kohl, A. Weickenmeier, W. Knüpfer, J.P.F. Sellschop, Appl. Phys. Lett. **57**, 2956 (1990).

[Gen96] H. Genz, L. Groening, P. Hoffmann-Staschek, A. Richter, M. Höfer, J. Hormes, U. Nething, J.P.F. Sellschop, C. Toepffer, M. Weber, Phys. Rev. B **53**, 8922 (1996).

[Gou82] M. Gouanere, D. Sillou, M. Spighel, N. Cue, M.J. Gaillard, R.G. Kirsch, J.-C. Poizat, J. Remillieux, B.L. Berman, P. Catillon, L. Roussel, G.M. Temmer, Nucl. Instrum. Meth. **194**, 225 (1982).

[Gou88] M. Gouanere, D. Sillou, M. Spighel, N. Cue, M.J. Gaillard, R.G. Kirsch, J.-C. Poizat, J. Remillieux, B.L. Berman, P. Catillon, L. Roussel, G.M. Temmer, Phys. Rev. B **38**, 4352 (1988).

[Gri00a] L.Sh. Grigoryan, A.R. Mkrtchyan, B.V. Khachatryan, H.F. Khachatryan, H. Prade, W. Wagner, Rad. Eff. & Def. in Solids, vol. **152**, 269 (2000).

[Gri00b] L.Sh. Grigoryan, A.H. Mkrtchyan, H.F. Khachatryan, R.P. Vardapetian, H. Prade, W. Wagner, Rad. Eff. & Def. in Solids **152**, 225 (2000).

[Gri00c] L.Sh. Grigoryan, A.R. Mkrtchyan, H.F. Khachatryan, A.H. Mkrtchyan, H. Prade,

W. Wagner, Rad. Eff. & Def. in Solids **153**, 13 (2000).

[Gri01a] L.Sh. Grigoryan, A.R. Mkrtchyan, A.H. Mkrtchyan, H.F. Khachatryan, W. Wagner, M.A. Piestrup, Rad. Eff. & Def. in Solids **153**, 212 (2001).

[Gri01b] L.Sh. Grigoryan, A.R. Mkrtchyan, A.H. Mkrtchyan, H.F. Khachatryan, W. Wagner, M.A. Piestrup, Rad. Eff. & Def. in Solids **153**, 289 (2001).

[Gri01c] L.Sh. Grigoryan, A.R. Mkrtchyan, A.H. Mkrtchyan, H.F. Khachatryan, W. Wagner, M.A. Piestrup, Rad. Eff. & Def. in Solids **153**, 307 (2001).

[Gri01d] L.Sh. Grigoryan, A.R. Mkrtchyan, A.H. Mkrtchyan, H.F. Khachatryan, H. Prade, W. Wagner, M.A. Piestrup, Nucl. Instrum. Meth. B **173**, 132 (2001).

[Gri01e] L.Sh. Grigoryan, A.R. Mkrtchyan, A.H. Mkrtchyan, H.F. Khachatryan, H. Prade, W. Wagner, M.A. Piestrup, Nucl. Instrum. Meth. B **173**, 184 (2001).

[Gri03a] L.Sh. Grigoryan, A.H. Mkrtchyan, H.F. Khachatryan, V.U. Tonoyan, W. Wagner, Nucl. Instrum. Meth. B **201**, 25 (2003).

[Gri03b] L.Sh. Grigoryan, A.H. Mkrtchyan, H.F. Khachatryan, W. Wagner, A.A. Saharian, K.S. Baghdasaryan, Nucl. Instrum. Meth. B **212**, 51 (2003).

[Hig79] V.L. Highland., Nucl. Instrum. Methods **129**, 497 (1975); ibid. **161**, 171 (1979).

[Jac75] J.D. Jackson, *Classical Electrodynamics* (Wiley, New York, 1975) p. 713.

[Kep89] J.O. Kephart, R.H. Pantell, B.L. Berman, S. Datz, H. Park, R.K. Klein, Phys. Rev. B **40**, 4249 (1989).

[Kep91] J.O. Kephart, B.L. Berman, R.H. Pantell, S. Datz, R.K. Klein, H. Park, Phys. Rev. B 44, 1992 (1991).

[Kle85] R.K. Klein, J.O. Kephart, R.H. Pantell, H. Park, B.L. Berman, R.L. Swent, S. Datz, R.W. Fearick, Phys. Rev. B **31**, 68 (1985).

[Kum76] M.A. Kumakhov, Phys. Lett. **57**, 17 (1976).

[Kum89] M.A. Kumakhov, F.F. Komarov, *Radiation from Charged Particles in Solids*

(AIP, New York, 1989).

[Kum91] M.A. Kumakhov, R. Wedell, *Radiation of Relativistic Light Particles during Interaction with Single Crystals* (Spektrum Akademischer Verlag, Heidelberg, 1991).

[Lin65] J. Lindhard, Kong. Danske Vid. Selsk. Mat. Fys. Medd. **14**, 34 (1965).

[Mir79] I.I. Miroshnichenko, J.J. Murray, R.O. Avakyan, Th. Fieguth, Sov. JETP Lett. **29**, 722 (1979).

[Mkr86] A.R. Mkrtchyan, R.H. Gasparyan, R.G. Gabrielyan, Phys. Lett. A **115**, 410 (1986).

[Mkr87] A.R. Mkrtchyan, R.H. Gasparyan, R.G. Gabrielyan, Sov. Phys. JETP **66**, 248 (1987).

[Mkr88] A.R. Mkrtchyan, R.H. Gasparyan, R.G. Gabrielyan, A.G. Mkrtchyan, Phys. Lett. A **126**, 528 (1988).

[Mol69] B.R. Mollow, Phys. Rev. **188**, 1969 (1969).

[Mol70] B.R. Mollow, Phys. Rev. B **2**, 76 (1970).

[Net94] U. Nething, PhD thesis, TH Darmstadt (1994).

[Net94] U. Nething, M. Galemann, H. Genz, M. Höfer, P. Hoffmann-Staschek, J. Hormes, A. Richter, J. P. F. Sellschop, Phys. Rev. Lett. **72**, 2411 (1994).

[Neu07] W. Neubert, B. Azadegan, W. Enghardt, K. Heidel, J. Pawelke, W. Wagner, Nucl. Instrum. Meth. B **254**, 319 (2007).

[Ogn94] L.I. Ognev, Nucl. Instrum. Meth. B **84**, 319 (1994).

[Par83] H. Park, R.L. Swent, J.O. Kephart, R.H. Pantell, B.L. Berman, S. Datz, R.W. Fearick, Phys. Lett. **96A**, 45 (1983).

[Rad70] G. Radi, Acta Crystallogr., Sect. A: Cryst. Phys., Diffr., Theor. Gen. Crystallogr. **26**, 41 (1970).

[Rei99] I. Reiz, Diploma thesis, TU Darmstadt (1999);
H. Genz, in *Proc. NATO Advanced Research Workshop on Electron-Photon Interaction in Dense Media, Nor-Hamberd, Yerevan, Armenia (2001*) ed. H. Wiedemann,

NATO Science Series II, vol. 49, 217 (Kluwer Acad. Publ., Dordrecht, 2002).

[Rob62] M.T. Robinson, Appl. Phys. Lett. **1**, 49 (1962).

[Rob63] M.T. Robinson, O.S. Oen, Appl. Phys. Lett. **2**, 30 (1963).

[Sae85] A.W. Sáenz, H. Überall, *Coherent Radiation Sources* (Springer, Berlin-Heidelberg, 1985).

[Smi63] G.S. Smith, L.E. Alexander, Acta Crystallogr. **16**, 462 (1963).

[Swe84] R.L. Swent, R.H. Pantell, H. Park, J.O. Kephart, R.K. Klein, S. Datz, R.W. Fearick, B.L. Berman, Phys. Rev. B **29**, 52 (1984).

[Tsa74] Y.S. Tsai, Rev. Mod. Phys. **46**, 815 (1974).

[Tul81] A.V. Tulupov, Sov. Phys. JETP **54**, 872 (1981).

[Ugg66] E. Uggerhøj, Phys. Lett. 22, 382 (1966).

[Van57] V. Vand, T.F. Eiland, R. Pepinsky, Acta Crystallogr. **10**, 303 (1957).

[Wag04] W. Wagner, A. Panteleeva, J. Pawelke, W. Enghardt, Wiss.–Tech. Berichte FZR-**401**, 56 (2004).

[Wag05a] W. Wagner, B. Azadegan, A. Panteleeva, J. Pawelke, and W. Enghardt, in *Proc. Internat. Conf. on Charged and Neutral Particles Channeling Phenomena, Frascati, Italy (2004*) ed. S. B. Dabagov (SPIE, vol. **5974**, Bellingham, 2005).

[Wag05b] W. Wagner, F. Müller, A. Nowack, M. Sobiella, J. Steiner, W. Enghardt, Wiss.–Tech. Berichte FZR-**423**, 72 (2005).

[Wag05c] W. Wagner, B. Azadegan, J. Pawelke, W. Enghardt, Wiss.–Tech. Berichte FZR-**423**, 69 (2005).

[Wag07] W. Wagner, B. Azadegan, L.Sh. Grigoryan, J. Pawelke, Europhys. Lett. 78, 56004 (2007).

[Web95] M. Weber, PhD thesis, University of Erlangen (1995).

[Whe65] M.J. Whelan, J. Appl. Phys. **36**, 2103 (1982).

Acknowledgements

I would like to gratefully acknowledge the support of this work by the administration of the Institute of Radiation Physics of the Forschungszentrum Dresden-Rossendorf, by my colleagues from the Department of Radiation Physics and by scientific workers and engineers from other divisions of the FZD.

I wish to thank my academic supervisor Prof. Dr. Eckart Grosse, head of the Institute of Radiation Physics until March 2007, for giving me the possibility of a PhD fellowship at this institute. I am very thankful to Prof. Dr. Wolfgang Enghardt, head of the Department of Radiation Physics until October 2005, for his invitation to Forschungszentrum Dresden-Rossendorf and for the conceptual formulation of this thesis.

I wish to thank my scientific supervisor Dr. Wolfgang Wagner for his valuable and great scientific guidance, for sharing the knowledge in this field or research, for the steady discussion of forthcoming work and for the warm hearted cooperation. I also want to cordially thank Dr. Jörg Pawelke for the management of the experiments performed at ELBE and for his inexhaustible activity during the measurements.

I am very thankful to Dr. Waldemer Neubert for fruitful discussions and for a first correction of this work.

I want to thank Dr. Anna Lehnert who introduced me into the software Mathematica and shared her experience with this program package. I would like to thank my colleagues Elke Beyreuther, Dr. Paulo Crespo, Fine Fiedler, Elisabeth Lessmann, Daniela Möckel, Uwe Reichelt, Georgy Shakirin, Karl Zeil, who went with me through these years and created the nice atmosphere during and out of the work time.

I am indebted to the crew of the Radiation source ELBE headed by Dr. Peter Michel, especially to Dr. Ulf Lehnert for delivering excellent electron beams, to Michael Freitag for the installation of necessary equipment at the electron beam line, to Dr. Hartmut Büttig for his active support in RF techniques and to Ulrich Wolf for his kind assistance.

I very would like to thank Manfred Sobiella for the rapid construction and modification of the RF cavities and the workshop of the IRP for the immediate manufacturing of these devices.

I acknowledge the funding of my research work abroad by the Ministry of Science, Research and Technology of the Islamic Republic of Iran from November 2003 to November 2007. It is also a great pleasure for me to thank all my teachers during my undergraduate studies at the Ferdowsi University of Mashad. I especially thank Prof. Dr. Rahim Kohi Faegh and Dr. Jafar Shoja Taheri for sharing their knowledge in physics and numerical methods.

My warmest thanks goes to my family, my parents, my sister and my brother for their help to go abroad and for their patience during living at more than 4000 km distance from each other. I wish to express my great love to my wife Batoul for her steady and uncomplaining support of my research work and for her

care at home. Thanks also to my wonderful children, to Ayda for her perseverance in learning German at school and parallel her mother language Persian at home, and to our little Atrin who was born during my stay in Dresden.

Versicherung

Hiermit versichere ich, dass ich die vorliegende Arbeit ohne unzulässige Hilfe Dritter und ohne Benutzung anderer als der angegebenen Hilfsmittel angefertigt habe; die aus fremden Quellen direkt oder indirekt übernommenen Gedanken sind als solche kenntlich gemacht. Die Arbeit wurde bisher weder in Inland noch im Ausland in gleicher oder ähnlicher Form einer anderen Prüfungsbehörde vorgelegt.

Dresden, den Behnam Azadegan

Erklärung

Die vorliegende Arbeit wurde am Institut für Strahlenphysik des Forschungszentrums Dresden-Rossendorf (FZD) angefertigt. Die wissenschaftliche Betreuung erfolgte durch Herrn Prof. Dr. E. Grosse seitens der Fachrichtung Physik der Technischen Universität Dresden und durch Herrn Dr. rer. nat. W. Wagner seitens der Abteilung Strahlungsphysik des Instituts für Strahlenphysik des FZD.
Die Promotionsordnung der Fakultät für Mathematik und Naturwissenschaften der Technischen Universität Dresden wird von mir anerkannt.

Dresden, den Behnam Azadegan